Advances in Materials Science and Engineering

Biomass Materials for Metallurgical Applications

Lead Guest Editor: Liming Lu
Guest Editors: Xianchun Li, Merrick Mahoney, and Zhiqiang Zhang

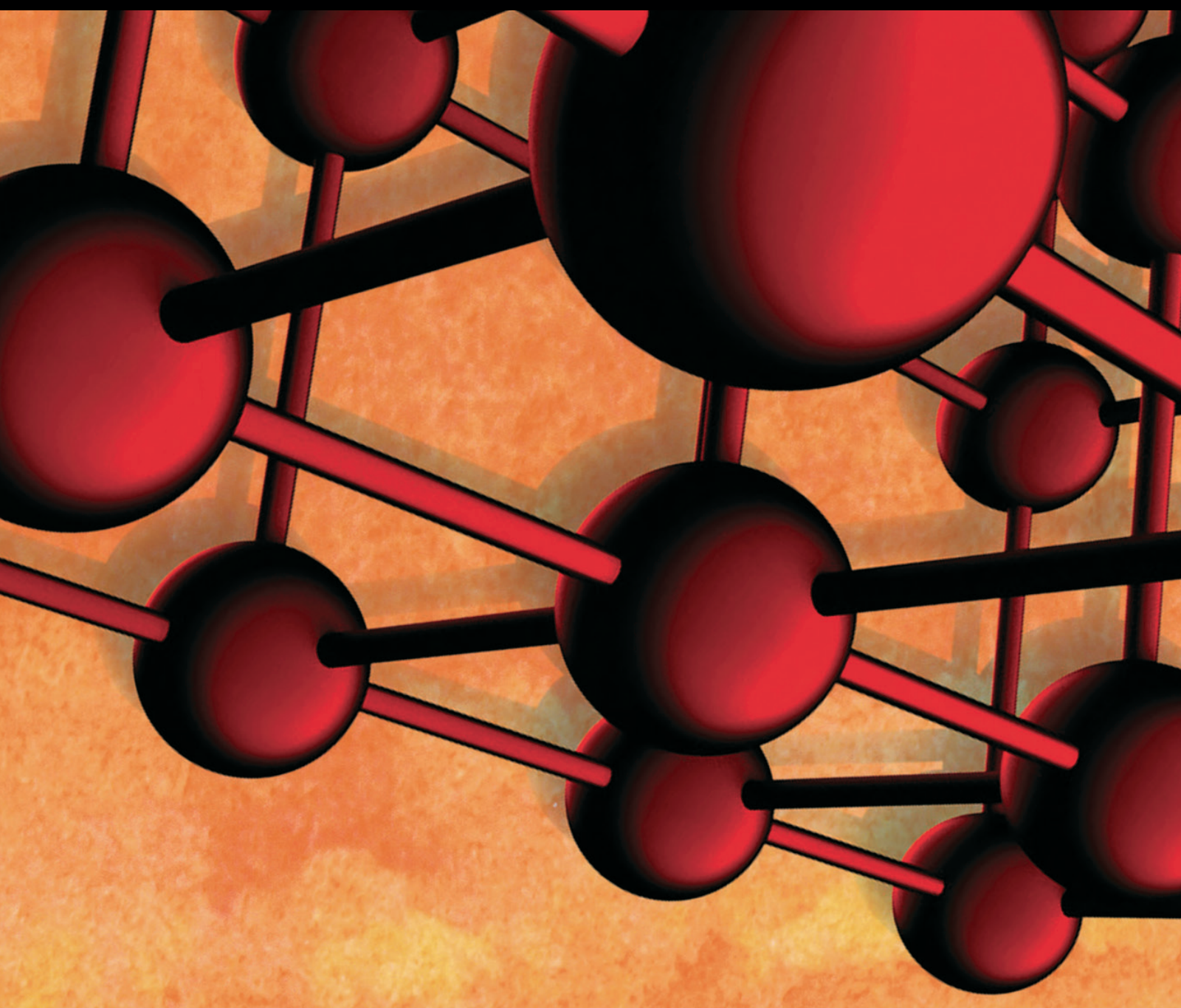

Biomass Materials for Metallurgical Applications

Advances in Materials Science and Engineering

Biomass Materials for Metallurgical Applications

Lead Guest Editor: Liming Lu
Guest Editors: Xianchun Li, Merrick Mahoney,
and Zhiqiang Zhang

Editorial Board

Contents

Hindawi
Advances in Materials Science and Engineering
Volume 2018, Article ID 7297136, 1 page
https://doi.org/10.1155/2018/7297136

Editorial

Biomass Materials for Metallurgical Applications

Liming Lu,[1] **Xianchun Li**,[2] **Merrick Mahoney**,[3] **and Zhiqiang Zhang**[2]

[1]*CSIRO Mineral Resources, Technology Court, Pullenvale, QLD 4069, Australia*
[2]*University of Science and Technology Liaoning, Anshan, Liaoning, China*
[3]*Newcastle Institute for Energy and Resources, University of Newcastle, University Drive, Callaghan, NSW 2308, Australia*

Correspondence should be addressed to Liming Lu; liming.lu@csiro.au

Received 25 February 2018; Accepted 25 February 2018; Published 27 May 2018

Steels are by far the most widely used of metallic materials and will continue to be vitally important to our society. However, production of steel from virgin raw materials is currently energy intensive, requires substantial use of fossil-based carbon sources, such as coal and coke, and results in high CO_2 emissions. Based on the statistics available, worldwide steel production is believed to contribute to about 5–6% to total world greenhouse gas emissions. Hence there have been considerable efforts over the years in examining the use of biomass-based materials in primary metal production as a fuel and reductant in place of fossil fuel carbon sources. The biomass material is not only CO_2 neutral but also likely contains less S, N, Cl, and other heavy metal elements, which are harmful to both the environment and human health as well as metal quality.

The special issue on the biomass materials for metallurgical applications is dedicated to the recent advances in the characterisation, processing, and utilisation of biomass materials for metallurgical operations. Among the six papers collected, four papers endeavoured to develop new iron ore-carbon composite pellets in which biomass materials are used as a reductant, while the other papers studied the possibility to use biomass materials as an alternative fuel in the sintering processes. The papers evaluated a wide range of biomass materials from raw biomass such as cow manure and wood to pretreated biomass materials such as biochars from rice husk, peanut shell, oil palm empty fruit bunch (EFB), and acutissima.

Clearly, we still have a long way to go for large-scale applications of biomass materials in metallurgical industries. First, the biomass materials need to achieve the qualities ideally suited to their potential applications, such as iron ore sintering and blast furnace iron making. In addition to the quality suitability of biomass materials for metallurgical applications, the availability and cost of biomass materials must also be considered. The availability and cost of biomass materials are two key factors hindering the introduction of biomass materials in metallurgical industries. More studies concentrating on the availability and possible production chain of biomass materials for metallurgical applications are urgently needed in order to develop and manage the biomass sources on a sustainable basis and to develop a high-capacity production technology at a low cost and less environmental impact.

Liming Lu
Xianchun Li
Merrick Mahoney
Zhiqiang Zhang

Hindawi
Advances in Materials Science and Engineering
Volume 2018, Article ID 4067237, 7 pages
https://doi.org/10.1155/2018/4067237

Research Article

Innovative Process to Enrich Carbon Content of EFB-Derived Biochar as an Alternative Energy Source in Ironmaking

Hadi Purwanto, Alya Naili Rozhan, and Hamzah Mohd Salleh

Faculty of Engineering, IIUM, P.O. Box 10, 50728 Kuala Lumpur, Malaysia

Correspondence should be addressed to Alya Naili Rozhan; alyanaili@iium.edu.my

Received 26 May 2017; Revised 15 September 2017; Accepted 8 January 2018; Published 14 March 2018

Academic Editor: Zhiqiang Zhang

This paper describes the mechanism of a developed process—an integrated pyrolysis-tar decomposition process—to produce oil palm empty fruit bunch- (EFB-) derived biochar with additional solid carbon within the biochar bodies, produced by decomposition of tar vapor on its pore surface, using the chemical vapor infiltration (CVI) method. The product, carbon-infiltrated biochar, was characterized to investigate the possibility to be used as partial coke breeze replacement in ironmaking. Carbon-infiltrated biochar is proposed to be utilized for a sintering process that could reduce the consumption of coke and CO_2 emission in iron-steel industry.

1. Introduction

Being one of the largest palm oil producers, Malaysia has abundance of oil palm residues generated throughout the year. The high volume of oil palm biomass residues incurs high management and disposal costs. The inefficiency of waste management also causes environmental deterioration because of the natural methanation process from biomass dumping [1].

We are interested in the utilization of oil palm empty fruit bunch (EFB), biomass that is abundantly available but marginally utilized in Malaysia. One of the thermochemical methods to harness biomass energy is pyrolysis—a process that produces biochar, biotar, and gases [2]. Gases produced can be directly used as a renewable fuel source, mainly in electric power generation in Malaysia. Biochar (the main product of slow pyrolysis) and biotar (the main product of fast pyrolysis) contain carbon that can be collected and used as a fuel source as well. Different pyrolysis conditions resulted in different products, and each pyrolysis process has to be well executed by following the objectives of the biomass treatment. Several techniques have been carried out by researchers to obtain the desired products, and they are mostly achieved by controlling the important processing parameters such as temperature and heating rates.

This paper discusses the mechanism of carbon-infiltrated biochar production by the integrated pyrolysis-tar decomposition process. The experimental part of the production was already presented [3], which was a combination of slow and fast pyrolysis processes of coarse and fine EFB particles, respectively. Slow pyrolysis of coarse EFB produces biochar that is highly porous and is able to be utilized as a substrate for the biotar decomposition process to take place. Chemical vapor infiltration (CVI) technology was employed to implement integrated fast pyrolysis—tar decomposition over porous EFB biochar—to produce a value-added EFB biochar.

An important product of using the technology is carbon-infiltrated biochar containing increased carbon content and calorific value, which is able to partially substitute coke breeze. Coke breeze is generally a by-product of metallurgical coke production for blast furnace, and it is in the form of fine particles. Coke breeze has been used in a sintering machine as a heat source. Carbon-infiltrated biochar, with increased carbon but decreased volatile matters content, can be considered as a supplementary fuel in a sintering plant to reduce the usage of coke breeze. Utilization of an EFB-derived product to partially substitute this fossil fuel is expected to reduce CO_2 emission into the environment.

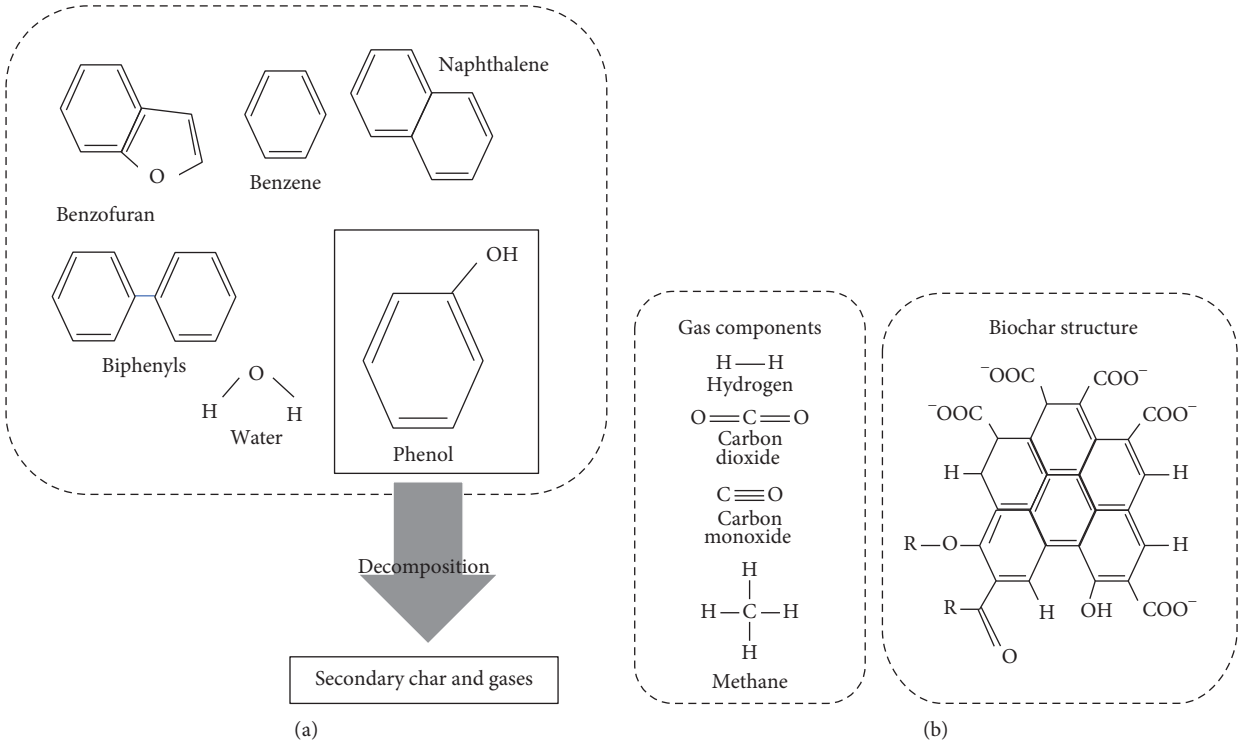

Figure 1: (a) Chemical structure of biotar components produced by the fast pyrolysis process at 500–600°C. (b) Chemical structures of gas components and biochar produced by the pyrolysis process.

2. Characterization Method

Carbon-infiltrated biochar produced using the integrated pyrolysis-tar decomposition process was characterized for its carbon type and microstructure, as well as to understand the mechanism of the developed process. This carbon deposition process came from decomposition of EFB-derived biotar that took place within the pores of EFB-derived biochar. The conversion of EFB into porous biochar involved decomposition of its components, hemicellulose, cellulose, and lignin. The chemical and physical properties of deposited carbon within the porous biochar were investigated. The chemical structures for components of tar produced by fast pyrolysis, components of gases, and structure of biochar are presented.

In order to study the physical properties of the carbon-infiltrated biochar, FE-SEM observation was performed. In relation to the morphologies, pore size distribution of biochar samples before and after tar carbonization was investigated by adsorption isotherms of nitrogen gas on meso- and micropores and the data were collected by employing the Dubinin–Astakhov (DA) method. This method was chosen because it is the most suitable method for biochar, a heterogenous carbonaceous material.

The deposited carbon within the porous biochar was analyzed using the Renishaw inVia micro-Raman spectrometer, equipped with a CCD detector to investigate its sp^3 content. The spectra for measurement were selected to be in the range of 900–2000 cm^{-1}, and the measurement was done at least three times to confirm reproducibility. The properties of carbon-infiltrated biochar were then compared to those of the commercial coke breeze. This material is proposed to be an alternative or a partial substitute to coke breeze in a sintering machine for ironmaking.

3. Results and Discussion

Generally, for a lignocellulosic biomass such as EFB, cellulose and hemicellulose decompose into volatiles, whereas lignin normally decomposes into residual ash or biochar depending on the process parameters [4]. Figure 1 (a) presents the structure of tar components produced from the fast pyrolysis process at 500–600°C adapted from a review done by Li and Suzuki [5]. The main component in tar produced at these temperatures is phenol, and phenol is a product based from lignin. Therefore, this tar was anticipated to be able to decompose into a large amount of pyrolytic carbon or secondary char, as compared to tar produced at other temperatures. Figure 1(b) depicts the structure of gases and biochar produced in this process.

Figure 2 shows the FE-SEM photos of biochar materials at 100,000x magnification. This result revealed the shape of biochar pores that appeared to be similar to nano-sized cracks. This clearly supports the notion that the EFB biochar was a heterogeneous material consisting of micropores, mesopores, and macropores. It could be seen that the pores narrowed after the tar carbonization process within the pores. Figure 3 shows the pore size distributions of biochar

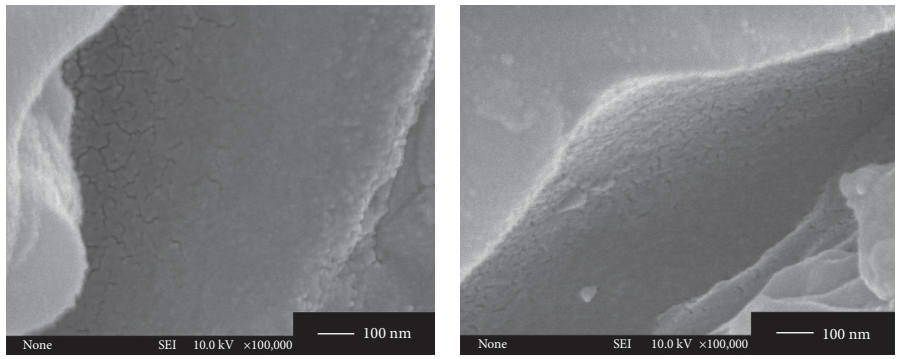

(a) (b)

Figure 2: Morphology of biochar particles showing the shape of the pores (magnification 100,000x). (a) Biochar produced at 400°C; (b) biochar after carbon deposition within the pores.

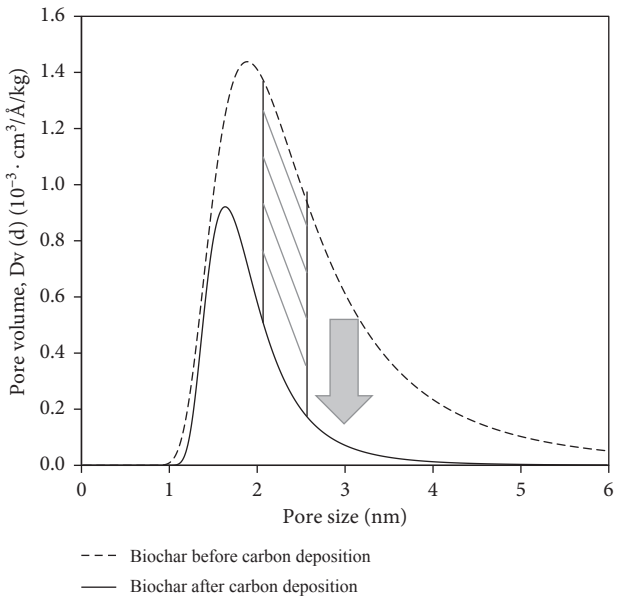

Figure 3: Changes in pore size distribution of biochar particles before and after carbon deposition using the Dubinin–Astakhov (DA) method.

before and after tar carbonization analyzed using the nitrogen adsorption method. The Dubinin–Astakhov equation was employed for this type of material and presented by a nonlinear curve fitting to the adsorption isotherm. From this figure, it can be clearly seen that the pores were "consumed" after the tar carbonization process, and pores with 2.0–2.5 nm size range were found to have the most "pore consumption." This phenomenon was attributed to the carbon deposition within the pores. It can be deduced that, for biochar, 2–2.5 nm is the range of pore size suitable for the carbon deposition process. In addition, the process to produce more pores of the mentioned size range in a biochar must be controlled by using slow heating rate and low processing temperature.

Figure 4 presents the types of diffusion in porous materials, and these include molecular diffusion, Knudsen diffusion, and a mixture of both diffusion types [6]. In relation to the study of the CVI process within biochar, Knudsen diffusion was the most favorable diffusion type to ensure that the maximum amount of carbon could be deposited within the pore network in the biochar particles. The vapor diffused through the macropores to reach the mesopores where the decomposition took place, to finally fill up the pores with carbon deposit. Figure 5 presents the mechanism of Knudsen diffusion in relation with this tar carbonization process by the CVI method.

The chemical reaction of tar decomposition to produce carbon deposit is as described below:

$$\begin{aligned}\mathrm{Tar}\left(\mathrm{C}_n\mathrm{H}_m\right) + \mathrm{CO}_2 + \mathrm{H}_2\mathrm{O} \rightarrow{}& \mathrm{C}_{n-1}\mathrm{H}_m + \mathrm{C} + \mathrm{H}_2 + \mathrm{CO} \\ &+ \mathrm{CH}_4 + \mathrm{C}_2\mathrm{H}_x \\ &+ \text{other hydrocarbons}\end{aligned} \quad (1)$$

Smaller pore sizes and low reaction temperatures were particularly important to ensure that a pure Knudsen diffusion occurred so that the pores were not clogged, as they would be if molecular diffusion also came into effect. Small pore size would enhance the colliding of the molecules with the walls which were the pore surface. In addition, low-temperature reaction is necessary so that the molecules move slowly, suppressing the possibility for them to collide with each other. In this study, tar vapor decomposed into solid carbon and gases when the molecules collided with the pore surface, leaving the solid carbon deposited properly on the pore surface, which consequently could result in the pores to be filled up with this additional carbon to the maximum amount possible. For larger pore sizes, molecular diffusion will take place where the tar will mostly be decomposed into gases instead of solid carbon. This type of diffusion might also cause clogging, which leads to very little or no proper deposition of solid carbon.

On the other hand, low reaction temperature for tar carbonization was also important to avoid unwanted reactions from taking place during the process that could lead to decrease of carbon content of the final product. Reactions that may take place during the tar carbonization process are methanation and Boudouard reactions. The reactions are as described below:

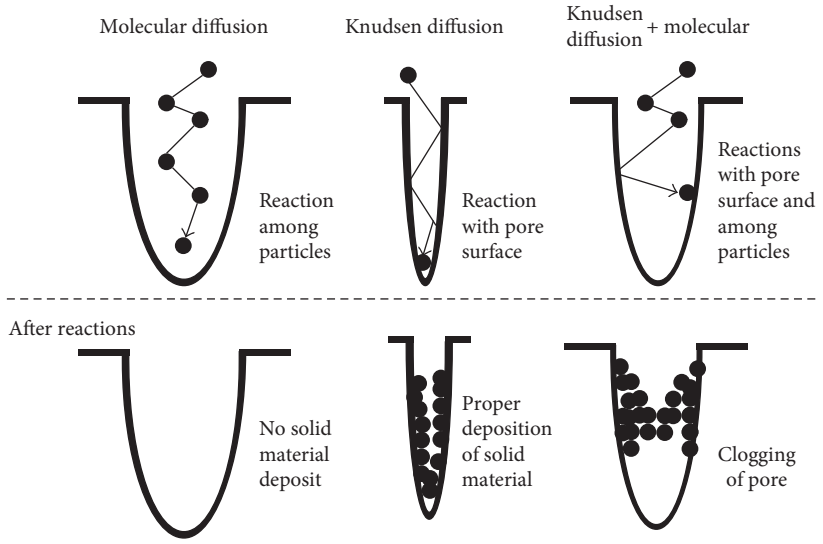

Figure 4: Types of diffusion in porous materials.

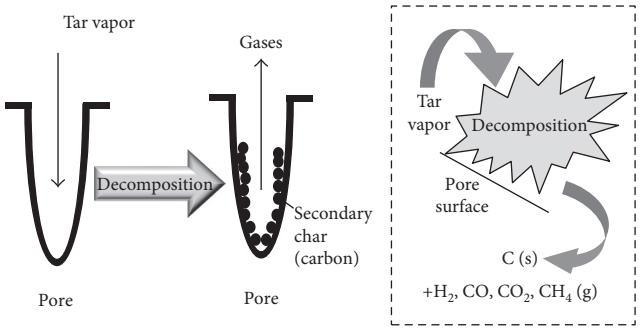

Figure 5: Mechanism of Knudsen diffusion to decompose tar vapor into carbon and gases by the CVI method.

$$\text{methanation}: \quad \begin{aligned} &CH_4 + H_2O \leftrightarrow CO + 3H_2 \\ &CO_2 + 4H_2 \leftrightarrow CH_4 + 2H_2O \\ &C + 2H_2 \leftrightarrow CH_4 \end{aligned} \tag{2}$$

$$\text{Boudouard}: \quad C + CO_2 \leftrightarrow 2CO \tag{3}$$

Standard methanation and Boudouard reactions occurred at around 700°C and 680°C, respectively. However, if the carbon is of amorphous type with high porosity, the temperatures required for these reactions to take place might be lower than those reported. In addition, for the Boudouard reaction, as the temperature increased further, production of CO would be more likely to occur which in turn could cause the carbon content of biochar to be consumed, reducing the total amount of solid carbon.

Figure 6 shows the Raman spectra of deposited carbon from the tar carbonization process by utilization of EFB and those of metallurgical coke breeze for comparison. The Raman spectra were characterized by two strong main peaks: D (Defect of Disorder) peak and G (Graphitic) peak. In relation to ideal graphitic lattice, D peak and G peak appeared at around 1350 cm^{-1} and 1580 cm^{-1}, respectively [7].

There are few methods to evaluate the disordered structure of a material based on Raman spectra, and these include peak intensity ratio, G peak position, and peak area ratio [8, 9]. Using the D and G peak intensities, I_D and I_G, respectively, cluster diameter of the structure can be estimated using the ratio of I_D to I_G (I_D/I_G). In addition, the sp^3 fraction of an amorphous carbon can be calculated by using the G peak position, ω_G [10].

Figure 6 also depicts the Raman spectra with the respective sp^3 fraction of metallurgical coke breeze, biochar, and deposited carbon. As the G peak shifted slightly towards the right, the extent of graphitization increased. Metallurgical coke breeze was found to be having a higher degree of graphitization, indicating a more ordered carbon structure as compared to the EFB-derived products. As compared to biochar produced by the slow pyrolysis process, the deposited carbon which was originated from tar produced by fast pyrolysis showed a slight shift towards the right in the G peak position. At higher temperatures, the sp^3 content was smaller because of increase in graphitization, which also resulted in a more ordered carbon structure and the existence of large carbon crystallites [11].

The results for cluster diameter and sp^3 content of the metallurgical coke breeze, EFB biochar, and deposited carbon are plotted in Figure 7. The cluster diameter for coke breeze was the smallest (2.40 nm) followed by EFB biochar (3.28 nm) and deposited carbon (3.90 nm). On the other hand, biochar had the highest sp^3 content, followed by deposited carbon and coke breeze. A material with high sp^3 content is a highly disordered material having a dispersive structure. Therefore, the results suggested that a biochar produced by the slow pyrolysis process is the most disordered material as compared to coke breeze and the deposited carbon, a fast pyrolysis product. This is the reason it was selected as the medium for tar decomposition reaction to take place. In the view of cluster diameter, the deposited carbon recorded the biggest cluster diameter that had been opened up, and this is due to the high processing

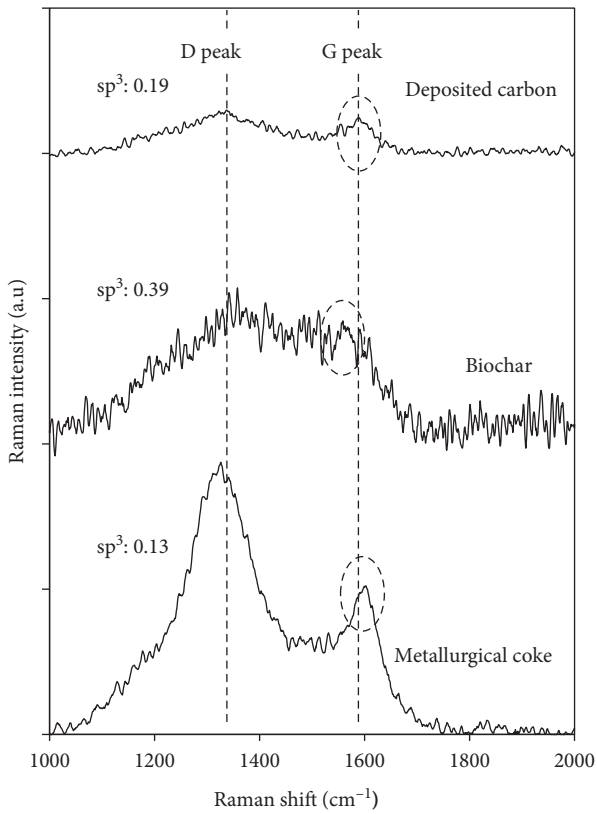

Figure 6: Raman spectra of deposited carbon, biochar substrate, and commercial metallurgical coke breeze, indicating the D and G peaks.

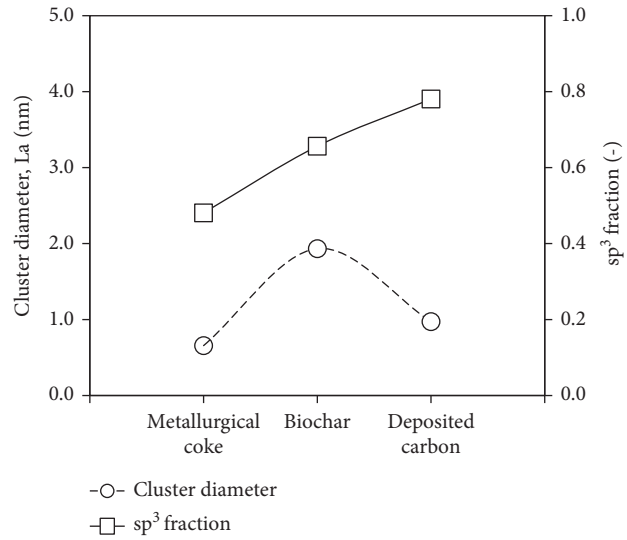

Figure 7: Estimation of cluster diameter and sp^3 fraction of metallurgical coke breeze, biochar substrate, and the deposited carbon after the tar decomposition process.

temperature and a rapid heating rate than those required to produce biochar.

3.1. Application of Carbon-Infiltrated Biochar in Sintering Plant. A sintering plant functions at high temperatures to agglomerate small particles of iron ore together with coke breeze and other fine materials to prepare suitable feedstock for the blast furnace. In a sintering plant operation, coke breeze is the main energy source that undergoes combustion through an oxidation process. This process consumes high energy and produces a large amount of CO_2 because of the coke breeze and coke oven gas (COG) combustion. It is crucial to efficiently control the amount of fuel consumption in a sintering plant because it plays a key role in production costs [12].

On the other hand, the effects of biochar utilization as a substitute to coke breeze in a sintering plant on the sinter productivity and quality were reported that an increase of biochar amount in the sintering plant is able to increase the fuel combustion rate. In addition to that, the extent of reduction was also increased in biochar sinter due to its porous structure. However, an approximate 20–25% replacement of coke breeze with an agricultural residue-derived biochar was found suitable to obtain optimum sinter productivity and sinter quality [13].

Table 1 presents the comparison of EFB-derived biochar and carbon-infiltrated biochar with the commercial coke breeze used in a sintering process. The values for EFB biochar and carbon-infiltrated biochar were obtained from experimental data [3], whereas the values for coke breeze were obtained from commercial coke and/or coke breeze data. Having a similar range of particle sizes, carbon content of biochar increased from 63.7 to 69.8 mass% after the developed integrated pyrolysis-tar decomposition process, which was approaching the minimum carbon content of a commercial coke breeze, 75 mass%. Interestingly, the carbon content of the final carbon-infiltrated biochar product was believed able to be increased further by increasing the amount of tar source [14]. Nevertheless, in this work, the limitation was with the equipment, where the amount of tar source had to be restricted. The calorific value (dry basis, d.b.) of the carbon-infiltrated biochar was also found to be approaching that of a commercial coke breeze. From the values shown Table 1, it can be seen that this developed process to produce carbon-infiltrated biochar managed to help increase and upgrade the value of an EFB-derived biochar to be used as a solid biofuel, with more efficient exergetic performance as compared to conventional biochar production from EFB.

Therefore, utilization of carbon-infiltrated EFB biochar in a sintering plant is deemed to be a promising alternative to coke breeze in the ironmaking industry. Moreover, the gases produced after the tar decomposition process could be used as an energy source as well to become a partial substitute to COG. Figures 8(a) and 8(b) illustrate the schematic diagram of conventional and proposed systems where the proposed system consequently could help to reduce the consumption of coke breeze in a conventional sintering machine. Instead of coke breeze being the only fuel in the sintering plant, carbon-infiltrated biochar is proposed to be used as a partial substitute in order to reduce the consumption of the fossil fuel. Carbon-infiltrated biochar will be able to be produced by using EFB via the integrated pyrolysis-tar decomposition process in the CVI reactor. The utilization of this EFB-derived carbon-infiltrated

Table 1: Comparison of EFB-derived biochar and carbon-infiltrated biochar with the commercial coke breeze.

Material	EFB biochar**	C-infiltrated biochar**	Coke breeze
Particle size (mm)	1.0–3.0	1.0–3.0	0.0–3.0
Carbon content (%mass)	62.9–64.4	68.7–70.5	75.0–85.0
Calorific value (d.b.*) (MJ/kg)	22.9–24.3	25.3–27.2	27.9–30.2

*d.b. = dry basis; **data collected from the previous study [3].

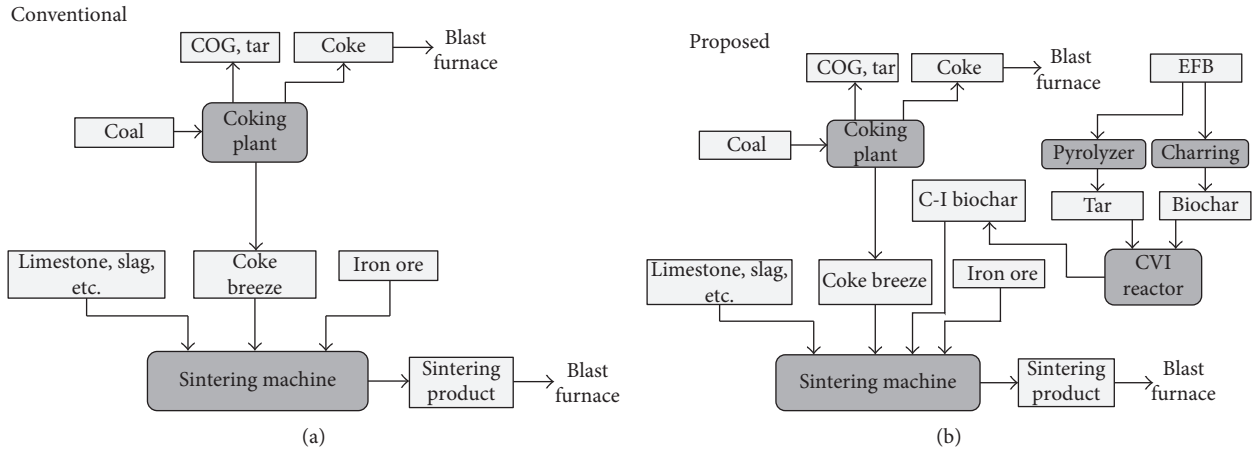

Figure 8: (a) Schematic diagram of conventional system in the sintering machine. (b) Schematic diagram of proposed system for utilization of carbon-infiltrated biochar as a partial substitute to coke breeze in the sintering machine.

biochar could also reduce the emission of CO_2 into the environment.

4. Conclusion

The mechanism of diffusion was investigated. In this study, for low temperature of biochar production, 400°C was selected in order to produce biochar having a small average pore size suitable for Knudsen diffusion to take place. For the tar carbonization process, a low reaction temperature of 400°C was selected so that the molecules of tar vapor were less active, to ensure pure Knudsen diffusion to occur, maximizing the amount of carbon able to be deposited within the porous network of biochar. From the pore size distribution plots, the most pores being filled up were the pores in a size range of 2.0–2.5 nm.

The sp^3 fractions of the EFB-derived products were calculated in comparison with those of commercial metallurgical coke breeze. The biochar substrate and deposited carbon were categorized as amorphous carbon having 38.67% and 19.45% of sp^3 content, respectively. As the sp^3 contents are higher, the materials become highly reactive due to their dispersive structure. This reactivity characteristic is also important for the product to be used as an energy source in a sintering machine besides its carbon content and calorific value. Metallurgical coke breeze recorded 13% of sp^3 content, which indicated that the produced carbon-infiltrated biochar is more reactive than the commercial coke breeze.

Conflicts of Interest

The authors declare that they have no conflicts of interest.

Acknowledgments

This research is partially supported by International Islamic University Malaysia through IIUM Research Initiative Grant Scheme (RIGS 16-353-0517).

References

[1] Agensi Inovasi Malaysia, *National Biomass Strategy 2020: New Wealth Creation for Malaysia's Palm Oil Industry*, Agensi Inovasi Malaysia, Cyberjaya, Malaysia, 2011, http://biomass-sp.net/wp-content/uploads/2012/11/5-Bas-Melssen.pdf.

[2] M. Gavrilescu, "Biomass power for energy and sustainable development," *Environmental Engineering and Management Journal*, vol. 7, no. 5, pp. 617–640, 2008.

[3] A. N. Rozhan, R. B. Cahyono, N. Yasuda, T. Nomura, S. Hosokai, and T. Akiyama, "Carbon deposition of biotar from pine sawdust by chemical vapor infiltration on steelmaking slag as a supplementary fuel in steelworks," *Energy & Fuels*, vol. 26, no. 6, pp. 3196–3200, 2012.

[4] S. H. Kong, S. K. Loh, R. T. Bachmann, S. A. Rahim, and J. Salimon, "Biochar from oil palm biomass: a review of its potential and challenges," *Renewable and Sustainable Energy Reviews*, vol. 39, pp. 729–739, 2014.

[5] C. Li and K. Suzuki, "Tar property, analysis, reforming mechanism and model for biomass gasification—An overview," *Renewable and Sustainable Energy Reviews*, vol. 13, no. 3, pp. 594–604, 2009.

[6] J. Welty, C. E. Wicks, G. L. Rorrer, and R. E. Wilson, *Fundamentals of Momentum, Heat and Mass Transfer*, John Wiley & Sons Inc., Hoboken, NJ, USA, 2007.

[7] Y. Kameya and K. Hanamura, "Kinetic and raman spectroscopic study on catalytic characteristics of carbon blacks in

methane decomposition," *Chemical Engineering Journal*, vol. 173, pp. 627–635, 2011.

[8] M. A. Capano, N. T. McDevitt, R. K. Singh, and F. Qian, "Characterization of amorphous carbon thin films," *Journal of Vacuum Science and Technology A: Vacuum, Surfaces, and Films*, vol. 14, pp. 431–435, 1996.

[9] M. Kawakami, T. Karato, T. Takenaka, and S. Yokoyama, "Structure analysis of coke, wood charcoal and bamboo charcoal by raman spectroscopy and their reaction rate with CO_2," *ISIJ International*, vol. 45, pp. 1027–1034, 2005.

[10] S. Zeb, M. Sadiq, A. Qayyum, G. Murtaza, and M. Zakaullah, "Deposition of diamond-like carbon film using dense plasma focus," *Materials Chemistry and Physics*, vol. 103, pp. 235–240, 2007.

[11] X. Zhu and C. Sheng, "Influences of carbon structure on the reactivities of lignite char reacting with CO_2 and NO," *Fuel Processing Technology*, vol. 91, pp. 837–842, 2010.

[12] T. Kronberger, M. Schaler, and C. Schönegger, "Latest generation sinter process optimization systems," in *Sintering-Methods and Products*, V. Shatokha, Ed., InTech, Shanghai, China, 2012.

[13] E. A. Mousa, A. Babich, and D. Senk, "Iron ore sintering process with biomass utilization," in *Proceedings of the METEC and 2nd European Steel Technology and Application Days Conference (METEC and 2nd ESTAD)*, pp. 1–13, Düsseldorf, Germany, 2015.

[14] A. N. Rozhan, M. H. Ani, H. M. Salleh, T. Akiyama, and H. Purwanto, "Development of carbon-infiltrated bio-char from oil palm empty fruit bunch," *ISIJ International*, vol. 55, no. 2, pp. 436–440, 2015.

Hindawi
Advances in Materials Science and Engineering
Volume 2018, Article ID 3807609, 14 pages
https://doi.org/10.1155/2018/3807609

Research Article

Evaluation of Carbonisation Gas from Coal and Woody Biomass and Reduction Rate of Carbon Composite Pellets

Tateo Usui,[1] **Hirokazu Konishi**,[2] **Kazuhira Ichikawa**,[3] **Hideki Ono**,[2] **Hirotoshi Kawabata**,[2] **Francisco B. Pena**,[4,5] **Matheus H. Souza**,[6] **Alexandre A. Xavier**,[7] **and Paulo S. Assis**[8]

[1]*Osaka University, 2-1 Yamadaoka, Suita, Osaka 565-0871, Japan*
[2]*Graduate School of Engineering, Osaka University, 2-1 Yamadaoka, Suita, Osaka 565-0871, Japan*
[3]*Osaka University, JFE Steel Corporation, 1 Kawasaki-cho, Chuo-ku, Chiba 260-0835, Japan*
[4]*School of Mines, Federal University of Ouro Preto (UFOP), 35400-000 Ouro Preto, MG, Brazil*
[5]*Vanzolini Foundation, University of São Paulo, Avenida Paulista, 967-3° Floor, 01311-100 São Paulo, SP, Brazil*
[6]*School of Mines, UFOP, Campus Morro do Cruzeiro, 35400-000 Ouro Preto, MG, Brazil*
[7]*School of Mines, UFOP, 522 Igaporã, 46490-000, BA, Brazil*
[8]*Materials and Metallurgy, UFOP/REDEMAT, Praça Tiradentes 20, 35400-000 Ouro Preto, MG, Brazil*

Correspondence should be addressed to Tateo Usui; usui@mat.eng.osaka-u.ac.jp

Received 26 June 2017; Accepted 28 September 2017; Published 11 March 2018

Academic Editor: Liming Lu

Carbon composite iron oxide pellets using semichar or semicharcoal were proposed from the measured results of the carbonisation gas release behaviour. The carbonisation was done under a rising temperature condition until arriving at a maximum carbonisation temperature $T_{c,\max}$ to release some volatile matter (VM). The starting point of reduction of carbon composite pellets using semicharcoal produced at $T_{c,\max} = 823$ K under the rising temperature condition was observed at the reduction temperature $T_R = 833$ K, only a little higher than $T_{c,\max}$, which was the aimed phenomenon for semicharcoal composite pellets. As $T_{c,\max}$ increases, the emitted carbonisation gas volume increases, the residual VM decreases, and, as a whole, the total heat value of the carbonisation gas tends to increase monotonically. The effect of the particle size of the semicharcoal on the reduction rate was studied. When T_R is higher than $T_{c,\max}$, the reduction rate increases, as the particle size decreases. When T_R is equal to $T_{c,\max}$, there is no effect. With decreasing $T_{c,\max}$, the activation energy E_a of semicharcoal decreases. The maximum carbonisation temperature $T_{c,\max}$ may be optimised for reactivity ($1/E_a$) of semicharcoal and the total carbonisation gas volume or the heat value.

1. Introduction

The exhaustion of natural resources (quantity and quality) and CO_2 emission controls are becoming increasingly important in steel industry. A lot of steel engineers studied various means to decrease reducing agents at blast furnace for reduction of CO_2 emissions [1]. For example, injection of waste plastics [2] and carbon-neutral materials such as biomass into the blast furnace is a better alternative [3, 4]. Especially, biomass has novel advantages, namely, no CO_2 emissions because of carbon neutral. Production of carbon composite iron ore agglomerates having good reducibility and strength is becoming one of the most important subjects [5].

In previous work, effective use of coal especially the carbonisation gas was discussed in prereduction of iron oxide pellets for total smelting reduction process [6–8]. From these carbonisation data, it was proposed that novel carbon composite iron oxide pellets using semichar or semicharcoal and the residual volatile matter (VM) in char or charcoal could be used effectively. On this basis, data analyses of the carbonisation gases from coal and woody biomass have also been carried out to evaluate their chemical and thermal possibility.

2. Background for the Present Work

Prereduction experiments of iron oxide pellets for the total smelting reduction process were carried out with coal

Table 1: Analyses of the samples used.

	mass%							
Sample	FC	VM	Ash	S	C	H	O	N
Newlands coal	58.9	25.9	15.2	0.50	71.5	5.24	6.15	1.40
Newcastle blend coal	58.7	32.8	8.5	0.54	74.8	4.90	9.27	1.97
Muswellbrook coal	55.2	36.5	8.3	0.70	76.0	4.93	8.51	1.57
Japanese cedar	12.05	87.38	0.57	0.01	52.52	6.76	40.4	0.03
Japanese cypress	8.12	90.8	1.08	0.014	50.7	6.16	41.1	1.01

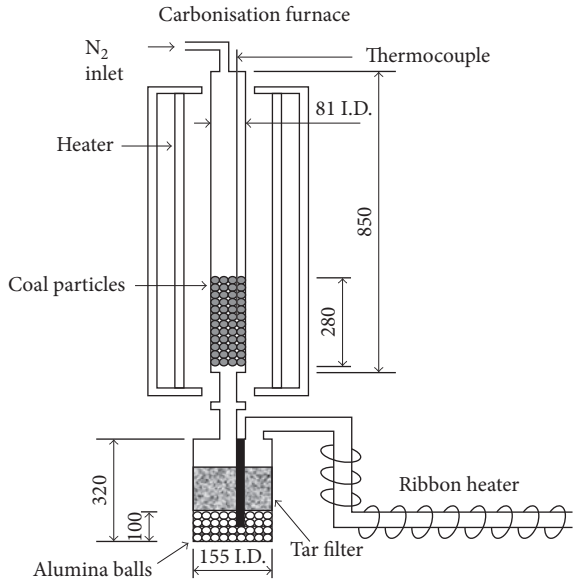

Figure 1: Schematic view of experimental apparatus for carbonisation of coal (or wood chips) (dimensions in mm).

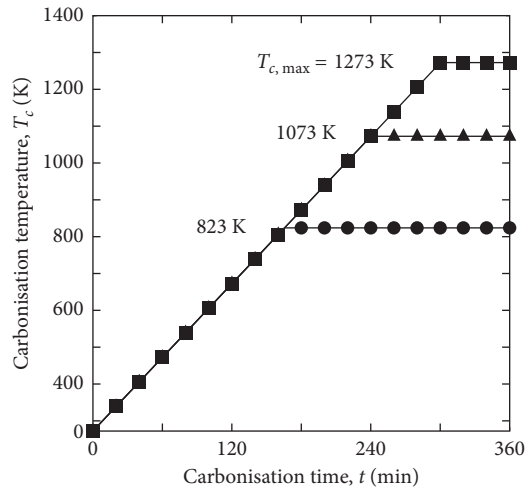

Figure 2: Typical heating patterns of coal carbonisation from room temperature to maximum carbonisation temperature $T_{c,\max} = 823$, 1073, and 1273 K at a heating rate of 200 K/h and maintained at $T_{c,\max}$ until total carbonisation time reached 360 min.

carbonisation gas [6–8]. In other words, coal carbonisation gases from various coals under different heating patterns were evaluated through the degree of prereduction at various reduction temperatures.

In the first step, three sorts of bituminous coal were carbonised under various rising temperature conditions (Table 1, Figures 1 and 2). In Table 1, samples (including two sorts of wood) are arranged in order of increasing volatile matter (VM). In Figure 1, schematic diagram of the experimental apparatus for carbonisation of the coal (or wood chips) is shown. Constant flow rate of N_2 was added to determine the flow rates of carbonisation gas components as follows [7]: the volume ratios of carbonisation gas components and N_2 were measured by a gas chromatograph, and then, the comparison of each gas component to N_2 yielded the absolute flow rate of each gas component [7]. Subsequently, the carbonisation gas mixed with N_2 gas flowed out from the exit of the reactor and was filtered and cooled to remove the tar and the water, respectively. After that, the gas without tar and water was analysed by gas chromatography (Figure 3). In Figure 2, typical heat patterns of carbonisation at a heating rate $r_h = 200$ K/h are shown. After arriving at the maximum carbonisation temperature $T_{c,\max}$, the carbonisation temperature T_c was maintained at $T_{c,\max}$ until total carbonisation time reached 360 min.

Variation of each gas component with time was measured by gas chromatography (Figure 4). The reason to express the sum $(C_2H_4 + C_2H_6 + C_3H_8)$ for higher hydrocarbons is as follows: the present gas chromatograph could not divide the peaks of C_2H_4 and C_2H_6 and, moreover, the flow rates of C_2H_4, C_2H_6, and C_3H_8 were very small in comparison with the other gas components. In general, there was experimental error among each data set.

Figure 4 shows the total flow rate V_{Total} (above) and mole fraction (below) of the carbonisation gas for Muswellbrook coal as a function of carbonisation time t. At $t = 240$ min, the carbonisation temperature arrived at $T_{c,\max} = 1073$ K and was maintained at $T_{c,\max}$ until 360 min had elapsed. After 240 min, the total flow rate decreased gradually. Around the carbonisation time of 0–120 min and 300–360 min, the total flow rate was relatively low; in these cases, the accuracy of the mole fraction would not be high. However, the overall picture of the gas composition can be seen easily. Hydrogen evolved at rather higher temperatures. Methane evolved from relatively lower carbonisation temperatures and continued across the temperature range. Higher hydrocarbons emitted within a lower temperature range. Both CO and CO_2 evolved at

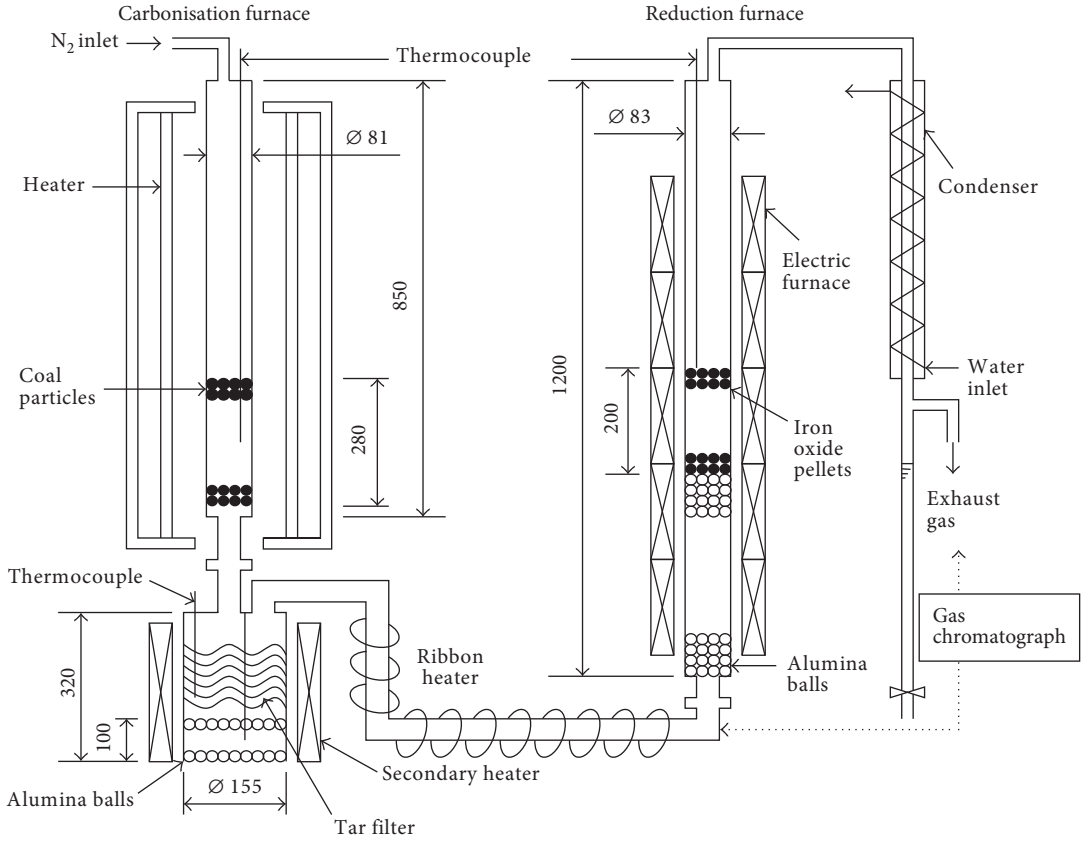

Figure 3: Schematic of the experimental apparatus for prereduction of iron oxide pellets by coal carbonisation gas (dimensions in mm).

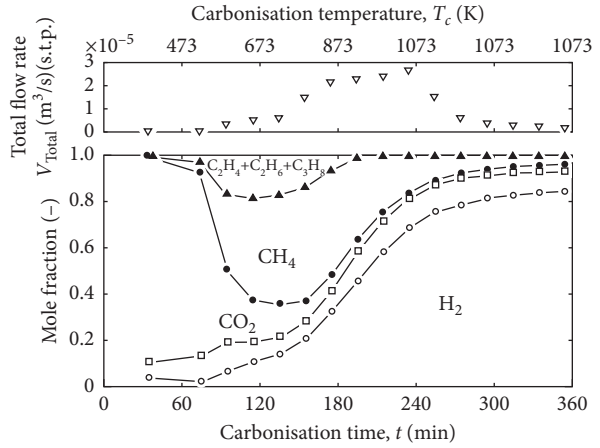

Figure 4: Mole fraction of carbonisation gas as a function of carbonisation time t [6]. Carbonisation conditions: Muswellbrook coal: 1 kg, carrier gas: N_2 1.0 L/min (s.t.p.), maximum carbonisation temperature ($T_{c,max}$): 1073 K, and heating rate (r_h): 200 K/h; heating pattern is shown in Figure 2.

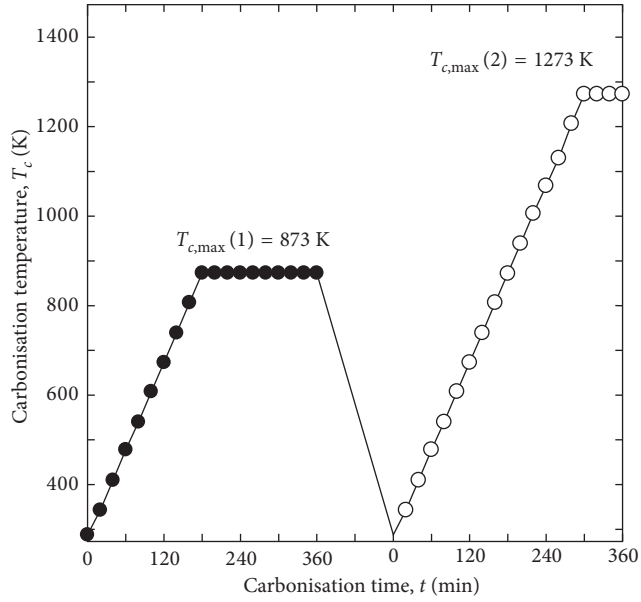

Figure 5: Two-step heat pattern of carbonisation (heating rate $r_h = 200$ K/h).

rather constant rates all over the carbonisation time. This fact introduced the concept of the use of semichar in a carbon composite pellet and will be discussed later (Figures 5 and 6).

In the second step, carbonisation gas was used to prereduce iron oxide pellets (Figures 3 and 7) for the iron bath smelting reduction process. The resultant char was evaluated as a reducing agent and a heat source for iron bath by simulation (calculation only); optimum amount of coal in the total iron bath smelting reduction process including the proposed prereduction stage was estimated and compared with the amount of coking coal required

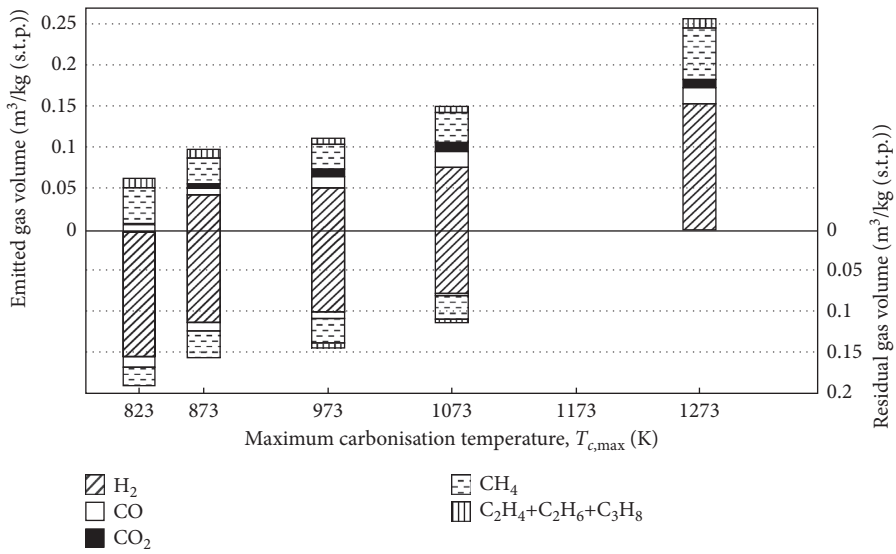

Figure 6: Emitted carbonisation gas volume and residual gas volume as a function of $T_{c,max}$ (Newcastle blend coal, $r_h = 200$ K/h).

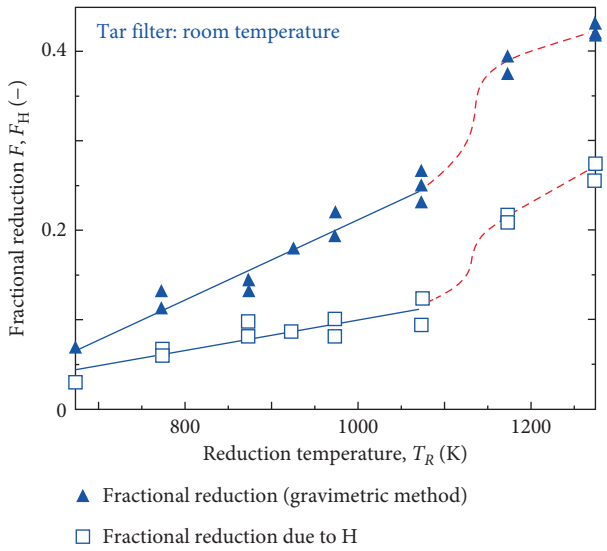

Figure 7: Variations of final fractional reductions F and F_H with reduction temperature T_R [7]. Experimental conditions: carbonisation of Muswellbrook coal (1 kg), $T_{c,max} = 1273$ K, $r_h = 200$ K/h (Figure 2), carrier gas: N_2 1.0 L/min (s.t.p.), secondary heater: off (Figure 3), and reduction of Nibrasco pellets (2 kg).

for a conventional blast furnace route. The proposed route was shown to be marginally better than the conventional blast furnace route in terms of coal consumption rate [9].

Figure 3 shows schematic diagram of the experimental apparatus for the prereduction of iron oxide pellets by coal carbonisation gas. The carbonisation reactor is the same as shown in Figure 1. Fractional reduction was evaluated from the loss in weight of the packed pellets. Fractional reduction by H was also evaluated by the condensed water vapour. The secondary heater can be used for heating the tar to produce the secondary carbonisation gas.

Figure 7 shows the final fractional reduction calculated by the gravimetric method, F, and by the final fractional reduction due to H, F_H, as a function of reduction temperature T_R, where H originated in hydrogen gas and hydrocarbons and was measured as condensed water vapour from the exhaust gas after reduction. Both F and F_H tend to increase linearly between $T_R = 673$ K and 1073 K, and increase more than the extrapolated lines for $T_R > 1073$ K, which suggests the contribution of hydrocarbons to reduction reaction at higher reduction temperatures, maybe by the catalytic effect of reducing iron oxides or reduced iron. The ratio of F_H to F can be seen about 0.5, which means very large contribution of H from hydrogen gas and hydrocarbons. The ultimate analysis is shown in Table 1. In Table 1, the values are written in mass% and mass% H is not so large, but mol% is important in chemical reactions and 4.93 mass% is large enough from this viewpoint.

3. Experimental Procedure

Carbon composite iron oxide pellets using semichar [10–12] were proposed from the measured results of the coal carbonisation gas release behaviour shown in the above section. Newlands coal, Newcastle blend coal, and Muswellbrook coal were used as samples of coal. Japanese cedar and Japanese cypress were used as samples of woody biomass. The analyses of the samples demonstrate that the woody biomass has much more VM and O and much less FC, ash, and S than the coals (Table 1). The carbonisation was done under a rising temperature condition at the same heating rate until arriving at the maximum carbonisation temperature $T_{c,max}$ in order to release some VM (Figure 2). The experiment was carried out by placing chips of the sample in the carbonisation reactor (Figure 1). Partly because some of the experimental items are the same as in Section 2 and partly because the present work covers many experimental items, the present experimental details are written in Section 4.

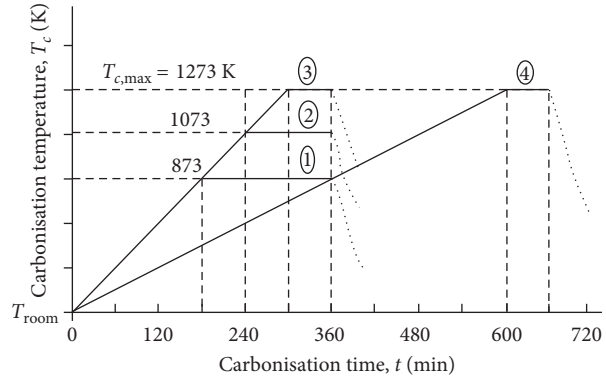

Figure 8: Heat patterns of carbonisation for Muswellbrook coal.

Table 2: Carbonisation gas from Muswellbrook coal.

	[m^3/kg (s.t.p.)]			
Case (Figure 8)	1	2	3	4
r_h (K/h)	200	200	200	100
$T_{c,\max}$ (K)	873	1073	1273	1273
H_2	0.0326	0.0936	0.1252	0.1327
CO	0.0086	0.0212	0.0242	0.0232
CO_2	0.0084	0.0102	0.0112	0.0092
CH_4	0.0387	0.0515	0.0484	0.0516
$C_2H_4 + C_2H_6 + C_3H_8$	0.0071	0.0071	0.0065	0.0066
Total	0.0955	0.1837	0.2155	0.2231

4. Results and Discussion

4.1. Heating Rate of Carbonisation. In the case of Muswellbrook coal, two heating rates (r_h), 100 and 200 K/h, were used as shown in Figure 8; only carbonisation condition 4 (Case 4) was the lower heating rate of 100 K/h, applied to the Muswellbrook coal. This was applied to examine the effect of heating rate. When Case 4 in Figure 8 was applied, a little more total carbonisation gas was released, as shown in Table 2. However, the difference between total carbonisation gases of Cases 3 and 4 was only 3.4%, and therefore, it is assumed that the sample obtained by Case 3 in Figure 8 released all the volatile matter. It is also assumed that the sample carbonised at $T_{c,\max} = 1273$ K under the heating rate of 200 K/h released all the volatile matter for every coal sample.

4.2. Carbon Composite Iron Oxide Pellets Using Semichar

4.2.1. Two-Step Carbonisation Behaviour. It was inferred from the carbonisation experiments under rising temperature conditions (Figure 4) that when the carbonisation was interrupted, the volatile matter release would also be interrupted, and that when the carbonisation under rising temperature conditions was started again, the release of the residual volatile matter would begin at the same interrupted carbonising temperature. This inference was demonstrated by the following two-step carbonisation. Figure 5 shows the schematic heat pattern for two steps: the first

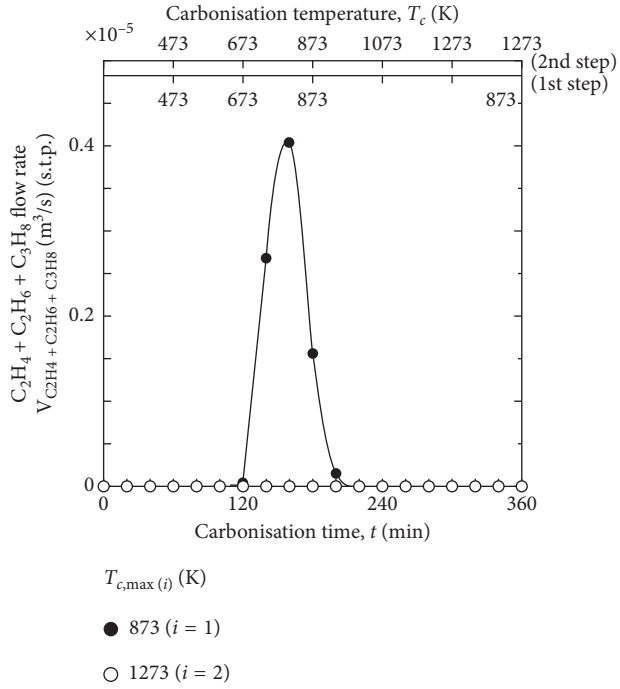

Figure 9: Variations of ($C_2H_4 + C_2H_6 + C_3H_8$) flow rate with carbonisation time in the two-step carbonisation [10].

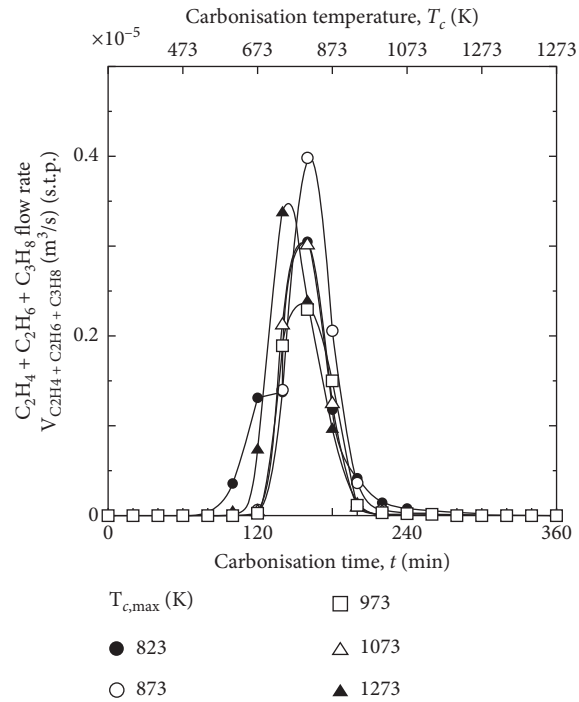

Figure 10: Variations of ($C_2H_4 + C_2H_6 + C_3H_8$) flow rate with carbonisation time in the one-step carbonisation [10].

carbonisation at $T_{c,\max}$ (1) = 873 K and the second one at $T_{c,\max}$ (2) = 1273 K.

Figures 9 through 13 in [10] show flow rates of the emitted gas components H_2, CO, CO_2, CH_4, and ($C_2H_4 + C_2H_6 + C_3H_8$) by two-step carbonisation of Newcastle blend coal at each

maximum carbonisation temperature $T_{c,\max}$ under the heating rate $r_h = 200$ K/h. After the first carbonisation at $T_{c,\max}$ (1) = 873 K, when the carbonisation was started again (the second carbonisation at $T_{c,\max}$ (2) = 1273 K), the release of the residual volatile matter began at almost the same interrupted carbonising temperature $T_c = 873$ K. In Figure 9, cited from Figure 13 of [10], the total flow rate of ($C_2H_4 + C_2H_6 + C_3H_8$) is negligibly small all over ($t = 0$–360 min) for the second carbonisation at $T_{c,\max}$ (2) = 1273 K, which can be easily understood from Figure 10, cited from Figure 7 of [10]; almost all the higher hydrocarbons ($C_2H_4 + C_2H_6 + C_3H_8$) are released at $T_c = 873$ K.

Moreover, from Figure 14 of [10], the total and individual carbonisation gas volumes for one-step ($T_{c,\max} = 1273$ K) and two-step ($T_{c,\max}$ (1) = 873 K and $T_{c,\max}$ (2) = 1273 K) carbonisation were almost the same.

From these findings, novel carbon composite pellets were proposed, in which the semichar including the residual volatile matter was used as the carbonaceous material. When fully carbonised char is used as the carbonaceous material, the reduction of carbon composite pellets initially occurs as a solid/solid reaction under rising temperature conditions as in a blast furnace.

Whereas, when semichar is used as the carbonaceous material, the reduction of carbon composite pellets starts earlier as a gas/solid reaction just after the reduction temperature T_R arrives at $T_{c,\max}$. In general, in the case of the semichar produced at lower maximum carbonisation temperature, $T_{c,\max}$, the carbon composite pellets started the reduction reaction at the reduction temperature only a little higher than $T_{c,\max}$ under a rising temperature condition (see Figure 11 for semicharcoal composite pellets). The starting temperature of reduction and the quantity of residual volatile matter (VM) can be changed simultaneously (but not independently) by controlling $T_{c,\max}$. Coal type could also be selected on the basis of VM content.

Therefore, the first benefit is the decrease in the starting temperature of reaction, and the second one is the improved rate of reduction reaction by the residual volatile matter. The decrease in the starting temperature of reduction reaction of iron ore in a blast furnace leads to the decrease in consumption of reducing agents and hence, a productivity improvement.

4.2.2. Reduction Behaviour of Carbon Composite Iron Oxide Pellets Using Semichar. Preparation of carbon composite iron oxide pellets was as follows:

Mass ratio semichar: $Fe_2O_3 = 1:4$.
Particle size: less than 63 μm.
Binder: bentonite (1 mass% added).
Pellet size: about 15 mm.
Drying at 378 K for 24 h to remove water.

Reagent grade hematite (95 mass% Fe_2O_3, particle size: less than 44 μm) was used for iron oxide. The chemical analysis of the bentonite is shown in Table 3, from which almost no effect of the bentonite is expected upon the reduction reaction because Fe_2O_3 content is as low as 3 mass% and the addition of the bentonite is 1 mass%. The semichar used was produced from Newcastle blend coal (Table 1).

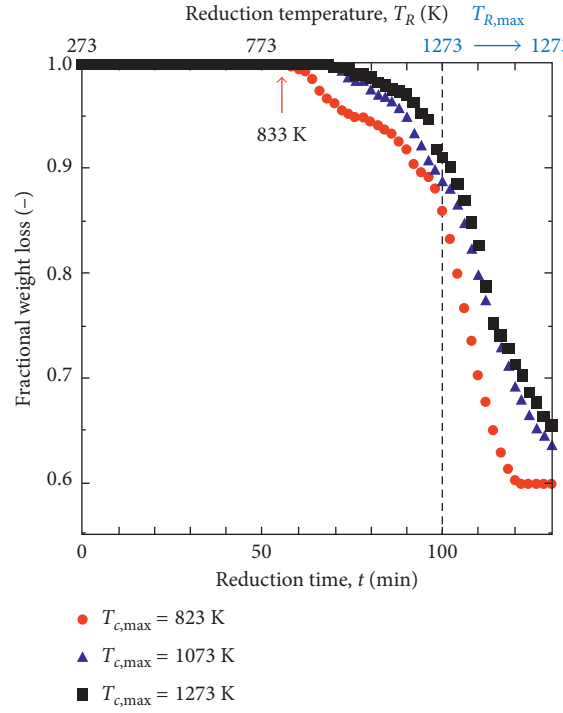

Figure 11: Weight loss curves in N_2 gas atmosphere for carbon composite pellets using semicharcoal produced at $T_{c,\max} = 823$, 1073, and 1273 K ($r_h = 200$ K/h) from Japanese cypress under the rising temperature condition at 10 K/min. Particle size range for the semicharcoal is 63–75 μm.

Table 3: Chemical analysis of the bentonite used.

mass%						
SiO_2	Al_2O_3	Fe_2O_3	CaO	MgO	K_2O	Na_2O
58.79	14.27	2.99	0.70	1.28	0.70	3.42

Table 4: Analyses of semichar carbonised from Newcastle blend coal at $T_{c,\max} = 823$, 1073, and 1273 K ($r_h = 200$ K/h).

	mass%							
$T_{c,\max}$ (K)	FC	VM	Ash	S	C	H	O	N
Initial	58.7	32.8	8.5	0.54	74.8	4.90	9.27	1.97
823	72.17	15.93	11.90	0.53	75.33	2.87	7.31	2.06
1073	82.70	4.43	12.87	0.42	81.52	1.54	1.91	1.74
1273	83.21	2.51	12.28	0.52	81.69	0.90	1.34	1.27

Newcastle blend coal was carbonised from room temperature to $T_{c,\max} = 823$, 873, 973, 1073, or 1273 K at a heating rate of 200 K/h under the same heating time of 360 min, as shown in Figure 2. The obtained semichar was mixed with reagent grade hematite along with bentonite as a binder in order to strengthen. The semichar composite pellet was prepared by hand rolling.

Emitted and residual carbonisation gas volumes as a function of $T_{c,\max}$ are shown in Figure 6. As $T_{c,\max}$ increases,

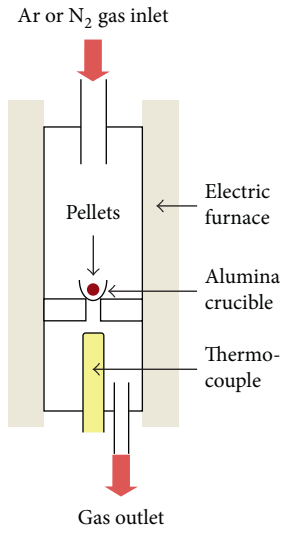

Figure 12: Experimental apparatus for reduction of carbon composite pellets.

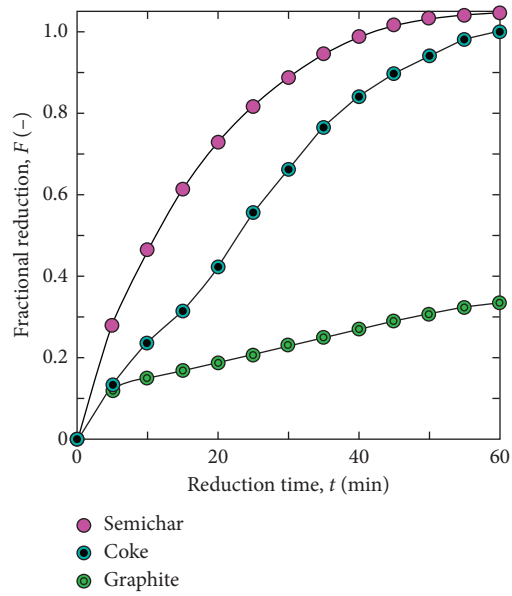

Figure 13: Comparison of reduction curves for carbon composite pellets using semichar, coke, and graphite (T_R = 1273 K).

emitted gas volumes of H_2 and CO increase and consequently residual gas volumes of H_2 and CO decrease. The residual gas volume was calculated under the assumption that all the carbonisation gas components were emitted at $T_{c,\max} = 1273$ K, as mentioned previously.

Table 4 shows the analyses of semichar carbonised from Newcastle blend coal at $T_{c,\max} = 823$, 1073, and 1273 K. As $T_{c,\max}$ increases, the residual volatile matter (VM) decreases clearly in Proximate analysis and H and O decrease gradually in Ultimate analysis, while FC in Proximate analysis and C in Ultimate analysis increase gradually.

Figure 12 shows schematic view of experimental apparatus for reduction of carbon composite iron oxide pellets in Ar or N_2 gas atmosphere. Constant flow rate of N_2 was added to determine the flow rates of exhaust gas components [7]; the generated gases of H_2, CO, CO_2, CH_4, ($C_2H_4 + C_2H_6 + C_3H_8$), and H_2O along with N_2 were analysed by the gas chromatography and the quadrupole mass spectrometry. Fractional reduction F (–) was calculated by

$$F = \frac{\left(M_{O \text{ in reaction gas}} - M_{O \text{ in volatile matter}}\right)}{R_O}, \quad (1)$$

where $M_{O \text{ in reaction gas}}$ is the total mole of oxygen in generated gases on iron oxide reduction (mol), $M_{O \text{ in volatile matter}}$ is the total mole of oxygen in the released gas on carbonisation of carbonaceous materials (mol), and R_O is the total mole of oxygen in case of reducing Fe_2O_3 as an iron oxide sample perfectly (mol) [13].

Figure 13 shows the comparison of reduction curves (fractional reduction F versus reduction time t) at reduction temperature $T_R = 1273$ K in N_2 gas atmosphere for carbon composite iron oxide pellets using semichar from Newcastle blend coal ($T_{c,\max} = 823$ K and $r_h = 200$ K/h), coke (VM = 0.6 mass%), and graphite (purity 98%). Particle size ranges for the semichar and coke are less than 63 μm and for the graphite less than 43 μm. The effect of the residual volatile matter in the semichar reductant can be easily seen with reduction occurring earlier and at a faster rate. The reduction rate of the graphite is much less than that of the coke, which can be explained by the degree of crystallization; the degree of crystallization of the graphite is higher than that of the coke (for another example, see Figure 14, which shows that the semichar has a crystalline structure but semicharcoal shows amorphous nature. In general, when the degree of crystallization is lower, the gasification rate is higher, and therefore, the reduction of carbon composite pellets using semicharcoal proceeds faster than that using semichar).

4.3. Carbon Composite Iron Oxide Pellets Using Semicharcoal. Semicharcoal [13–15] was also used to produce carbon composite pellets. The use of semicharcoal is aimed at not only because of carbon-neutral material but also because of high reactivity (reactivity = $1/E_a$, Table 5).

4.3.1. Carbonisation Gases from Woods in Comparison with Those from Coals. Figure 15 depicts total and individual components of carbonisation gases for Japanese cypress (200 g) as a function of the maximum carbonisation temperature $T_{c,\max}$, where the heating patterns are the same as in Figure 2. As $T_{c,\max}$ increases, H_2 emission increases significantly, but the other components are relatively stable across the temperature range. The ratios of CO and CO_2 are large, and those volumes are much the same with each other.

Table 6 shows the analyses of semicharcoal carbonised from Japanese cypress at $T_{c,\max} = 823$, 1073, and 1273 K with coke included for comparison. As $T_{c,\max}$ increases, the residual volatile matter (VM) decreases clearly in Proximate analysis and H and O also decrease clearly in Ultimate analysis, while FC and C increase gradually. The residual volatile matter value in the semicharcoal carbonised from Japanese cypress at $T_{c,\max} = 1273$ K is relatively large and

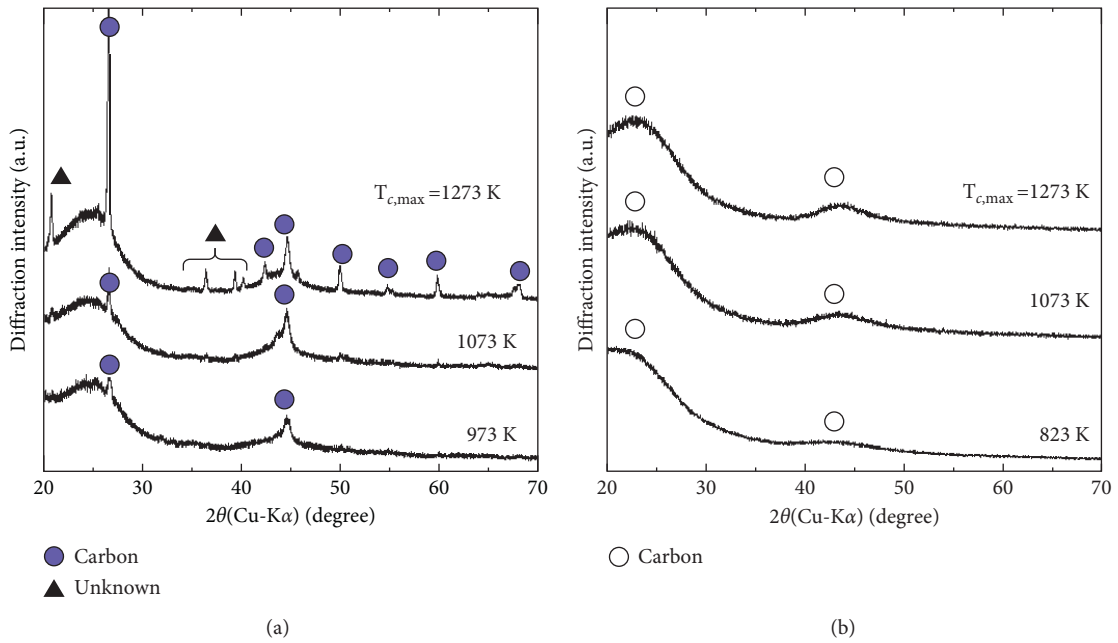

Figure 14: Comparison between the crystal structures of semichar (Newcastle blend coal) and semicharcoal (Japanese cypress) by XRD measurements. (a) Semichar. (b) Semicharcoal.

Table 5: Comparison of activation energies for various carbonaceous materials.

Carbonaceous material	Activation energy E_a (kJ/mol)
Graphite	217 [16]
Bintyo char	182 [16]
Bamboo char	181 [16]
Coke	200 [16]
Glassy carbon	211 [16]
Activated carbon	149 [16]
Semicharcoal at $T_{c,max} = 823$ K	138*
Semicharcoal at $T_{c,max} = 1073$ K	139*
Semicharcoal at $T_{c,max} = 1273$ K	162*
Semichar at $T_{c,max} = 1073$ K	174*
Coke	219*

*Present work (by gasification experiments), where the semicharcoal was obtained from Japanese cypress and semichar from Newcastle blend coal (Table 1), and the analyses of the coke are shown in Table 6.

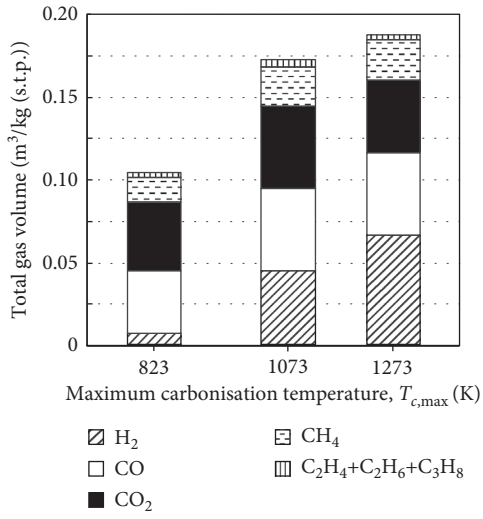

Figure 15: Total and individual components of carbonisation gases for Japanese cypress as a function of $T_{c,max}$ ($r_h = 200$ K/h).

much larger than the one in the semichar carbonised from Newcastle blend coal at $T_{c,max} = 1273$ K (Table 4).

Figure 16 shows surface views of Japanese cypress carbonised at $T_{c,max} = 823$ and 1273 K by using an optical microscope. Semicharcoal has many micropores with the size of about 10 μm.

Figure 17 illustrates comparisons of carbonisation gas volumes for all the analysed samples at $T_{c,max} = 1073$ and 1273 K and $r_h = 200$ K/h. From Figure 17, it can be seen that coal and wood release almost similar total quantities of carbonisation gas. The first important point is the clear difference between the kinds of carbonisation gas components released from coals and woods. The second important point is large quantities of H_2 and CH_4 released from the samples of coal. This can be explained by the structure of the coal, which is composed of mainly carbon and hydrogen. The third important point is that wood releases great amount of CO and CO_2 because of the large quantity of oxygen in its structure (Table 1). From Figure 6, it can be seen that the carbonisation gas will stay more within coal (or wood) especially in the residual VM, as the maximum carbonisation temperature decreases. Naturally, the total volume of carbonisation gas released at $T_{c,max} = 1273$ K is always higher than the one at $T_{c,max} = 1073$ K for all the samples used, which leads to results of the total amount of heat discussed later (Figure 18).

Table 6: Analyses of semicharcoal carbonised from Japanese cypress at $T_{c,\max} = 823$, 1073, and 1273 K ($r_h = 200$ K/h) in comparison with coke.

		mass%							
	$T_{c,\max}$ (K)	FC	VM	Ash	S	C	H	O	N
Japanese cypress	—	8.12	90.8	1.08	0.014	50.7	6.16	41.1	1.01
Semicharcoal	823	80.60	18.65	0.76	0.01	85.8	2.93	9.89	0.60
	1073	89.35	9.64	1.01	0.03	91.2	1.33	5.89	0.55
	1273	91.80	7.00	1.16	0.04	92.6	0.56	4.81	0.82
Coke	—	87.1	0.97	11.97	0.60	84.6	0.26	1.35	1.22

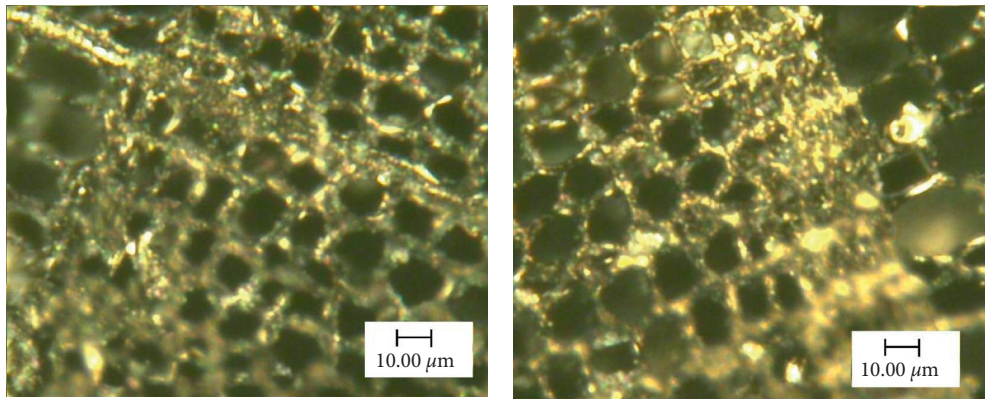

(a) (b)

Figure 16: Surface views of Japanese cypress carbonised at $T_{c,\max} = 823$ and 1273 K ($r_h = 200$ K/h); photos were taken by an optical microscope. (a) $T_{c,\max} = 823$ K. (b) $T_{c,\max} = 1273$ K.

Figure 19 summarizes total carbonisation gas volumes as a function of $T_{c,\max}$. On the whole, total carbonisation gas volumes for all the samples used increase monotonically with $T_{c,\max}$.

4.3.2. Starting Point of Reduction of Semicharcoal Composite Pellet under Rising Temperature. Figure 20 shows schematic view of experimental apparatus for measuring weight loss of a sample by a gravimetric method; in the upper box, a strain gauge-type transducer was equipped to measure the weight loss of the sample. The balance was used to counter the initial weight to be zero. Inside of the box was cooled by an N_2 flow to keep the transducer at a constant temperature.

Figure 11 shows weight loss curves in N_2 gas atmosphere for carbon composite iron oxide pellets using semicharcoal produced at $T_{c,\max} = 823$, 1073, and 1273 K from Japanese cypress under the rising temperature condition at 10 K/min (reduction temperature T_R from room temperature till the maximum temperature $T_{R,\max} = 1273$ K). At $T_{c,\max} = 823$ K, the weight loss started at $T_R = 833$ K, which is only slightly higher than $T_{c,\max}$.

4.3.3. Effect of Particle Size of Semicharcoal upon the Reduction Rate. In order to clarify the effect of particle size of semicharcoal upon the reduction rate of the composite pellets, variations of reduction curves at the reduction temperature $T_R = 1073$ and 1273 K in N_2 gas atmosphere for carbon composite iron oxide pellets using semicharcoal produced at $T_{c,\max} = 1073$ K from Japanese cypress with the particle size are depicted in Figure 21.

In this experiment, the apparatus used is the same as shown in Figure 12 and fractional reduction F was calculated by (1).

By using sieves, the particle size ranges were divided into the following three: 23–35, 63–75, and 105–150 μm. In the case of Figure 21(a) at $T_R = 1073$ K, the particle size dependence cannot be distinguished. In this case, the residual VM is unable to be released because $T_R = T_{c,\max}$. On the other hand, in the case of Figure 21(b) at $T_R = 1273$ K, the residual VM is able to be released because $T_R > T_{c,\max}$, and moreover, the effect of particle size is very clear; the reduction rate of the composite pellet increases, as the particle size decreases, as a consequence of the specific surface area increasing.

4.3.4. Comparison between Semichar and Semicharcoal. The rate enhancement effect of reduction for semicharcoal composite pellets is stronger than that for semichar composite pellets [15] because the gasification rate of semicharcoal is higher than that of semichar (Figures 22 and 23). This is caused by the following reasons: semicharcoal has an amorphous nature, while semichar has a more crystalline structure (Figure 14), and the activation energy of semicharcoal is lower than that of semichar (Table 5).

Figure 14 in [15] shows the comparison between the reduction curves of carbon composite pellets using

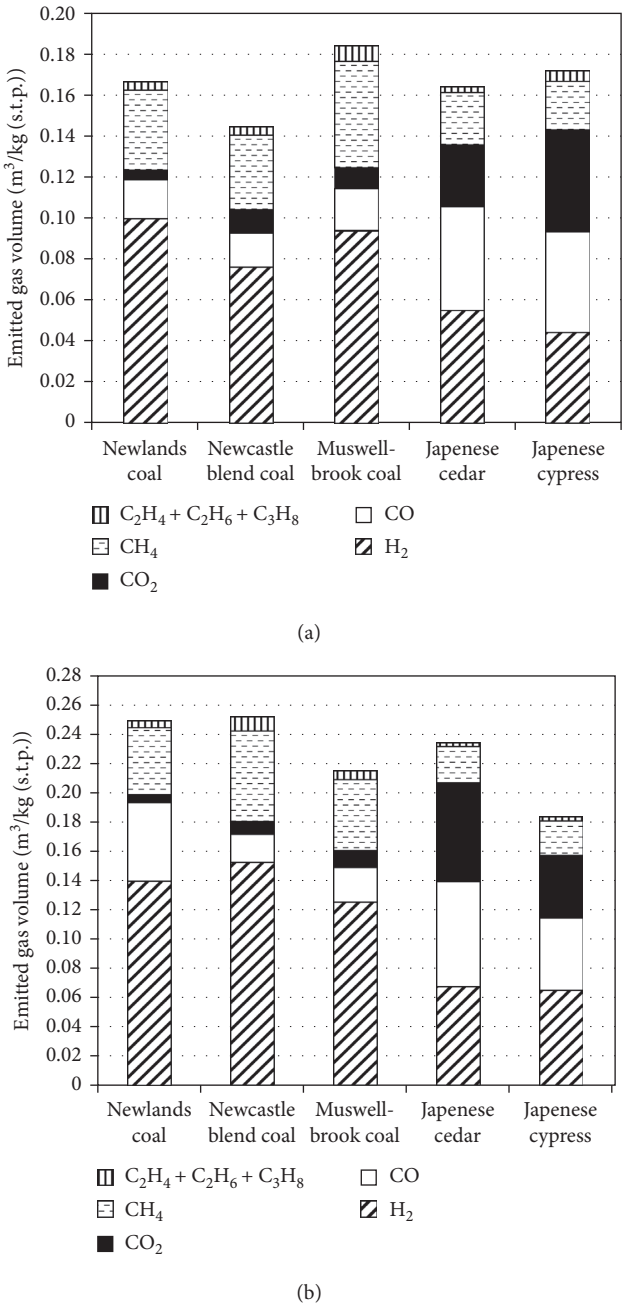

FIGURE 17: Carbonisation gas volumes at $T_{c,\max} = 1073$ and 1273 K and $r_h = 200$ K/h. (a) $T_{c,\max} = 1073$ K. (b). $T_{c,\max} = 1273$ K.

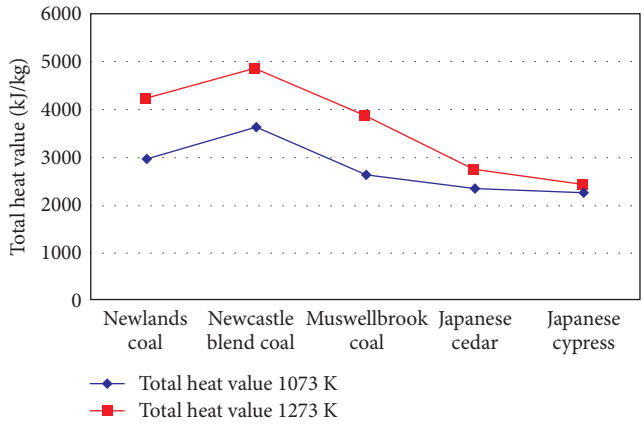

FIGURE 18: Total amount of heat (kJ/kg) of each sample at the maximum carbonisation temperature $T_{c,\max} = 1073$ and 1273 K ($r_h = 200$ K/h).

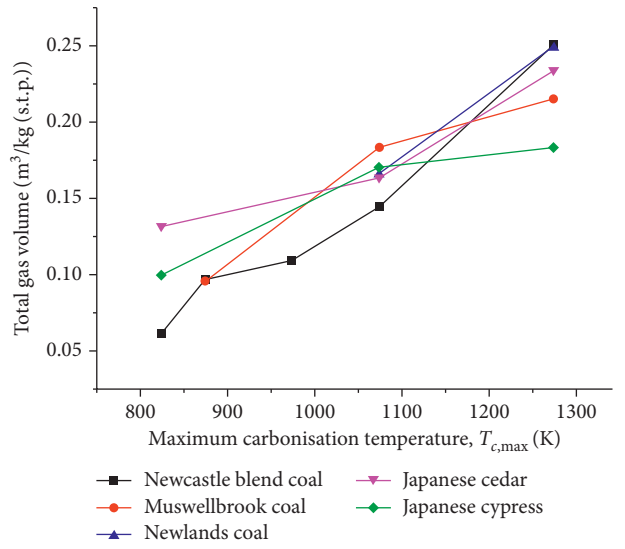

FIGURE 19: Total carbonisation gas volumes for all the samples used as a function of the maximum carbonisation temperature ($r_h = 200$ K/h).

semicharcoal (Japanese cypress) and semichar (Newcastle blend coal) carbonised at $T_{c,\max} = 823$, 1073, and 1273 K and $r_h = 200$ K/h at reduction temperature $T_R = 1273$ K in an N_2 gas atmosphere. The reduction of carbon composite pellets using semicharcoal (Japanese cypress) proceeded faster than that using semichar (Newcastle blend coal).

Figure 22 shows weight loss curves of semichar from Newcastle blend coal obtained by carbonisation at $T_{c,\max} = 823$, 1073, and 1173 K and a coke sample (Table 6) at a gasification temperature $T_G = 1273$ K in CO_2 gas atmosphere. The experimental apparatus for measuring the weight loss due to gasification of carbonaceous materials by a gravimetric method is the same as shown in Figure 20. Figure 23 shows weight loss curves of semicharcoal made from Japanese cypress obtained by carbonisation at $T_{c,\max} = 823$, 1073, and 1273 K and a coke sample at $T_G = 1273$ K in CO_2 gas atmosphere. From comparison of these figures, it can be concluded that the gasification rate of semicharcoal is higher than that of semichar.

In Figure 14, XRD measurements are shown; Semicharcoal has an amorphous nature, while semichar has a more crystalline structure. As shown in Figure 16, semicharcoal is very porous. From these facts, semicharcoal can be expected to be very reactive.

Figure 24 shows Arrhenius plots of the reaction rate of gasification for semichar and semicharcoal produced at $T_{c,\max} = 1073$ K as well as for coke, which are the

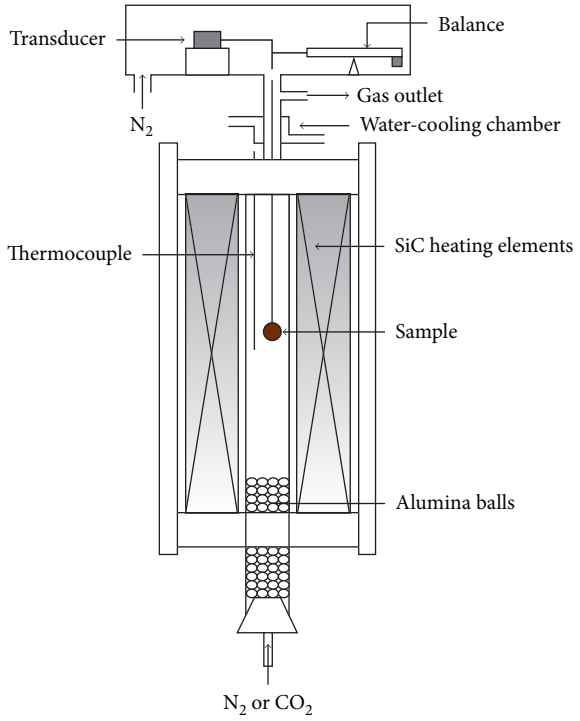

FIGURE 20: Experimental apparatus for measuring weight loss of a sample by the gravimetric method.

same as in Figures 22 and 23. The reaction rate r (1/s) is given by

$$r = \frac{dX}{dt}, \tag{2}$$

where t = reaction time (s) and $X = (W_0 - W_t)/W_0$, in which W_0 is the initial mass (g) and W_t is the mass at reaction time t (g). The gradient for semicharcoal is the smallest, and hence, its activation energy is the lowest. Table 5 shows comparison of activation energies for various carbonaceous materials from Kawakami et al. [16] and the data derived from this study. The most active one (the lowest activation energy) in this table is "semicharcoal at $T_{c,\max} = 823$ K." The activation energy for "semicharcoal at $T_{c,\max} = 1073$ K" is lower than that for "semichar at $T_{c,\max} = 1073$ K," which means that semicharcoal is more reactive than semichar.

4.4. Heat Value of Carbonisation Gas. In order to evaluate the thermal potential of the gas components, the amount of heat (kJ/kg) has been calculated as for Newcastle blend coal in Table 7. As $T_{c,\max}$ increases, the amounts of heat of H_2 and CO also increase. The amounts of heat of CH_4 within the temperature range of $T_{c,\max} = 823$ to 973 K are much the same within some experimental error, but those from $T_{c,\max} = 973$ to 1273 K increase monotonically. With regard to higher hydrocarbons, almost all these carbonisation gases (C_2H_4, C_2H_6, and C_3H_8) are evolved before the carbonisation temperature reaches at a little above 823 K, and therefore, the amounts of heat values for

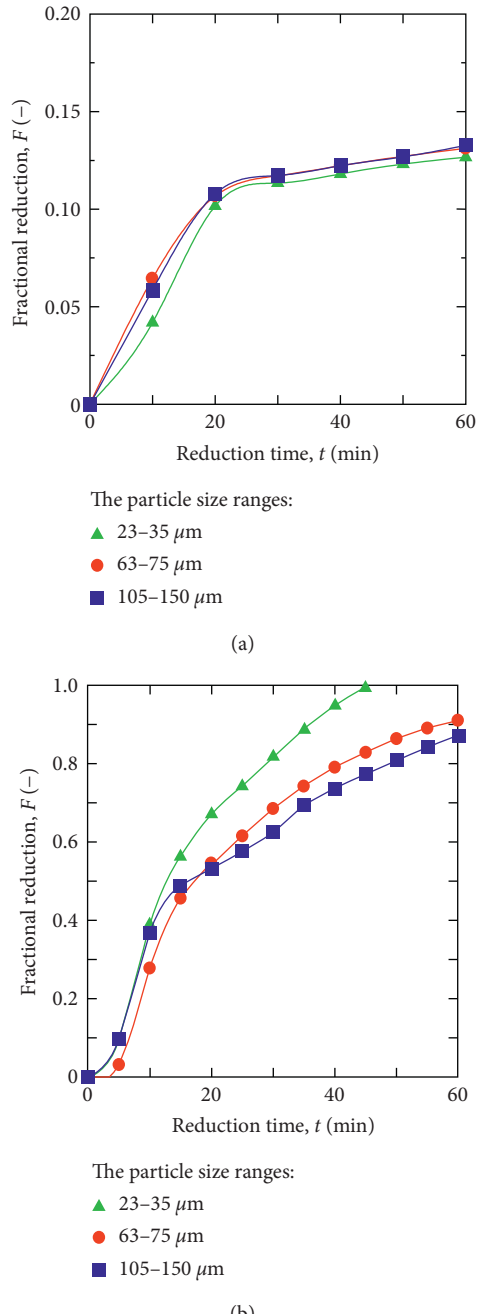

FIGURE 21: Influence of particle size of semicharcoal upon the reduction curves at the reduction temperature $T_R = 1073$ and 1273 K in N_2 gas atmosphere for carbon composite iron oxide pellets using semicharcoal produced at $T_{c,\max} = 1073$ K and $r_h = 200$ K/h from Japanese cypress. (a) $T_R = 1073$ K. (b) $T_R = 1273$ K.

$C_2H_4 + C_2H_6 + C_3H_8$ have no dependence upon the maximum carbonisation temperature $T_{c,\max}$ over the $T_{c,\max}$ range from 823 to 1273 K but are scattered randomly. These tendencies can be easily understood by observing each gas emission behaviour at each $T_{c,\max}$ for Newcastle blend coal (see Figures 3 to 7 in [10]; Figure 7 in [10] is shown in this paper as Figure 10) or mole fraction variation for Muswellbrook coal (Figure 4). As a whole, the

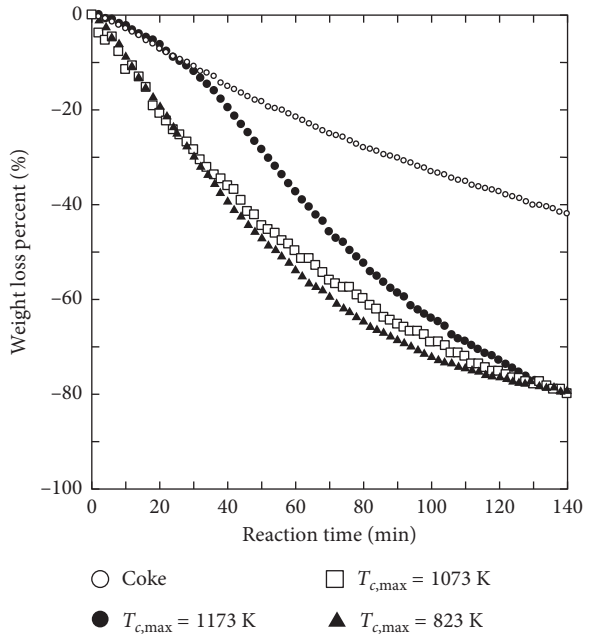

Figure 22: Weight loss curves of semichar samples (Newcastle blend coal) obtained by carbonisation at $T_{c,max} = 823$, 1073, and 1173 K and a coke sample (Table 6) at a gasification temperature $T_G = 1273$ K in CO_2 gas atmosphere.

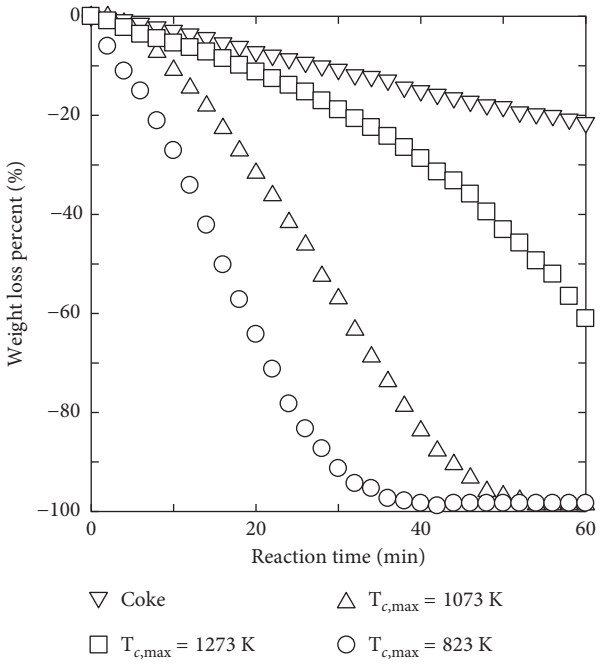

Figure 23: Weight loss curves of semicharcoal samples (Japanese cypress) obtained by carbonisation at $T_{c,max} = 823$, 1073, and 1273 K and a coke sample (Table 6) at $T_G = 1273$ K in CO_2 gas atmosphere.

total heat values tend to increase almost monotonically, as $T_{c,max}$ increases.

Figure 18 shows the comparison among the total amounts of heat for all the samples used at $T_{c,max} = 1073$ and 1273 K. Amounts of heat for coal are somewhat higher

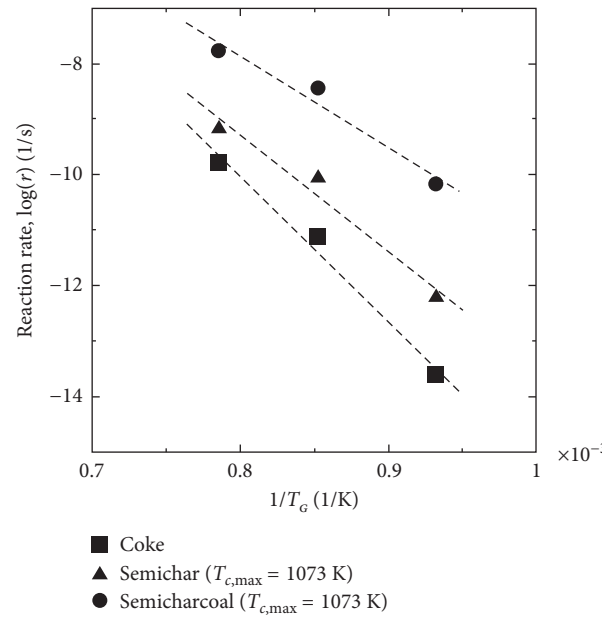

Figure 24: Arrhenius plots of the reaction rate of gasification for semichar and semicharcoal produced at $T_{c,max} = 1073$ K as well as for coke, which are the same as in Figures 22 and 23. The reaction rate r (1/s) is defined by (2) and T_G: gasification temperature (K).

Table 7: Amount of heat (kJ/kg) of each gas component as a function of maximum carbonisation temperature $T_{c,max}$ (Newcastle blend coal, $r_h = 200$ K/h).

$T_{c,max}$ (K)	823	873	973	1073	1273
H_2	24	453	555	1010	1648
CO	64	109	163	267	254
CH_4	1384	1079	1145	1842	2206
$C_2H_4 + C_2H_6 + C_3H_8$	688	725	320	509	725
Total	2160	2366	2183	3628	4833

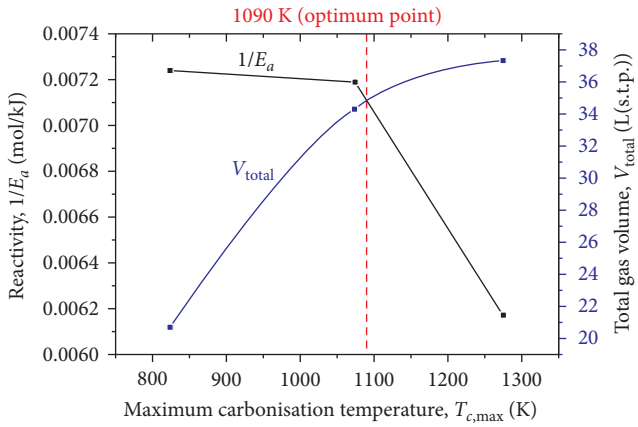

Figure 25: Reactivity of semicharcoal and total carbonisation gas volume as a function of the maximum carbonisation temperature $T_{c,max}$ ($r_h = 200$ K/h) for Japanese cypress (sample weight in wood stage: 200 g).

than those for wood. The total amount of heat at $T_{c,\max} = 1273$ K is always higher than the one at $T_{c,\max} = 1073$ K for all the samples used.

4.5. Reactivity of Semicharcoal and the Total Carbonisation Gas Volume. Figure 25 shows the reactivity of semicharcoal and the total carbonisation gas volume for Japanese cypress as a function of the maximum carbonisation temperature $T_{c,\max}$. The reactivity was calculated by the reciprocal of the activation energy E_a (kJ/mol) (Table 5). Because the scales of both ordinates are arbitrary, the optimum point cannot be considered absolute. However, we can envisage that there will be an optimum point for both high reactivity of semicharcoal and large volume of the emitted carbonisation gas, or biogas. Such an optimum point should be determined in consideration of the usage of the semicharcoal and carbonisation gas.

5. Conclusions

Carbon composite iron oxide pellets using semichar or semicharcoal were proposed from the measured results of the coal carbonisation gas release behaviour for prereduction of iron oxide, which was a part of the fundamental study for smelting reduction total process. The samples used were Newlands coal, Newcastle blend coal, Muswellbrook coal, Japanese cedar, and Japanese cypress to prepare semichar and semicharcoal as carbonaceous materials, and coke was also used for reference. The carbonisation was completed under rising temperature conditions at a constant heating rate (mainly at 200 K/h) until arriving at the maximum carbonisation temperature $T_{c,\max}$ in order to release some volatile matter (VM). Conclusions obtained are as follows:

(1) Comparison of reduction curves for carbon composite pellets using semichar produced at $T_{c,\max} = 823$ K and coke and graphite at the reduction temperature $T_R = 1273$ K showed that the reduction rate of the semichar composite pellet was the highest and that of graphite was the lowest.

(2) From [14], the rate of reduction for semicharcoal composite pellets was greater than that for semichar composite pellets because the gasification rate of semicharcoal is higher than that of semichar for the following reasons: the amorphous nature of semicharcoal is stronger than that of semichar, and the activation energy of semicharcoal is lower than that of semichar.

(3) The starting point of reduction of the carbon composite pellet using semicharcoal produced at $T_{c,\max} = 823$ K in N_2 gas atmosphere was observed to be at the reduction temperature $T_R = 833$ K, only a little higher than $T_{c,\max}$, which was the target of the experiment.

(4) For all the samples, the total carbonisation gas volume increases, as the maximum carbonisation temperature $T_{c,\max}$ increases. The heat value of the carbonisation gas depends on $T_{c,\max}$ and consequently the emitted gas volume and the composition. As a whole, the total heat value tends to increase almost monotonically, as $T_{c,\max}$ increases.

(5) Large quantities of H_2 and CH_4 are released from the sample coals. This can be explained from the structure of the coal, which is mainly composed of carbon and hydrogen. In contrast, large amounts of CO and CO_2 are released from the sample woods because of the large quantity of oxygen in its structure.

(6) The effect of the particle size of the carbonaceous material on the reduction rate was studied by using semicharcoal composite pellets. When T_R is higher than $T_{c,\max}$, the reduction rate increases, as the particle size decreases. When T_R is equal to $T_{c,\max}$, there is almost no effect.

(7) The maximum carbonisation temperature $T_{c,\max}$ can be used to control the evolved and residual gas volumes. With decreasing $T_{c,\max}$, the activation energy E_a of semicharcoal decreases, or the reactivity $1/E_a$ of semicharcoal increases. The maximum carbonisation temperature $T_{c,\max}$ may be optimised for reactivity of semicharcoal and the total carbonisation gas volume or the heat value.

Conflicts of Interest

All authors declare that there are no conflicts of interest regarding the publication of this paper.

Acknowledgments

The authors wish to express their thanks to Mr. Kazuhiro Azuma (Bachelor of Engineering), Mr. Takeshi Harada (Master of Engineering), Mr. Atsushi Yamashita (Master of Engineering), and Mr. Shiro Fujimori (Bachelor of Engineering), graduated students of Osaka University, at the time of study, for their help. The authors would like to express their gratitude to FAPEMIG, Brazil, for their financial support.

References

[1] T. Ariyama and M. Sato, "Optimization of ironmaking process for reducing CO_2 emissions in the integrated steel works," *ISIJ International*, vol. 46, no. 12, pp. 1736–1744, 2006.

[2] M. Asanuma, T. Ariyama, M. Sato et al., "Development of waste plastics injection process in blast furnace," *ISIJ International*, vol. 40, no. 3, pp. 244–251, 2000.

[3] T. Ariyama, R. Murai, J. Ishii, and M. Sato, "Reduction of CO_2 emissions from integrated steel works and its subject for a future study," *ISIJ International*, vol. 45, no. 10, pp. 1371–1378, 2005.

[4] T. Matsumura, M. Ichida, T. Nagasaka, and K. Kato, "Carbonization behaviour of woody biomass and resulting metallurgical coke," *ISIJ International*, vol. 48, no. 5, pp. 572–577, 2008.

[5] M. Nakano, M. Naito, K. Higuchi, and K. Morimoto, "Non-spherical carbon composite agglomerates: lab-scale manufacture and quality assessment," *ISIJ International*, vol. 44, no. 12, pp. 2079–2085, 2004.

[6] T. Usui, T. Yokoyama, T. Nakahashi, and Z. Morita, "Effective use of hydrogen within coal in pre-reduction of iron oxide for minimizing the amounts of coal used and CO_2 exhausted in an iron bath smelting reduction process," in *Proceedings of Ironmaking Conference*, vol. 52, pp. 389–398, The Iron and Steel Society of AIME, Dallas, Texas, USA, March 1993.

[7] T. Usui, N. Inoue, T. Watanabe, T. Yokoyama, T. Oyama, and Z. Morita, "Influence of reduction temperature on pre-reduction of iron oxide with coal carbonisation gas without tar," *Ironmaking and Steelmaking*, vol. 31, no. 6, pp. 479–484, 2004.

[8] N. Inoue and T. Usui, "Influence of combined water in coal on pre-reduction of iron oxide with coal carbonization gas in low, middle and high volatile matter coal," *Journal of High Temperature Society*, vol. 35, no. 1, pp. 26–32, 2009.

[9] T. Usui, T. Yokoyama, T. Ohyama, T. Nakahashi, M. Nonaka, and Z. Morita, "Effective use of volatile matter in pre-eduction of iron oxide for minimizing the amounts of coal used in an in-bath smelting reduction process," in *Proceedings of the Second International Symposium on Metallurgical Processes for the Year 2000 and Beyond and the 1994 TMS Extraction and Process Metallurgy Meeting*, Vol. I, pp. 693–714, TMS (The Minerals, Metals and Materials Society), San Diego, CA, USA, September 1994.

[10] H. Konishi, T. Usui, and K. Azuma, "The preparation and reduction behavior of carbon composite iron oxide pellets using semi-coal-char," *Tetsu-to-Hagané*, vol. 92, no. 12, pp. 802–808, 2006.

[11] H. Konishi, A. Yamashita, and T. Usui, "Effect of residual volatile matter on reduction of iron oxide in carbon composite pellets," *Journal of JSEM (Japanese Society for Experimental Mechanics)*, vol. 8, Special Issue, pp. 142–146, 2008.

[12] H. Konishi, T. Usui, and A. Yamashita, "Effect of residual volatile matter on reduction reaction between semi-coal-char and iron oxide," *Tetsu-to-Hagané*, vol. 95, no. 6, pp. 467–472, 2009.

[13] H. Konishi, K. Ichikawa, and T. Usui, "Effect of residual volatile matter on reduction of iron oxide in semi-charcoal composite pellets," *ISIJ International*, vol. 50, no. 3, pp. 386–389, 2010.

[14] H. Konishi, T. Usui, and T. Harada, "The preparation and reduction behavior of charcoal composite iron oxide pellets," *Journal of High Temperature Society*, vol. 34, no. 1, pp. 14–19, 2008.

[15] H. Konishi, S. Fujimori, and T. Usui, "Reduction behavior of iron oxide in semi-charcoal composite pellets," *Journal of High Temperature Society*, vol. 35, no. 1, pp. 33–39, 2009.

[16] M. Kawakami, H. Taga, T. Takenaka, and S. Yokoyama, "Micro pore structure and reaction rate of coke, wood charcoal and graphite with CO_2," *ISIJ International*, vol. 44, no. 12, pp. 2018–2022, 2004.

Hindawi
Advances in Materials Science and Engineering
Volume 2018, Article ID 2138268, 6 pages
https://doi.org/10.1155/2018/2138268

Research Article

Carbothermal Reduction of Iron Ore in Its Concentrate-Agricultural Waste Pellets

Zhulin Liu,[1] Xuegong Bi,[2] Zeping Gao,[1] and Wei Liu[2]

[1]*School of Metallurgical and Materials Engineering, Hunan University of Technology, Zhuzhou 412007, Hunan, China*
[2]*State Key Laboratory of Refractory Materials and Metallurgy, Wuhan University of Science and Technology, Wuhan 430081, Hubei, China*

Correspondence should be addressed to Xuegong Bi; 1575595611@qq.com

Received 22 May 2017; Accepted 24 August 2017; Published 17 January 2018

Academic Editor: Liming Lu

Carbon-containing pellets were prepared with the carbonized product of agricultural wastes and iron concentrate, and an experimental study on the direct reduction was carried out. The experimental results demonstrated that carbon-containing pellets could be rapidly reduced at 1200 to 1300°C in 15 minutes, and the proper holding time at high temperature was 15 to 20 min. The degree of reduction gradually increased with temperature rising, and the appropriate temperature of reducing pellets was 1200°C. The weight loss rate and reduction degree of pellets increased with the rise of carbon proportion, and the relatively reasonable mole ratio of carbon to oxygen was 0.9. A higher content of carbon and an appropriate content of volatile matters in biomass char were beneficial to the reduction of pellets. The carbon-containing pellets could be reduced at high speeds in the air, but there was some reoxidization phenomenon.

1. Introduction

In recent years, the research of carbon-containing pellets has attracted great attention of metallurgists. The carbon-containing pellets are composed of iron-containing powders and carbonaceous additives (coke breeze, petro-coke, pulverized coal, peat moss, and charcoal) blended with appropriate binders [1]. They are carbon- and iron-containing pellets or cold/hot briquettes made through pelletizing in a balling disc or through briquetting in a molding machine after thorough mixing. Carbon-containing pellets were originally used for the production of high-quality sponge iron [2, 3], and they could also be fed into the blast furnace. Yokoyama et al. [4] prepared ore/coal briquettes with cement as the binder (blending ratio was 10-11 mass%) and conducted a 80 day 54 kg/t charge test at Oita BF No. 2. A substantial reduction of fuel rate was confirmed by this test. It was attempted to partially substitute biomass char from Japanese cedar for pulverized coal in the preparation of carbon-containing iron ore hot briquettes [5]. The difference of reactivity between wood charcoal, bamboo charcoal, and coal were also investigated [6]. The raw material source of biomass char is wide; however, in China, the forest resource is poor, but the agricultural waste output is great. Charcoal bars made with agricultural crops as raw materials gradually form market for home heating in winter.

It was reported that the carbon content in wheat and corn crops is about 40% and exceeds 43% in rice hull. The derived biomass char contains less ash, and the content of impurities such as sulfur and phosphorus are also very low. To apply it for producing carbon-containing pellets will not only contribute to the solution of the puzzle of effectively using agricultural waste in large scale but also improve the quality of iron and steel products.

Effect of several factors such as maximum carbonization temperature of Japanese cypress, reduction temperature, and heating profile on fractional reduction F (%) after 60 min was experimentally studied in the laboratory by Hirokazu et al. [7]. Effect of coal content on the apparent density and the cold crushing strength and melt-down temperature of coal composite iron ore hot briquettes was investigated by Hayashi [8]. Kunishi et al. [9] confirmed by the XRD analysis

of the reduced pellets that the carbon composite iron oxide pellets using the semi-Newcastle blend coal-char at a lower maximum carbonization temperature (823 K) have the highest reducibility of the iron oxide. Ariyama et al. [10] prepared the composite composed of iron oxide and plastic wastes and confirmed the importance of the composite structure and temperature profile on the effective utilization of pyrolysis gas released from plastics.

Also was studied the impact of residual volatile matters in semicharcoal biomass on the reduction performance of iron ore pellets [11]. Because the reactivity of biomass char outclasses coke, Ueda et al. [12] carried out a research on how biomass char improved the reactivity of carbon-containing pellets. The mole ratio of carbon to oxygen, represented as C/O ratio hereinafter, was selected as 1.0. Japanese cedar-derived biomass char, and iron ore powders with no binders were mixed uniformly and pressed in a 10 mm die at 9.8 MPa to form a tablet of the sample. The temperature inside the test furnace was increased to 1000°C at a rate of 0.167°C/s, simulating the blast furnace shaft condition. The following main results were obtained: (1) the gasification reaction rate of biomass char is faster than that of coke in a couple of dozen times; (2) the reduction of the composite begins at about 550°C, and the reactivity of the carbon iron ore composite with biomass char is remarkably faster than that with coke; and (3) the reaction rate of carbon iron ore composite with highlyreactive reducing agent is controlled from both reaction rate of carbon gasification and iron ore reduction.

Takyu et al. [13] tried to understand the reduction mechanism of iron ore and carbon composite by volatile matters in biomass char at low temperature. The iron ore and carbon composite were heated at a constant rate to 1473 K, and the CO and CO_2 concentrations in waste gases were analyzed by an infrared absorption analyzer. It was found that the reduction degree at 1100 K increased with the amount of volatile matters. By making a comparison between the sample mixed with Biomass char 3 and the sample mixed with coal char, the CO content was decreased at temperatures below 1000 K while it was increased at higher temperatures. As for the CO_2 content, it was increased when the temperature exceeded 900 K and reached the maximum at about 950 K, implying the indirect reduction reaction was expedited.

The reducing agents applied in the study of carbon-containing pellets in China and abroad were so far coal and biomass char derived from wood materials. In this paper, the local abundant resource of rice hull and peanut shell in Hunan Province was utilized as raw materials to prepare biomass char, which was used to replace pulverized coal for preparing carbon-containing pellets and to study in laboratory the improvement effect of biomass char on pellets reducibility.

2. Materials and Methods

2.1. Experimental Materials. The concentrate for pellet preparation was provided by Xianggang Company, and the chemical composition is listed in Table 1. The reducing agent was biomass chars prepared from rice husk and peanut shell through crushing, molding, and low temperature carbonization (300–350°C). In this work, two kinds of biomass chars with different chemical compositions were applied, aiming at studying the influence of char composition on reduction process of carbon-containing pellets. Their chemical compositions are given in Table 2. Bentonite was used as the binder, and its chemical composition is shown in Table 3.

Table 1: Chemical composition of the concentrate (mass%).

T.Fe	S	P	FeO	SiO_2	CaO	Al_2O_3	MgO	MnO	H_2O^*
63.55	0.05	0.01	27.02	5.47	2.86	0.93	1.00	0.33	10.20

*Free water content.

Table 2: Approximate analysis of biomass chars (mass%).

Char	FC_d	V_{daf}	A_d	$S_{t,d}$	M_{ad}
A	61.82	32.1	3.48	0.05	2.60
B	59.79	25.88	14.2	0.05	5.13

Note. A_d: air dry ash content; V_{daf}: air dry and ash free volatile content; FC_d: air dry fixed carbon content; $S_{t,d}$: air dry total sulfur content; M_{ad}: internal water content.

Table 3: Chemical component of bentonite (mass%).

	Al_2O_3	CaO	MgO	SiO_2	K_2O	Na_2O	I.L
Bentonite	12.65	1.02	4.19	53.25	0.43	0.3	14.39

It is seen from Table 1 that FeO content of the concentrate was 27.02%. The Fe_2O_3 content calculated from FeO% and the T.Fe% was 60.76%, and the corresponding total oxygen content was 24.23%, stating that this concentrate was a pure magnetite with T.Fe/FeO = 2.35.

It can be seen from Table 2 that the ash content and sulfur content in biomass char are low. Lower ash content benefits improving the blast furnace performance in terms of the reduction of flux consumption and the smelting of low silicon content pig iron. That the fixed carbon content is low and the volatile content is high is mainly because rather low carbonization temperatures were accepted in the preparation of biomass char, leading to an incomplete pyrolysis. But residual volatile matters will play the role of reduction in the reduction process of pellets because these materials begin to crack and generate H_2 and C as temperature reaches nearly the maximum carbonization temperatures [11]. Also, the temperature range of the pyrolysis is much lower than that of starting reduction of iron oxide; it is therefore essential to design the composite structure and the temperature profile for realizing this temperature difference of the reactions simultaneously in the composite, in order to effectively utilize the pyrolysis gas as a reductant [10].

2.2. Carbon Proportioning. Three molar ratios of carbon to oxygen in pellets were selected for this study, that is, 0.8, 0.9, and 1.0. The corresponding amount of biomass char required for 1 kg iron ore concentrate, blend ratio of biomass char and carbon content in pellets could be calculated based on the mass balance of carbon and oxygen elements.

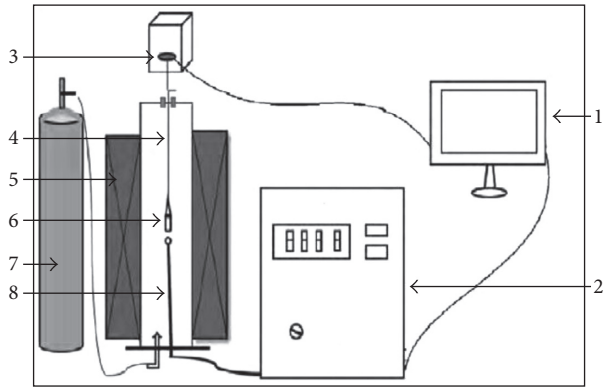

Figure 1: The schematic diagram of experimental apparatus. (1) Computer; (2) temperature controller; (3) electronic balance; (4) Mo wire; (5) $MoSiO_2$ bar; (6) basket and samples; (7) atmosphere controller; (8) thermocouple.

Uniformly mix the concentrate, biomass char and bentonite (additional 6 mass%) weighed, pelletize the mixture in a balling disc and sift out the 8–12 mm section. In order to prevent pellets from breaking due to thermal stress in the preheating stage, it is needed to preheat green balls at 105°C for 2 h.

2.3. Equipment and Procedure. By applying the thermogravimetry technique (TG), carbon-containing pellets were heated and reduced in a $MoSi_2$ bar electric resistant furnace, and the test apparatus is shown in Figure 1. The temperature of the furnace was measured with a Pt-30%Rh/Pt-6%Rh thermocouple, and the sample weight was measured with a 1 kg electronic balance of 0.001 g precision. The upper Fe–Cr–Mo wire basket with 30 mm ID and 100 mm height was connected with the electronic balance. Ten pellets of 25–30 g total weight with similar diameter were selected for one test, and before use, they were dried at 105°C for 2 h. The furnace heated up at 10°C/min as it was below 200°C while the heating rate was changed to 15°C/min as it was beyond 200°C. When the specified experimental temperature was reached, a N_2 gas flow was purged at a rate of 3 L/min. The temperature was kept constant for 5 min, then the basket was quickly put into the furnace together with the sample, and its weight was continuously recorded.

The experiment was conducted isothermally, the reduction temperature was respectively 1000, 1100, 1200, and 1300°C, and reduction time was respectively 5, 10, 15, and 20 min. After reduction, the sample was quickly taken out from the furnace and put into a tubular furnace purged with nitrogen for cooling to the room temperature.

2.4. Test Parameter Calculation. For usual iron ores, the degree of reduction can be calculated directly from the weight loss. In the weight loss of carbon-containing pellets, apart from oxygen loss, the carbon loss, the amount of volatile matters separated, and remaining water vaporized are also included. Most researchers made estimation according to the chemically analyzed value of total iron, metallic iron, and FeO contents in the reduced sample, this method can only obtain the final result of the degree of reduction and could not describe the reduction process. In this paper, the modified weight loss approach was utilized, that is, by taking carbon-containing alumina balls as a reference, to indirectly measure the separation ratio of volatile matters and water and to evaluate the degree of reduction with Equation (1), which originated from a reference and was modified in this work.

$$R = \frac{4}{7M_{\mathrm{O}}}\left(f_{\Sigma} - f_{A-P}\right)W \times 100\%, \quad (1)$$

where M_{O} is oxygen amount in iron oxides, g; f_{Σ} is the percentage of total weight loss, %; f_{A-P} is the percentage of weight loss of volatile matters and moisture in carbon-containing alumina balls, %; and W is the weight of carbon-containing pellets, g.

It is found in the experiment that release of volatiles is basically terminated at 5 min. The observed values of f_{A-P} at various temperatures and C/O ratios are shown in Table 4.

Table 4: f_{A-P} value of carbon-containing alumina balls under different conditions (%).

Temperature, °C	Molar ratio of carbon to oxygen, –	f_{A-P}, %
1000	0.8	5.76
	0.9	6.17
	1.0	6.74
1100	0.8	6.30
	0.9	6.64
	1.0	7.35
1200	0.8	6.32
	0.9	6.65
	1.0	7.49
1300	0.8	6.33
	0.9	6.66
	1.0	7.49

3. Results and Analysis

3.1. Effect of C/O Ratio on Reduction of Carbon-Containing Pellets. The plot of reduction degree of carbon-containing pellets with different C/O molar ratios at 1200°C against time are depicted in Figure 2.

As shown in Figure 2, the C/O ratio influences the reduction rate and the degree of reduction at 20 min. As the C/O ratio was increased from 0.8 to 0.9, the reduction was accelerated before 10 min, and it was more obviously accelerated as the C/O ratio was further increased to 1.0. The degree of reduction at 20 min was increased by 5.88% when the C/O ratio was increased from 0.8 to 0.9, but it almost did not change at all when the C/O ratio was further increased to 1.0, stating that it is reasonable to control the C/O ratio at a level of 0.9.

It was experienced that too high C/O ratios will deteriorate the ballability of pelletizing mixture and the strength of product pellets, which would also justify the use of 0.9 C/O ratio.

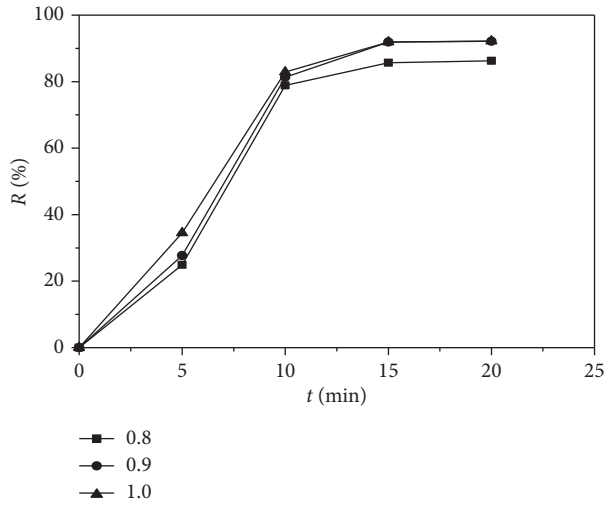

Figure 2: Variation of reduction degree of carbon-containing pellets of different C/O ratios with time at 1200°C.

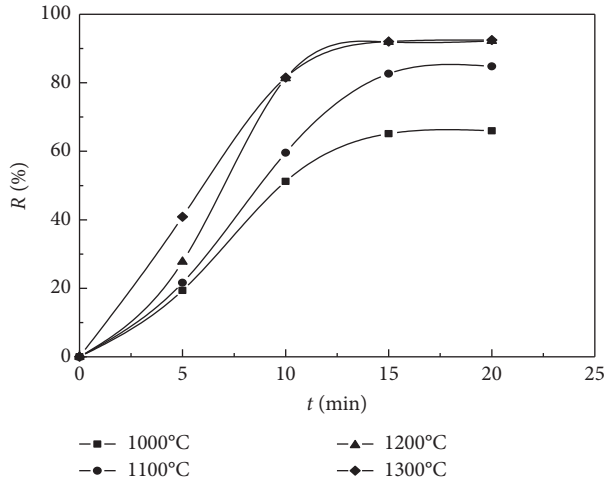

Figure 3: Reduction degree of carbon-containing pellets with C/O ratio of 0.9 at different temperatures.

3.2. Effect of Temperature on Reduction of Carbon-Containing Pellets. The plot of the degree of reduction of carbon-containing pellets (C/O = 0.9) against time at different temperatures is shown in Figure 3.

It is known from Figure 3 that when temperature is lower than 1200°C, increasing temperature can substantially promote reduction, and the degree of reduction at 1200°C could reach 92.17%, 7.37% higher than at 1100°C and 24.83% higher than at 1000°C, and that the effect of increasing temperature on reduction improvement was little when it exceeded 1200°C. It is known that during reduction of carbon-containing iron ore pellets, direct reduction as well as indirect reduction takes place simultaneously. Equilibrium concentration of CO of $C + CO_2 = 2CO$ is greater at higher temperatures, and consequently, an increase in temperature contributes to the improvement of indirect reduction of pellets from the view point of reaction kinetics. The direct reduction is an endothermic reaction, stating that an increase in temperature contributes to the improvement of direct reduction of pellets from the view point of reaction thermodynamics. Also, an increase in temperature will bring about a more complete escaping and pyrolysis of volatile matters in biomass char. As a result, the degree of reduction was increased with temperature increasing.

When temperature was over 1200°C, however, the benefit of these aspects reached the maximum, and the effect of further increasing temperature would thus not be substantial.

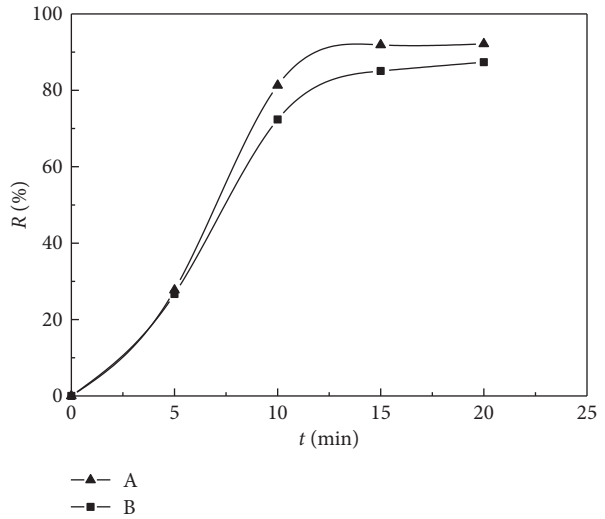

Figure 4: Plot of reduction degree of pellets blended with different biomass chars at 1200°C against time.

3.3. Composition of Biomass Char. The carbon-containing pellets blended with char B was reduced isothermally at 1200°C, and the variation of the degree of reduction with time is depicted in Figure 4. Also in this figure, the reduction experiment results of the carbon-containing pellets blended with char A was shown.

It can be seen from Figure 4 that, in the primary 5 minutes, the reduction behavior of these two kinds of pellets were basically the same, but soon afterwards, the reduction velocity of pellets blended with char B became more and more slowly, the difference with pellets blended with char A enlarged, and at 20 min the degree of reduction of this couple differed by 4.82%. The ratio of V_{daf} to FC_d of char A is 0.5192 while that of char B is 0.4328; it can thus be understood that at a same C/O ratio, the amount of volatile matters in pellets blended with char B is less than that in pellets blended with char A, meaning that the role played by volatile matters in pellet reduction is less. Furthermore, the escape of volatile matters during reduction will generate vacancies which are favorable for the quick diffusion of CO gas within pellets, contributing to the pellet reduction. The reason from these two aspects brings about that the degree of reduction of pellets blended with char B is not as high as that of pellets blended with char A, and the first reason is the prime.

3.4. Atmospheric Condition. The curve of reduction degree of pellets with 0.9 C/O ratio under air and N_2 atmospheres at 1200°C are shown in Figure 5.

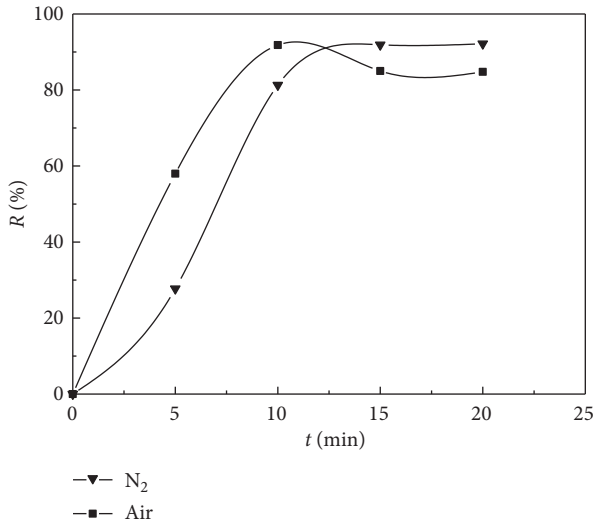

Figure 5: Plot of reduction degree of pellets under different atmospheres at 1200°C against time.

It can be seen from Figure 5 that, at 1200°C, pellets can be reduced at high speeds under the atmosphere of nitrogen and air, and the reduction speed under air atmosphere within the first 10 minutes is even faster. The blend ratio of biomass char in the 0.9 C/O ratio pellets was 18.60%, and char fines were surrounded by iron ore particles, implying the condition of combustion of char fines is poorer and that the weight loss caused by combustion of carbon would be small. Therefore, it is presumed that the promoted reduction in air would be mainly because CO gas generated from reduction reacts with oxygen in air and releases heat, supplying the heat consumed by the direct reduction, and that the generated CO_2 gas can also impede the reoxidation of iron. Till the final phases of reaction, however, the degree of reduction of pellets gradually decreases, resulted from that along with the combustion of carbon element, the amount of CO_2 that plays the role of protection becomes less and less, and part of iron will be reoxidized.

4. Conclusions

Carbon-containing pellets were produced with agricultural waste-derived biomass chars, and the influence of factors such as C/O ratio, temperature, and char chemical composition on the pellets reduction was experimentally studied, reaching the following conclusions:

(1) The appropriate C/O ratio is 0.9 and lower than 1.0, which is due to the occurrence of indirect reduction and that the volatile content in the biomass char is higher and the CO and H_2 gases generated by the pyrolysis of volatile materials during reduction also take part in the reduction of iron oxides.

(2) As lower than 1200°C, increasing temperature could substantially promote reduction, the degree of reduction at 1200°C could reach 92.17%, when temperature exceeds 1200°C; however, increasing temperature has little effect on reduction reaction.

(3) The chemical composition of biomass char has an important impact on the reducing properties of carbon-containing pellets, and higher carbon contents and bigger V_{daf}/FC_d ratios will promote the reduction reaction.

(4) Carbon-containing pellets could be quickly reduced even in the air atmosphere, in comparison with the reduction tests in the nitrogen atmosphere, and the reduction speed during the first 10 minutes is even higher and the maximum degree of reduction is bigger, but when the carbon blended is essentially completely consumed, the secondary oxidation phenomenon will take place.

Conflicts of Interest

The authors declare that there are no conflicts of interest regarding the publication of this paper.

Acknowledgments

The authors thank the Hunan Province (A research project supported by the Hunan Province Science and Technology Program Foundation Grant no. 2012FJ3037).

References

[1] J. E. Appleby and G. Shaw, "Carbonaceous additives in the pelletizing process," in *Proceedings of the 4th International Symposium on Agglomeration*, pp. 49–74, Toronto, ON, Canada, June 1985.

[2] W. L. Tennies, J. A. Lepinski, and J. T. Kopfle, "The Midrex Fastmet process a simple economic ironmaking option," *MPT*, vol. 14, no. 2, pp. 36–42, 1991.

[3] I. Kobayashi, Y. Tanigaki, and A. Uragami, "Direct reduction process using fine ore and coal," in *Proceedings of the Asia Steel' 2000*, Volume B: Ironmaking, pp. 132–139, Beijing, China, September 2000.

[4] H. Yokoyama, K. Higuchi, T. Ito, and A. Oshio, "Decrease in carbon consumption of a commercial blast furnace by using carbon composite iron ore," *ISIJ International*, vol. 52, no. 11, pp. 2000–2006, 2012.

[5] S. Hayashi and Y. Iguchi, "Reaction behavior of wood flour added coal composite iron ore hot briquettes at high temperatures," in *Proceedings of the Asia Steel International Conference*, pp. 372–377, Fukuoka, Japan, May 2006.

[6] M. Kawakami, T. Karato, T. Takenaka, and S. Yokoyama, "Structure analysis of coke, wood charcoal and bamboo charcoal by raman spectroscopy and their reaction rate with CO_2," *ISIJ International*, vol. 45, no. 7, pp. 1027–1034, 2005.

[7] K. Hirokazu, I. Kazuhira, and U. Tateo, "Preparation and reduction of semi-charcoal composite iron oxide pellets," in *Proceedings of the 5th International Congress on the Science and Technology of Ironmaking (ICSTI'09)*, pp. 287–291, Shanghai, China, October 2009.

[8] S. Hayashi, "Reaction behavior of coal composite iron ore hot briquettes in a laboratory scale blast furnace simulator," in *Proceedings of the 5th international Congress on the Science and Technology of Ironmaking (ICSTI'09)*, pp. 423–427, Shanghai, China, October 2009.

[9] H. Kunishi, T. Usui, K. Azuma, and A. Yamashita, "Preparation and reduction behavior of carbon composite iron oxide

pellets intentionally including residual volatile matter," in *Proceedings of the 4th Congress on the Science and Technology of Ironmaking (ICSTI'06)*, pp. 53–56, Osaka, Japan, November 2006.

[10] T. Ariyama, N. Hayashi, T. Murakami, and E. Kasai, "Reaction behavior of the composite composed of iron oxide and plastic wastes," in *Proceedings of the 4th Congress on the Science and Technology of Ironmaking (ICSTI'06)*, pp. 707–710, Osaka, Japan, November 2006.

[11] H. Konishi, K. Ichikawa, and T. Usui, "Effect of residual volatile matter on reduction of iron oxide in semi-charcoal composite pellets," *ISIJ International*, vol. 50, no. 3, pp. 386–389, 2010.

[12] S. Ueda, K. Watanabe, K. Yanagiya, R. Inoue, and T. Ariyama, "Improvement of reactivity of carbon iron ore composite with biomass char for blast furnace," *ISIJ International*, vol. 49, no. 10, pp. 1505–1512, 2009.

[13] Y. Takyu, T. Murakami, and E. Kasai, "Reduction mechanism of iron ore and carbon composite by volatile matters in biomass char at low temperature," *CAMP-ISIJ*, vol. 27, p. 681, 2014.

Hindawi
Advances in Materials Science and Engineering
Volume 2017, Article ID 1019438, 8 pages
https://doi.org/10.1155/2017/1019438

Research Article

Effects of Treated Cow Dung Addition on the Strength of Carbon-Bearing Iron Ore Pellets

Qing-min Meng,[1] Jia-xin Li,[1,2] Tie-jun Chun,[1] Xiao-feng He,[1] Ru-fei Wei,[1] Ping Wang,[1] and Hong-ming Long[1,3]

[1]*School of Metallurgical Engineering, Anhui University of Technology, Ma'anshan, Anhui 243002, China*
[2]*School of Metallurgy, Northeastern University, Shenyang 110819, China*
[3]*Key Laboratory of Metallurgical Emission Reduction & Resources Recycling, Anhui University of Technology, Ministry of Education, Ma'anshan 243002, China*

Correspondence should be addressed to Hong-ming Long; yaflhm@126.com

Received 25 June 2017; Accepted 25 September 2017; Published 2 November 2017

Academic Editor: Merrick Mahoney

It is of particular interest to use biomass as an alternative source of fuel in direct-reduction ironmaking to ease the current reliance on fossil fuel energy. The influence of cow dung addition on the strength of carbon-bearing iron ore pellets composed of cow dung, iron ore, anthracite, and bentonite was investigated, the quality of green and dry pellet was evaluated based on FTIR analysis, and the mechanism of strength variation of the reduced pellets was investigated by analysing the phase composition and microstructure using XRD and SEM. The results show that cow dung addition decreased the green pellet strength due to expansion of the amorphous region of the cellulose in the cow dung; however, the dry pellet strength increased substantially. In the process of reduction roasting, it was found that cow dung addition can promote aggregation of iron crystals and increase the density of the pellets, resulting in increased strength of the reduction roasted pellets, while excessive cow dung addition resulted in lower strength.

1. Introduction

With the gradual depletion of raw materials for the blast furnace, such as coke and quality iron ore, direct-reduction and smelting reduction technologies using gas, liquid fuels, and noncoking coal as energy sources were developed as cleaner, more environment friendly alternatives, which have been applied widely around the world [1–3]. However, the fuel sources of noncoking coal iron-making technology have not fundamentally changed, and there is a gap in product quality and energy consumption compared to the blast furnace. The use of biomass as an alternative fuel source, to further reduce the consumption of fossil fuels and emission of carbon in the steel-making industry, has become a hot topic among scholars [4–8]. Sterol [9] investigated the mechanisms of iron ore reduction with biomass wood waste. The results showed that the iron ore was successfully reduced to predominantly metallic iron when up to 30 wt% of biomass was introduced into the mixture and reduction commenced at approximately 943 K and was almost completed at 1473 K. Wei et al. [10] studied the characteristics and kinetics of iron oxide reduction by carbon in biomass composites. The result showed that iron oxide can be reduced by biomass very rapidly, and the degree of metallisation and reduction increased with temperature.

Iron oxide reduction by carbon in biomass can be divided into two stages, namely, reduction by volatile matter followed by reduction by nonvolatile carbon. The reduction times of the two stages both decrease with increasing temperature. Liu et al. [11] researched the reduction of carbon-bearing pellets, using the reducing agents prepared from carbonization products of rice husk, peanut shells, and wood chips. The result showed that the carbon-bearing pellets could be reduced rapidly between 1473 K and 1573 K in about 15 to 20 minutes, while the higher carbon content and appropriate volatile content in biological carbon were beneficial to the pellet reduction. Han et al. [12] studied the effect of biomass on the reduction of carbon-bearing pellets using charcoal, bamboo charcoal, and straw as reductant. The results showed that

Table 1: Chemical composition of iron ore (wt%).

TFe	FeO	SiO_2	Al_2O_3	CaO	MgO	P	S
61.4	23.5	3.3	1.1	1.0	0.2	0.028	0.328

Table 2: Proximate analysis of reducing agent (wt%).

Type of reducing agent	Fixed carbon	Ash	Volatile matter	P	S
Anthracite	78.8	13.4	7.9	0.024	0.580
Cow dung	7.7	24.9	67.4	0.001	0.270

Table 3: Raw material ratio of the carbon-bearing iron ore pellets.

Sample number	Iron ore	Anthracite	Cow dung	Bentonite	$C_{fix}/O_{iron\ oxide}$
1	82.5%	17.5%	0.0%	1.6%	1.0
2	79.4%	16.5%	4.1%	1.6%	1.0
3	76.7%	15.6%	7.8%	1.6%	1.0
4	74.2%	14.7%	11.1%	1.6%	1.0
5	72.1%	14.0%	14.0%	1.6%	1.0

the biomass reductants had little effect on metallisation rate, but certain biomass reductants had a substantial influence on the strength and volumetric shrinkage of the pellets. The compressive strength of pellets with straw was relatively higher, while the strength of pellets with charcoal or bamboo charcoal was low.

Biomass includes all animals, plants, and microorganisms, including organic waste residues. Thus, maximising the use of biomass could potentially relieve the global energy crisis. The large amount of animal dung produced as a by-product of the Agricultural Industry is causing an increasingly serious environmental problem [13], with the stock of cow dung topping the list. Researchers have made extensive studies regarding the issue of cow dung utilisation. Cow dung reclamation technology, such as energy, composting, and animal feed, has achieved considerable economic and social benefits [14–17]. Other than this, researchers are also exploring the applications of cow dung in areas such as new preparation methods of biomass carbon materials [18–20] and solid waste disposal [21, 22].

Similar to other plant biomass, cellulose, hemicellulose, and lignin are the main chemical constituents of dry cow dung. The similarity of organic components between cow dung and plant biomass makes it feasible to use cow dung as an alternative reducing agent in iron ore reduction, and this has been demonstrated in various studies. Rath et al. [23] used cow dung as a reductant in the reduction roasting of an iron ore slime containing 56.2% Fe. A concentrate of ~64% Fe, with a recovery of ~66 wt%, was obtained from the reduced product after being subjected to low intensity magnetic separation. Under similar conditions, a concentrate of ~66% Fe, with a recovery of only 35 wt%, was obtained after using conventional charcoal as the reductant (93.5% fixed carbon and 1.2% volatile matter), which demonstrated that cow dung was a better reductant.

The key purpose of this study is to investigate the effect of cow dung addition on the strength of carbon-bearing iron ore pellets and its mechanism. The influence of cow dung addition on the quality of green and dry pellets is evaluated based on FTIR analysis, and the mechanism of strength variation of reduction roasted pellets was investigated by analysing the phase composition and microstructure using XRD and SEM, to provide a benchmark for further utilisation of cow dung in direct-reduction ironmaking.

2. Materials and Methods

2.1. Materials. Carbon-bearing iron ore pellets were prepared by pressing a mixture consisting of iron ore, anthracite, bentonite, and different proportions of cow dung. The chemical composition of the iron ore used in this study is shown in Table 1, while the proximate analyses of the anthracite and the cow dung used as the reductant in this study are given in Table 2. The cow dung was obtained from the Mengniu Modern Animal Husbandry (Group), Maanshan Co. First, all of the raw materials were dried at 383 K for 24 h, individually ground in a ball mill to a passing size of 74 μm for the iron ore and 200 μm for the reducing agents. Mixtures of the ground materials were prepared according to the experimental plan given in Table 3. A little water was added, and 20 mm diameter pellets (molar ratio of $C_{fix}/O_{iron\ oxide}$ = 1) were prepared by pressing at 10 MPa.

2.2. Characterization Techniques. Characterization studies were undertaken on the raw materials and some reduction roasted products. The FTIR spectra were obtained with a Nicolet 8700 spectrophotometer by adding 32 scans at a resolution of 4 cm^{-1}, using KBr wafers containing about 0.5 g of sample, which had been dried at 393 K for 24 h before spectral analysis. XRD was carried out with a D8 Advance X-ray powder diffractometer using Cu-Kα radiation. The voltage and current of the machine were set at 60 kV and 80 mA, respectively, scanning from 20° to 80° using a step size of 0.02°. A scanning electron microscope (NOVA Nano SEM430, USA) equipped with EDS detector was used for the microstructure studies.

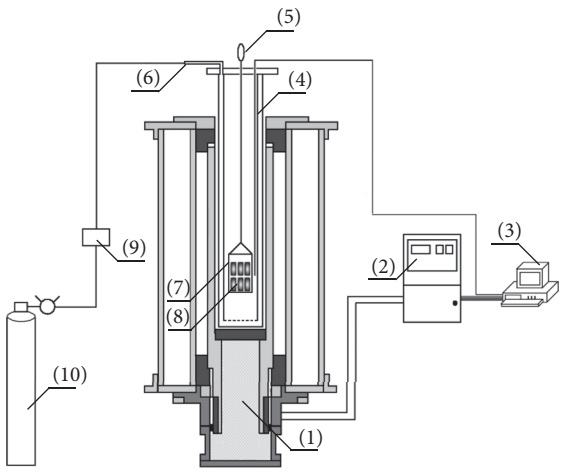

(1) Tubular furnace
(2) Temperature control panel
(3) Integrated console
(4) Thermocouple
(5) Hanging hook
(6) Inlet pipe
(7) Ni-Cr basket
(8) Carbon-bearing pellets
(9) Mass flow controller
(10) Nitrogen gas

Figure 1: A schematic of experimental apparatus of reduction roasting.

2.3. Strength Tests and Reduction Roasting. The compressive strength of green, dry, and reduction roasted pellets was measured with an automatic compressive strength tester, and each sample was tested 20 times under the same conditions and the results were averaged. A schematic of the reduction roasting experimental apparatus is shown in Figure 1. The furnace has a working temperature range of 298–1573 K, with ±1 K temperature control accuracy, and produces a 150 mm hot zone. The carbon-bearing pellets were placed in a Ni-Cr alloy basket which was hung over the hot zone, and the pellets were heated to 1523 K at a rate of 20 K/min. High-purity nitrogen gas was supplied at a constant flowrate of 1 l/min in the reaction tube. At the end of the experiment, the basket was quickly moved to the top of the furnace with high-purity nitrogen gas continuing to be supplied until the pellets cooled to room temperature.

3. Results and Discussion

3.1. Effects of Treated Cow Dung Addition on the Cold Strength of Carbon-Bearing Pellets. The cold strength test results of green and dry pellets with different proportions of cow dung addition are shown in Figure 2. The bar charts show that the strength of green and dry pellets varies with cow dung addition, but there is no clear correlation between the average compressive strength and the ratio of cow dung to anthracite added. The average strength of the green pellets containing cow dung decreased by 8–16% relative to pellets with no dung. For example, the strength of green pellets with no dung was 10.1 N/pellet, while green pellets with a dung-to-anthracite ratio of 1 : 4 (containing 4.1% cow dung) were 8.5 N/Pellet and the strength of green pellets with a dung-to-anthracite ratio of 3 : 4 (containing 11.1% cow dung) was 8.6 N/Pellet. In contrast, the average strength of dry pellets containing cow dung was between 33.5% and 56.6% higher than dry pellets with no cow dung. For example, the average strength of dry pellets with no cow dung was 18.2 N/pellet, while pellets with a dung-to-anthracite ratio of 1 : 4 had an average strength of 27.7 N/pellet.

The FTIR spectral analyses of different pellet samples are provided in Figure 3, which shows that the spectrum of the iron ore-anthracite sample (Figure 3(a)) aligns closely with the spectrum of the iron ore-anthracite-bentonite sample (Figure 3(b)). The main absorption peaks appear at 3413 cm^{-1} (stretching vibration centre of hydroxy-OH), 1619 cm^{-1} (anti-symmetric vibration peak of carboxyl-COOH) and 1032 cm^{-1} (Si-O bond stretching vibration of silicate impurities). This demonstrates that bentonite is not chemically adsorbed with the raw materials such as iron ore and anthracite, and it can be assumed that the strength of these green pellets with no cow dung was maintained by alternative strength mechanisms such as capillary and viscous forces.

A SEM backscattered image of a cross-sectioned dry pellet sample with no added cow dung is shown in Figure 4(a). The bentonite, iron concentrate, and finely pulverised coal particles have formed a gel, which has surrounded or coated the particles. The gel has a bridging effect and increases the bridge fluid viscosity and surface tension, strengthening the capillary and viscous forces that bind the particles in the green pellets [24]. In the drying process, the bentonite can make the solid particles be further drawn by the gel, the area of particle contact be increased, the intermolecular forces be strengthened, and the strength of the dry pellet be improved [25].

The FTIR spectra of a pellet sample containing anthracite, iron ore, and cow dung are shown in Figure 3(c), while a pellet sample containing anthracite, iron ore, cow dung, and bentonite is shown in Figure 3(d). The main absorption peaks in Figure 3(c) appear at 3423 cm^{-1}, 1631 cm^{-1}, 1423 cm^{-1}, and 1032 cm^{-1}, while the main peaks in Figure 3(d) appear at 3420 cm^{-1}, 1633 cm^{-1}, and 1032 cm^{-1}. The stretching vibration peak of hydroxy-OH and antisymmetric peak of carboxyl-COOH have shifted and increased in intensity. Near 1423 cm^{-1}, the lignin double bond or the hydroxy of carboxylic acid has generated an in-plane bending vibration peak, which suggests that chemical adsorption has probably occurred between the cellulose, hemicellulose, and free hydroxy of lignin and iron ore.

A SEM backscattered image of a cross-sectioned dry pellet sample containing 14.0% cow dung is shown in Figure 4(b). It can be seen in the figure that the bentonite, iron ore, and finely pulverised coal have formed a gel, infilled with or coating, particles, similar to that observed in the sample that did not contain cow dung (Figure 4(a)). The cellulose and hemicellulose in the particles of cow dung have a rope-shaped arrangement that reinforces the structure of the dry pellets and results in greater strength compared with the dry pellets that did not contain any cow dung.

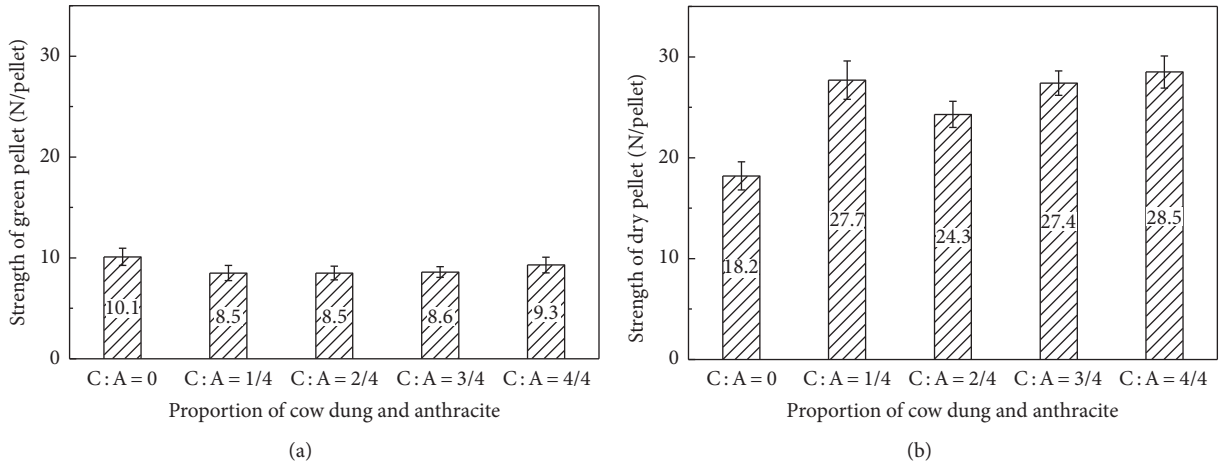

Figure 2: Cold strength of carbon-bearing pellets with different proportions of cow dung. (a) Green pellet; (b) dry pellet.

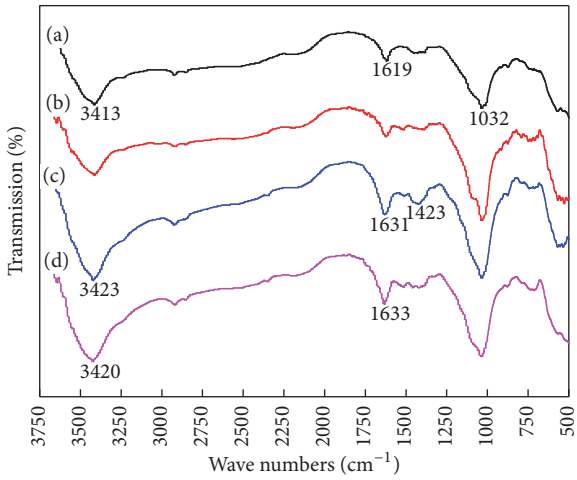

(a) Anthracite and iron ore
(b) Anthracite, iron ore, and bentonite
(c) Anthracite, iron ore, and cow dung (C : A = 4/4)
(d) Anthracite, iron ore, bentonite, and cow dung (C : A = 4/4)

Figure 3: FTIR spectra of carbon-bearing pellets, comparing different raw materials.

3.2. Effects of Treated Cow Dung Addition on the Strength of Carbon-Bearing Pellets after Reduction Roasting. The average strength of pellets that contained different proportions of cow dung after reduction roasting at 1523 K is given in Figure 5. The bar chart shows that the strength of the roasted sample with no cow dung was 2473 N/pellet. The pellets that had cow dung additive had a higher strength, but the strength decreased with increasing cow dung addition. The pellets containing 4.1% cow dung had a strength of 3106 N/pellet after reduction roasting, which was the highest strength obtained (an increase of 25.6%).

The strength of reduction roasted pellets is controlled by the rate of formation of intergrown iron crystals, their abundance, and physical structure, while the bentonite binder will have little effect on pellet strength after roasting [26]. When a mixture of anthracite and cow dung is used as a reducing agent in carbon-bearing pellets, the volatile matter in the cow dung cracks at about 773 K and will produce H_2, CO, CO_2, CH_4, and other gases [27]. Reduction reactions may occur directly between H_2, CO, and CH_4, while CO (which is a strong reductive agent) will be formed according to the Boudouard reaction between C (originating from the anthracite and cow dung additives) and CO_2. Devolatilisation generates pores within the carbon-bearing pellets, which increases their permeability to the reducing gases, promoting the rate of reduction and formation of intergrown iron crystals.

Table 4: Degree of metallization of carbon-bearing pellets after reduction roasting (%).

Sample number	Total Fe	Metal Fe	R_m
1	81.9	71.0	86.7
2	79.6	70.5	88.6
3	78.0	67.6	86.6
4	76.4	62.6	82.0
5	74.9	60.1	80.3

The size of the carbon-bearing pellets before and after reduction roasting is compared in Figure 6, which shows that the diameter of the sample with no cow dung contracted by 19%, and the sample with 7.8% cow dung contracted by 24%, while the sample containing 14.0% cow dung contracted by 28%. Thus, it can be concluded that the pellet shrinkage increases with increasing cow dung content. The shrinkage of reduction roasted pellets is mainly the result of aggregation of intergrown iron crystals, but porosity and the amount of low melting-point slag present may also influence the extent of pellet shrinkage [28]. However, Figures 5 and 6 show that the pellet shrinkage does not clearly correlate with higher pellet strength.

The metallisation degree of carbon-bearing pellets after reduction is shown in Table 4. It can be seen that the metal produced of reduction sample gradually decreases with increase of amount of the cow dung. The pellets containing 4.1% cow dung had a degree of metallisation of 88.6%

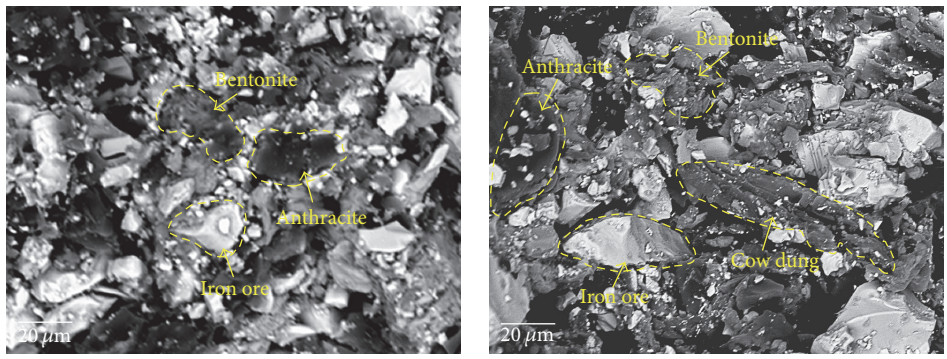

(a) (b)

Figure 4: SEM back scattered images of different carbon-bearing pellets after drying. (a) Dry pellet sample without cow dung; (b) dry pellet sample with 14.0% cow dung.

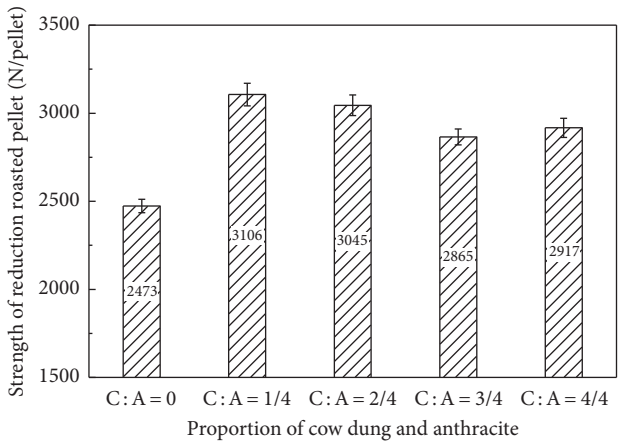

Figure 5: Strength of different carbon-bearing pellets after reduction roasting at 1523 K.

after reduction roasting, which was the highest degree of metallisation obtained.

3.3. Phase Analysis of Carbon-Bearing Pellets after Reduction Roasting. Figure 7 shows the XRD spectra of different pellet samples after reduction roasting at temperatures of 873, 1073, 1273, and 1523 K. It can be seen in Figure 7(a) that, after roasting at 873 K, the sample containing no cow dung additive was mainly composed of magnetite (Fe_3O_4) and a small amount of hematite (α-Fe_2O_3) and maghemite (γ-Fe_2O_3). In comparison, the peak intensity of α-Fe_2O_3 is smaller, while the peak intensity of Fe_3O_4 is larger, in the sample that originally contained 7.8% cow dung. When this sample (7.8% cow dung) was reduction roasted at 1073 K, diffraction peaks for wüstite (FeO) appeared, while the diffraction peaks of Fe_2O_3 were no longer detected (Figure 7(b)). After reduction roasting at 1273 K, diffraction peaks for metallic Fe were present, and their intensity was stronger in the sample with 7.8% cow dung compared to the sample with no cow dung (Figure 7(c)). Following reduction roasting at 1523 K, the XRD spectrum of the sample initially containing 7.8% cow dung consisted mainly of Fe diffraction peaks (Figure 7(d)). The results in Figure 7 demonstrated that cow dung addition and reduction temperature affect the extent of reduction of the iron oxides in the pellets. Taking into account the degree of metallisation in Table 4, it can be concluded that the extent of reduction at 1523 K decreases when the amount of cow dung additive exceeds about 4–8%.

SEM backscattered images of different carbon-bearing pellet samples reduction roasted at 1273 and 1523 K are shown in Figure 8. Figure 8(a) shows that the edges of iron ore particles were blurred and boundaries between some of the ore and reducing agent particles were hard to distinguish in the sample that had no cow dung addition after roasting at 1273 K. There were few small particles of reducing agent observed, and the structure of the pellet was relatively loose. For the sample with 7.8% cow dung (Figure 8(b)), whole iron ore particles were hard to distinguish, while some metallic iron had formed on the surface of some iron ore and reducing agent particles. The microstructure of the roasted samples that contained 7.8% and 14.0% cow dung (Figures 8(b) and 8(c)) was relatively similar. After reduction roasting at 1523 K, the discrete particles of iron ore, reducing agent, and other raw materials disappeared (Figures 8(d)–8(f)), and the reduction product was predominantly metallic iron with a minor amount of iron oxide. In the sample with no added cow dung (Figure 8(d)), the metallic iron phase is connected by a number of fine grains and there are a considerable number of pores or voids in the pellets. The metallic iron in the samples with 7.8% and 14.0% cow dung is flaky, but the sample with 14.0% cow dung has more voids and the amount of solid solution formed by the metallic iron and incompletely reduced iron oxide is more abundant.

Figures 7 and 8 demonstrate the effect of cow dung addition and the influence of temperature on the microstructure and phase composition of reduction roasted pellets. After reduction roasting at 1523 K, the intergrown iron crystals in pellets that contained cow dung are strongly clustered compared with the samples containing no cow dung. The higher ash content of the cow dung compared to the anthracite can improve the quaternary basicity (mass ratio of $(CaO + MgO)/(SiO_2 + Al_2O_3)$) of the carbon-bearing pellets,

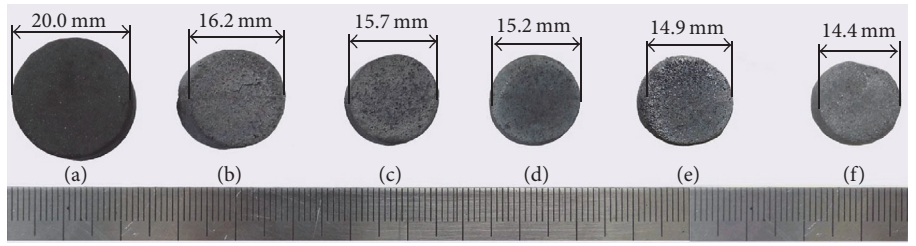

(a) Original sample
(b) Cow dung 0%
(c) Cow dung 4.1%
(d) Cow dung 7.8%
(e) Cow dung 11.1%
(f) Cow dung 14.0%

Figure 6: Size of the carbon-bearing pellets before and after reduction roasting.

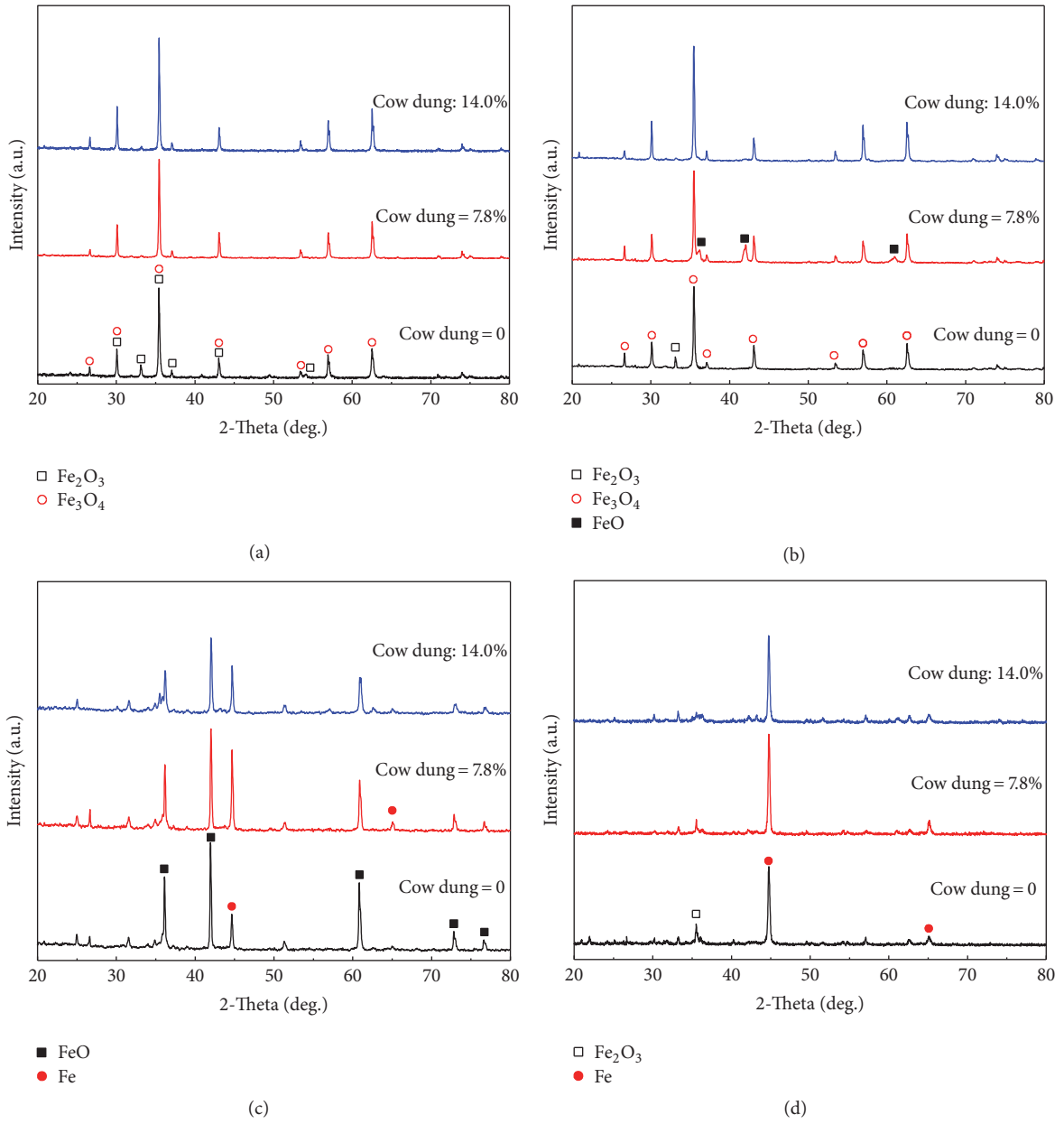

Figure 7: XRD of different carbon-bearing pellets after reduction at different temperatures. (a) 873 k; (b) 1073 k; (c) 1273 k; (d) 1523 k.

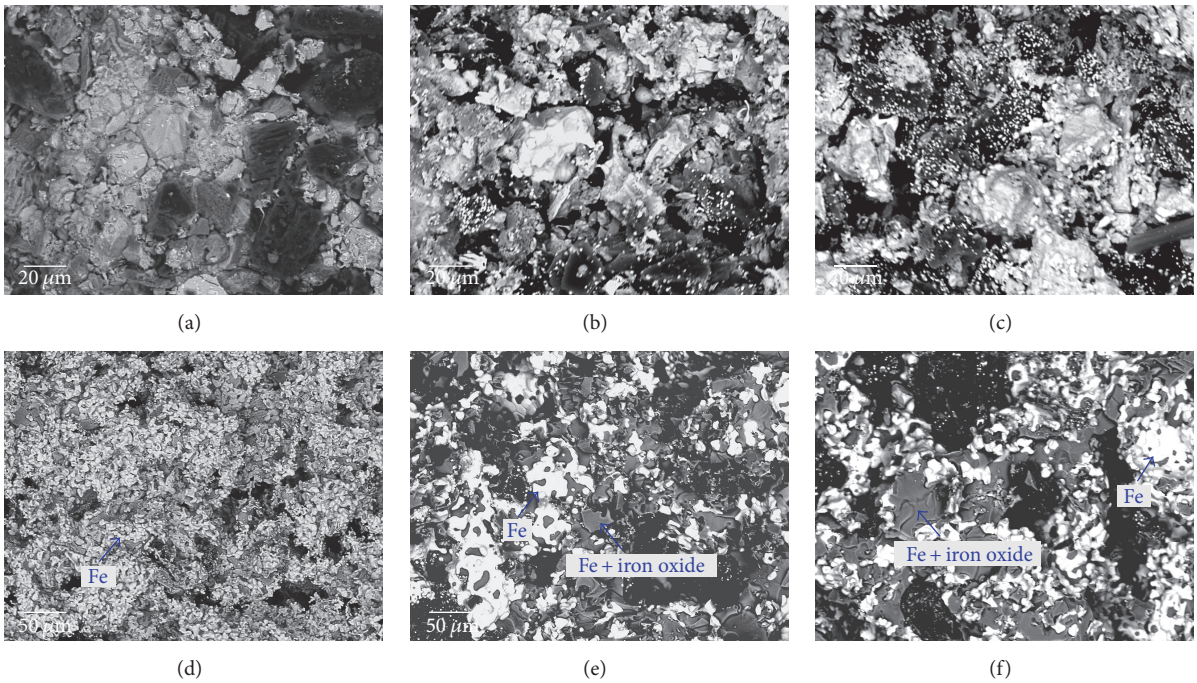

FIGURE 8: SEM backscattered images of different carbon-bearing pellets after reduction at 1273 and 1523 K. (a) 1273 k, cow dung 0%; (b) 1273 k, cow dung 7.8%; (c) 1273 k, cow dung 14.0%; (d) 1523 k, cow dung 0%; (e) 1523 k, cow dung 7.8%; (f) 1523 k, cow dung 14.0%.

promoting the reduction of iron oxides and facilitating the aggregation of intergrown iron crystals [29]. The larger amount of low melting-point amorphous slag produced can infill the pores, making the structure of the pellets stronger and more compact after reduction. However, an excessive addition of cow dung (of more than about 4–8%) will lead to more voids caused by hydrocarbon cracking and volatilisation, which will decrease the extent of metallisation during the reduction of iron oxides, resulting in a decrease pore filling by amorphous slag phases as well as decrease roasted pellet strength, compared with pellets that contained about 4% cow dung.

4. Conclusions

The following conclusions can be made through this study.

(1) The addition of cow dung affects the strength of carbon-bearing pellets. The green pellet strength decreased by about 8–16% and the dry strength increased by about 34–57% after adding cow dung. However, there was no obvious correlation between the quantity of cow dung added and the change in cold pellet strength. Compared with reduction roasted pellets containing no cow dung, roasted pellets containing cow dung had greater strength (ranging from about 16–26% stronger), but the strength decreased as the proportion of cow dung increased.

(2) The lower strength of green pellets containing cow dung was found to be due to expansion of the amorphous region of the cellulose contained in the cow dung. The greater strength of dry pellets containing cow dung was found to be the result of chemical adsorption among cellulose, hemicellulose, and free hydroxy in lignin and iron concentrate. The rope arrangement of cellulose and hemicellulose also positively reinforces the pellet structure.

(3) In process of reduction roasting of carbon-bearing pellets, cow dung additions is beneficial for aggregation of intergrown iron crystals and may help to increase the density of the physical structure of the pellets; thus the strength of the reduction roasted pellets is also improved. However, excessive addition of more than about 4–8% cow dung will result in lower pellet density and decreased strength compared with pellets containing about 4% cow dung.

Conflicts of Interest

The authors declare that they have no conflicts of interest.

Acknowledgments

The authors would like to acknowledge the funding from the Natural Science Foundation of China (Project no. 51574002).

References

[1] G. Q. Xu, "Newest advances and development prospect of COREX technology," *Ironmaking*, vol. 23, no. 2, pp. 50–55, 2004.

[2] W.-K. Lu and D. F. Huang, "The evolution of ironmaking process based on coal-containing iron ore agglomerates," *ISIJ International*, vol. 41, no. 8, pp. 807–812, 2001.

[3] S. L. Liu and C. G. Bai, "Technology research and development trend of direct reduction," *Journal of Iron and Steel Research*, vol. 23, no. 3, pp. 1–5, 2011.

[4] R. Wei, L. Zhang, D. Cang, J. Li, X. Li, and C. C. Xu, "Current status and potential of biomass utilization in ferrous metallurgical industry," *Renewable & Sustainable Energy Reviews*, vol. 68, pp. 511–524, 2017.

[5] Y. Ueki, R. Yoshiie, I. Naruse et al., "Reaction behavior during heating biomass materials and iron oxide composites," *Fuel*, vol. 104, pp. 58–61, 2013.

[6] G. Fick, O. Mirgaux, P. Neau, and F. Patisson, "Using biomass for pig iron production: A technical, environmental and economical assessment," *Waste and Biomass Valorization*, vol. 5, no. 1, pp. 43–55, 2014.

[7] M. Gan, X. Fan, X. Chen et al., "Reduction of pollutant emission in iron ore sintering process by applying biomass fuels," *ISIJ International*, vol. 52, no. 9, pp. 1574–1578, 2012.

[8] T. Kawaguchi and M. Hara, "Utilization of biomass for iron ore sintering," *ISIJ International*, vol. 53, no. 9, pp. 1599–1606, 2013.

[9] V. Strezov, "Iron ore reduction using sawdust: Experimental analysis and kinetic modelling," *Journal of Renewable Energy*, vol. 31, no. 12, pp. 1892–1905, 2006.

[10] R. Wei, D. Cang, Y. Bai, D. Huang, and X. Liu, "Reduction characteristics and kinetics of iron oxide by carbon in biomass," *Ironmaking and Steelmaking*, vol. 43, no. 2, pp. 144–152, 2016.

[11] Z. L. Liu, F. L. Wang, J. L. Wang, Z. P. Gao, and H. H. Liu, "Study on the Reduction Process of Carbon-Bearing Pellets from Agricultural Waste," *Journal of Hunan University of Technology*, vol. 28, no. 1, pp. 87–92, 2014.

[12] H. Han, P. Yuan, D. Duan, and D. Li, "Application of biomass to the RHF direct reduction process," *Chongqing Daxue Xuebao/Journal of Chongqing University*, vol. 38, no. 5, pp. 164–170, 2015.

[13] W. Li, M. Xu, and J. Li, "Prospect of resource utilization of animal faeces wastes," *Nongye Jixie Xuebao/Transactions of the Chinese Society for Agricultural Machinery*, vol. 44, no. 5, pp. 135–140, 2013.

[14] J. Liu, S. Wang, Q. Wei, and S. Yan, "Present situation, problems and solutions of China's biomass power generation industry," *Energy Policy*, vol. 70, pp. 144–151, 2014.

[15] S. Zhou, Y. Zhang, and Y. Dong, "Pretreatment for biogas production by anaerobic fermentation of mixed corn stover and cow dung," *Energy*, vol. 46, no. 1, pp. 644–648, 2012.

[16] T. Karak, I. Sonar, R. K. Paul et al., "Composting of cow dung and crop residues using termite mounds as bulking agent," *Bioresource Technology*, vol. 169, pp. 731–741, 2014.

[17] A. Kumar, N. Kumar, P. Baredar, and A. Shukla, "A review on biomass energy resources, potential, conversion and policy in India," *Renewable & Sustainable Energy Reviews*, vol. 45, pp. 530–539, 2015.

[18] K. S. Ro, K. B. Cantrell, and P. G. Hunt, "High-temperature pyrolysis of blended animal manures for producing renewable energy and value-added biochar," *Industrial & Engineering Chemistry Research*, vol. 49, no. 20, pp. 10125–10131, 2010.

[19] D. Bhattacharjya and J.-S. Yu, "Activated carbon made from cow dung as electrode material for electrochemical double layer capacitor," *Journal of Power Sources*, vol. 262, pp. 224–231, 2014.

[20] P. Vijayaraghavan, S. G. Prakash Vincent, and G. S. Dhillon, "Solid-substrate bioprocessing of cow dung for the production of carboxymethyl cellulase by *Bacillus halodurans* IND18," *Waste Management*, vol. 48, pp. 513–520, 2016.

[21] D. Singh and M. H. Fulekar, "Benzene bioremediation using cow dung microflora in two phase partitioning bioreactor," *Journal of Hazardous Materials*, vol. 175, no. 1-3, pp. 336–343, 2010.

[22] D. D. Das, R. Mahapatra, J. Pradhan, S. N. Das, and R. S. Thakur, "Removal of Cr(VI) from aqueous solution using activated cow dung carbon," *Journal of Colloid and Interface Science*, vol. 232, no. 2, pp. 235–240, 2000.

[23] S. S. Rath, D. S. Rao, and B. K. Mishra, "A novel approach for reduction roasting of iron ore slime using cow dung," *International Journal of Mineral Processing*, vol. 157, pp. 216–226, 2016.

[24] S. K. Kawatra and S. J. Ripke, "Effects of bentonite fiber formation in iron ore pelletization," *International Journal of Mineral Processing*, vol. 65, no. 3-4, pp. 141–149, 2002.

[25] S. K. Kawatra and S. J. Ripke, "Laboratory studies for improving green ball strength in bentonite- bonded magnetite concentrate pellets," *International Journal of Mineral Processing*, vol. 72, no. 1-4, pp. 429–441, 2003.

[26] J. Li, R. Wei, H. Long, P. Wang, and D. Cang, "Sticking behavior of iron ore-coal pellets and its inhibition," *Powder Technology*, vol. 262, pp. 30–35, 2014.

[27] K. B. Cantrell, P. G. Hunt, M. Uchimiya, J. M. Novak, and K. S. Ro, "Impact of pyrolysis temperature and manure source on physicochemical characteristics of biochar," *Bioresource Technology*, vol. 107, pp. 419–428, 2012.

[28] R. F. Wei, J. X. Li, G. W. Tang, and D. Q. Cang, "Strength and consolidation mechanism of iron ore and coal pellets," *Ironmaking and Steelmaking*, vol. 41, no. 7, pp. 514–520, 2014.

[29] T. Miki and Y. Fujita, "Reaction between iron oxide and gangue minerals at 1 373 K under Ar atmosphere," *ISIJ International*, vol. 55, no. 6, pp. 1206–1209, 2015.

Hindawi
Advances in Materials Science and Engineering
Volume 2017, Article ID 9404801, 8 pages
https://doi.org/10.1155/2017/9404801

Research Article

Gasification Reaction Characteristics between Biochar and CO_2 as well as the Influence on Sintering Process

Min Gan, Wei Lv, Xiaohui Fan, Xuling Chen, Zhiyun Ji, and Tao Jiang

School of Minerals Processing & Bioengineering, Central South University, Changsha, Hunan 410083, China

Correspondence should be addressed to Xiaohui Fan; csufxh@126.com

Received 4 June 2017; Accepted 17 September 2017; Published 23 October 2017

Academic Editor: Merrick Mahoney

For achieving green production of iron ore sintering, it is significant to substitute biochar, which is a clean and renewable energy, for fossil fuels. In this paper, the gasification reaction between CO_2 and biochar was investigated. The results showed the initial temperature and the final temperature of the gasification reaction between biochar and CO_2 were lower, while the maximum weight loss rate and the biggest heat absorption value were much higher than those of coke breeze, which indicated gasification reaction between the biochar and CO_2 occurred rapidly at lower temperature. The gasification activation energy of biochar was 131.10 kJ/mol, which was lower than that of the coke breeze by 56.26 kJ/mol. Therefore, biochar had a higher reactivity and easily reacted with CO_2 to generate CO. As a result, when biochar replaced coke powder at equal heat condition in sintering process, the combustion efficiency of fuel decreased and was disadvantage to the mineralization of iron ores at high temperature. With the increase of substitute proportion, the sinter yield, tumble strength, and productivity were decreased. The proportion of biochar replacing coke breeze should not be higher than 40%. By reducing the heat replacement ratio of biochar, the yield and quality of sinter got improved.

1. Introduction

The energy consumption of the iron ore sintering process generally accounts for about 10% of iron and steel enterprises, 75%~80% of which are consumed in the form of solid fossil fuels like coke breeze or anthracite [1, 2]. Fuel cost accounts for 40% or more of the sinter processing costs [3]. Also, previous research found that the combustion of solid fossil fuels served as the main source of CO_2, SOx, NOx, and so on in this process [4, 5]. To address these problems, substituting extensively distributed, renewable, and clean biochar for fossil fuels in sintering process was believed to be a promising strategy to reduce the emissions of CO_2, SOx, NOx, and so on [6–10].

CSIRO in Australia conducted a study on the application of charcoal in iron ore sintering process. The results showed that the ash content of charcoal produced by red eucalyptus was low and the residual impurities were few after burning. When applied to sintering process, the biochar could replace part of the coke breeze but reduced the strength of the sinter product. In particular, the tumble strength was reduced significantly when biochar dosage was high [11, 12]. The British and Dutch scholars of the Corus Technology and Development Research Center jointly conducted a series of sintering tests which used the sunflower seed shells to replace part of the coke breeze. The results showed that it was feasible to use sunflower seed shell to replace 10% coke breeze in iron ore sintering. The sintering characteristics were similar to the ones when using coke breeze only, while the sintering time shortened and the productivity was improved by 6.4%. However, when the substitution ratio was 20% or higher, the sintering production and quality indicators deteriorated seriously [13, 14]. Brazil research institutions used biochar powder with grain size of 5–10 mm to replace 6% and 12% coke breeze for sintering production, finding that sinter products with the large specific surface area and good metallurgical performance were obtained, and the products could meet the requirements of blast furnace although the tumble strength reduced [15]. Liming LU from CSIRO found that, compared with the sinter fired with coke breeze, the sinter from the mixtures with ≤50% coke powder replaced by charcoal was marginally weaker in terms of sinter yield, tumble strength, and reduction disintegration [16, 17]. Our

Table 1: Chemical compositions of raw materials and their proportions in mixture.

Types of raw materials	Chemical composition/wt-%							*Percent/wt-%
	TFe	FeO	SiO_2	CaO	MgO	Al_2O_3	LOI	
Iron ores blend	63.02	6.50	4.58	0.35	0.28	1.42	3.10	60.73
Dolomite	0.21	0.13	0.71	32.64	19.83	0.56	46.47	5.58
Limestone	0.14	0.10	1.49	50.66	2.28	0.43	40.72	2.16
Quicklime	0.4	0.23	2.86	76.69	1.18	1.20	12.36	4.62
Return fines	56.81	6.25	5.11	9.02	1.86	2.00	0.00	23.08

*The ratio was calculated when the proportion of coke was 3.85%.

Table 2: Ultimate and proximate analyses of solid fuels.

Fuel types	Ultimate analyses/wt-%			Proximate analyses (dry base)/wt-%			Calorific value/MJ·kg^{-1}
	C_{total}	S	N	Fixed carbon	Ash	volatile	
Coke breeze	78.89	0.500	0.72	74.68	19.54	5.88	26.84
Biochar	94.64	0.037	0.19	87.34	5.10	7.55	30.77

group also did a lot of work on the influences of biochar replacing coke breeze on sintering process. The research showed that it could reduce emissions of NOx, SOx, and so on when applying the carbonized products of straw, trees, and molded-sawdust [18–21].

There were lots of differences between biochar and conventional fuels in terms of chemical composition, physical properties, proximate analysis, and so on. Biochar replacing coke breeze would bring a series of changes to the behavior of the fuel in sintering process. Therefore, in this paper the differences between biochar and coke breeze in reactivity were studied, as well as the kinetic characteristics of biochar reacting with CO_2. In addition, the mechanism how biochar replacing coke breeze affected the yield and quality of sinter was revealed by researching the influences of biochar on combustion efficiency.

2. Materials and Methods

2.1. Raw Materials. Iron ore blend, solid fuels, fluxes (dolomite, limestone, and quicklime), and return fines were utilized to produce sinter. The chemical compositions of raw materials are shown in Table 1. Several kinds of iron ores were blended to satisfy the requirement of sinter compositions, with TFe (total iron content) of 57.5%, SiO_2 of 4.8% in sinter. Fluxes had the conventional compositions, and their percentages in mixture were calculated to meet basicity (CaO/SiO_2) of 2.0 and MgO of 2.0%.

Two types of solid fuels were applied in the experiments. One was coke breeze, which came from an industrial sintering plant, and the other was biochar carbonized from acutissima at 700°C for 30 min in nitrogen gas. Ultimate and proximate analyses of fuels are illustrated in Table 2. The chemical compositions of ash in fuels are shown in Figure 1. It can be seen that biochar had lower N and S contents, which was advantageous to reduce the generation of SOx and NOx. Compared with coke breeze, biochar was lower in ash content, but higher in fixed carbon, volatile, and calorific value.

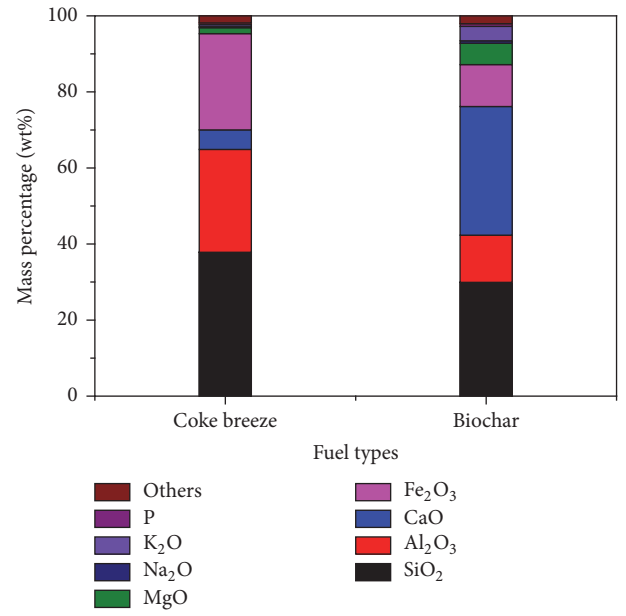

Figure 1: Chemical compositions of ash in fuels.

With the help of optical microscope, microstructures of coke breeze and biochar were obtained, as shown in Figure 2. Apparently, more microspores were distributed uniformly inside biochar and the majority of which were microscope. Porosity of biochar and coke breeze was measured by optical microscope, while specific surface areas were tested by Quantachrome Quadra Win. The biochar used in this paper was without activation, so nitrogen was used as adsorbate and BET method was used to calculate specific surface area. The porosity of biochar was 58.22%, which was higher than that of the coke breeze by 12.47%. The specific surface area of biochar was 54.76 m^2/g, which was 9.13 times bigger than that of coke breeze.

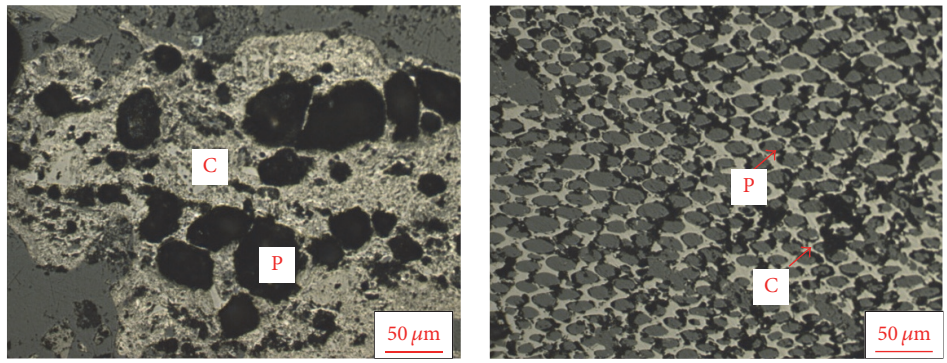

(a) (b)

Figure 2: Microstructure of solid fuels: (a) coke breeze; (b) biochar; C: carbon; P: pore.

2.2. Methods

2.2.1. Methods to Research Gasification Reaction Behavior. The reactivity of biochar under the nonisothermal condition was studied using the synchronous heat analyzer (NETZSCH STA 449C, German). 5.0 mg sample was put in the Al_2O_3 crucible of the thermobalance stent and heated by controlled computer process. The gas flow velocity was controlled, 0.5 m/s, and the speed of temperature increasing was 15°C/min. The TG-DTG curve and DSC curve of gasification reaction between the biochar and CO_2 were analyzed to obtain the characteristic parameters of gasification reaction, including reactions starting temperature (Ts), the end temperature (Te), the maximum weight loss rate (Vmax), and the maximum heat release (Qmax).

The reactivity of the biochar under isothermal conditions was studied in a vertical furnace. Using a fused silica tube with Φ38 × 550 mm as reaction tank, there was a cup for placing sample, which charged by 25 g dried fuel with a size fraction of 3 mm. The weight was measured and recorded by electronic balance and computer, respectively, and the system read the data every 20 s. Before starting the test, nitrogen as protective gas with flow rate of 5 L/min was passed into the tube until the temperature reached the preset temperature again. Then, the reaction tank was weighed and the nitrogen gas was cut off. Then inlet CO_2 with the flow rate of 10 L/min until the weight loss reached a constant value. Thus the gasification reaction conversion rate (x_c) and the instantaneous rate R at a certain time were calculated according to the weight loss value of each time. The formulas are as follows:

$$x_c = \left(1 - \frac{m}{m_0}\right) \times 100\%$$
$$R = -\frac{1}{m_0}\frac{dm}{dt}, \quad (1)$$

where x_c is conversion rate, %; R is reaction rate, %/min; m_0 is initial mass, g; m is the mass of reaction of the time t, g; dm/dt is weight loss rate at reaction of the time t, g/min.

The rate of gasification reaction was evaluated using the instantaneous rate $R_{1/2}$ at a fuel conversion of 50%.

2.2.2. Sintering Trials. Sintering process was simulated in a sinter pot of 180 mm diameter × 700 mm deep. The procedure involved ore proportioning, blending, granulation, ignition, sintering, and cooling. Raw materials were granulated in a drum of 600 mm diameter × 1400 mm deep for 4 min and then charged into the sinter pot. A hearth layer approximately 20 mm thick was used to protect the grate from thermal erosion. After charging, the fuel in the surface layer was ignited at 1150 ± 50°C for 1 min by an ignition hood. The combustion front moved downwards with the support of a downdraught system with a negative pressure of 10 kpa. In the sintering process, a infrared analyzer was used to detect the CO and CO_2 contents in exhaust gas, and combustion efficiency of $CO_2/(CO + CO_2)$ was calculated to assess the burning degree of fuels. After sinter cake discharging, dropping test (2 m ×3 times), screening, and tumble strength were carried out to evaluate the physical strength of sinter. Yield was the proportion of product sinter which deducted the hearth layer material and the fines −5 mm. Productivity was defined as the weight of product sinter produced per area per time. The test of tumble strength was conducted in a drum of Φ1000 × 500 mm where 7.5 kg product sinter was tumbled for 200r, then tumbled sinter was screened at 6.3 mm, and the proportion of +6.3 mm was treated as tumble strength. Sintering speed was the ratio between the height of sintering bed and the total sintering time.

During the sinter pot tests, the mass of biochar was calculated on the basis of replacement percentage biochar replacing coke and the heat replacement ratio by

$$m_b \cdot h_b \cdot a = m_c \cdot h_c \cdot r, \quad (2)$$

where m_b is the mass of biochar, kg; m_c is the mass of coke for the base case, kg; r is the percentage of biochar replacing coke, which means the reduction percentage of coke compared to the base case as biochar replacing coke; h_c is the calorific value of coke, MJ·kg^{-1}; h_b is the calorific value of biochar, MJ·kg^{-1}; a is the heat replacement ratio, which means that 1 kj heat released by biochar can replace the amount of heat released by coke; as $a = 1$, it means that the heat of biochar combustion was equivalent to that for the coke breeze substituted.

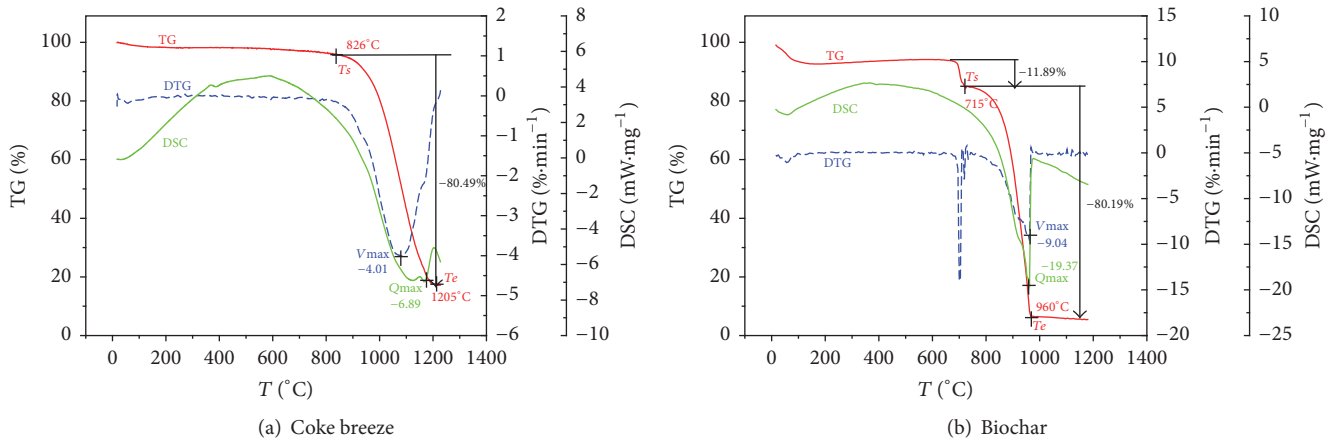

(a) Coke breeze (b) Biochar

Figure 3: TG-DSC curves of nonisothermal gasification of fuels.

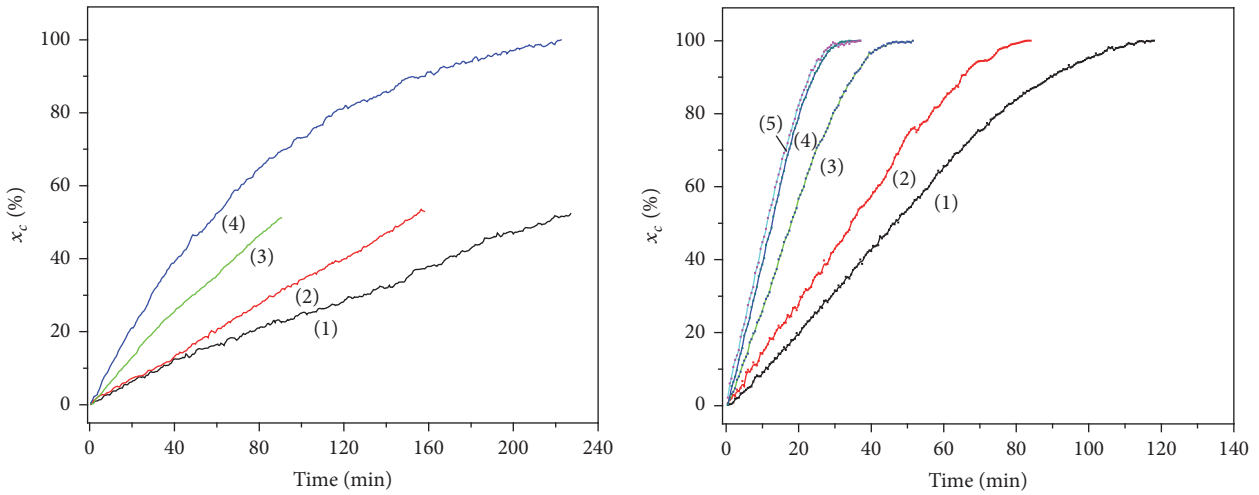

(1) 950°C
(2) 1000°C
(3) 1050°C
(4) 1100°C

(a) Coke breeze

(1) 900°C
(2) 950°C
(3) 1000°C
(4) 1050°C
(5) 1100°C

(b) Biochar

Figure 4: Effect of temperature on gasification of fuels.

3. Results and Discussion

3.1. Thermochemical Behavior of Biochar

3.1.1. Gasification Characteristic Parameters. The TG-DSC curves of nonisothermal gasification of fuels are shown in Figure 3. Biochar heated in CO_2 atmosphere went through four stages, which were drying, warming up, volatiles desorption, and gasification reaction of carbon, respectively. Volatile began to separate out when the temperature reached a certain value, compared with coke breeze, the weight loss of biochar during which process was more obvious and the volatile weight loss ratio could normally reach more than 8%. After the desorption of volatile, it came to the gasification of fixed carbon, and the weight loss ratio of fuel sped up significantly. The DTG and DSC curves of biochar showed sharp peaks, indicating that the reaction was more intense compared with coke breeze.

The TG-DTG and DSC curves of fuels' gasification were analyzed to obtain the characteristic parameters. It showed that biochar started to gasify at low temperature, and the reaction starting temperature (*Ts*) and the end temperature (*Te*) were both lower than those of the coke breeze, while the maximum weight loss rate (*V*max) and maximum heat absorption value (*Q*max) were both higher than those of the coke breeze. It manifested that biochar had a higher reactivity than coke breeze and easily reacted with CO_2 to generate CO.

3.1.2. Gasification Dynamics. The reaction rates of biochar and coke breeze with CO_2 were studied by isothermal thermogravimetric analysis and the conversion rates are shown in Figure 4. For comparing the gasification process between

Table 3: Activation energy of fuel gasification and the transition temperature of every zone.

Fuel	Activation energy/kJ·mol^{-1}			Transition temperature/°C	
	Chemical reaction	Internal diffusion	External diffusion	Chemical reaction → internal diffusion	Internal diffusion → external diffusion
Coke breeze	187.36	77.16	33.51	950	1100
Biochar	131.10	71.82	31.88	900	1000

fuel and CO_2, the rate of gasification reaction was evaluated by the instantaneous speed ($R_{1/2}$) when the conversion rate was 50%. It was known from Figure 3 that, at the same temperature, the gasification reaction rate of the biochar was 3.85%/min, which was faster than that of the coke breeze (0.57%/min) at 1050°C. With temperatures rising, gasification reaction speed of fuel got faster, which shortened the time during which fuel conversion rate reached 50%. When the temperature ranged from 950°C to 1100°C, the gasification reaction rate ($R_{1/2}$) of biochar increased from 1.50%/min to 4.35%/min, and $t_{1/2}$ decreased from 34.33 min to 11.52 min.

In this paper, a typical shrinking core reaction model was used to study the gasification reaction kinetics of solid fuels. The reaction can be divided into three zones: chemical reaction kinetics zone, inner diffusion zone, and outer diffusion zone. In the chemical reaction kinetics zone, the controlling factor of the reaction rate is the chemical reaction of coke and CO_2. In the outer diffusion zone, the controlling factor is the effect of CO_2 diffusing to coke surface, while the internal diffusion zone is affected by both chemical reaction and diffusion. Tseng and Edgar [22] analyzed the different reaction zones of coke. In the chemical reaction kinetics zone, the kinetic constant of coke gasification reaction is expressed by the following formula:

$$k_v = \frac{1}{P_{O_2} t_{1/2} S_0} \int_0^{0.5} \frac{S_0}{S} dx_c. \quad (3)$$

The internal diffusion rate constant of coke gasification in the internal diffusion zone is described in the following formula:

$$k_s = \frac{r_0}{P_{O_2}{}^a t_{1/2}} \left(1 - \sqrt[3]{\frac{1}{2}}\right). \quad (4)$$

In the outer diffusion zone, the external diffusion rate constant of coke gasification is represented by the following formula:

$$S_h = \frac{(1 - x_a)\, \rho_p r_0^2 RT}{D_b \omega P_{O_2} t_{1/2}} \left(1 - \sqrt[3]{\frac{1}{4}}\right). \quad (5)$$

In the formula, k_v is gasification rate constant; k_s is the internal diffusion rate constant; S_h is the outer diffusion rate constant; x_c is coke conversion rate; $t_{1/2}$ is the reaction time when the conversion rate reached 50%; S is specific surface area at any time during gasification process; P_{O_2} is the oxygen partial pressure; n is intrinsic reaction order; a is apparent reaction order; r_0 is initial particle radius of coke; D_b is diffusion coefficient of CO_2; x_a is ash ratio; ω is the amount of carbon consumed per mole of CO_2; R is gas constant.

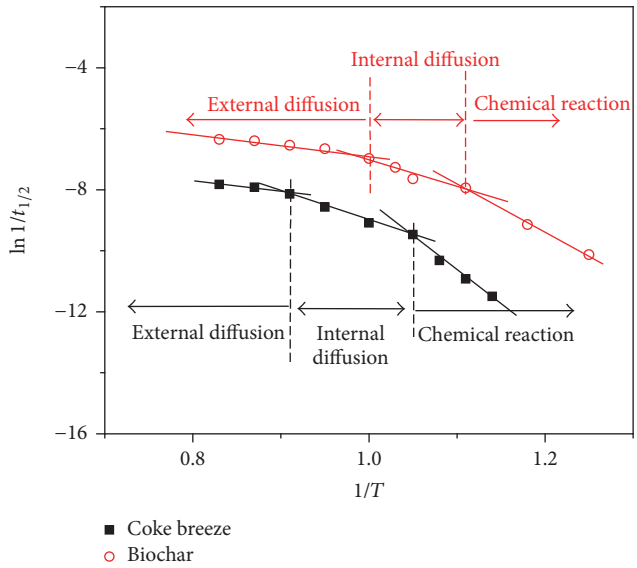

Figure 5: Relationship between ln $1/t_{1/2}$ and $1/T$ of fuel gasification.

The reaction rate constant $k(T)$ can be represented by the Arrhenius formula

$$k(T) = k_0 \exp\left(-\frac{E}{RT}\right). \quad (6)$$

Combining the above equations, the following formula (7) can be obtained:

$$\ln \frac{1}{t_{1/2}} = \ln \frac{k_0}{C} - \frac{E}{RT}. \quad (7)$$

The activation energy E of gasification can be obtained by the slope of ln $1/t_{1/2}$ and $1/T$. The change curve of ln $1/t_{1/2}$ of biochar and coke breeze with the change of $1/T$ was shown in Figure 5, and the activation energy and transition temperature were shown in Table 3.

It was shown in Table 3 that when the gasification reaction was in the external diffusion and internal diffusion control zone, the activation energy of biochar's gasification was slightly smaller than that of coke breeze, while, in the control of the chemical reaction zone, the activation energy of biochar's gasification was significantly lower than that of coke breeze. The activation energy of biochar's gasification was 131.10 kJ/mol, which was lower than that of coke breeze by 56.26 kJ/mol. Biochar's gasification transferred from chemical reaction control to internal diffusion control at 900°C, while transferring from internal diffusion control to external diffusion at 1000°C. Obviously, the transition temperature was lower than that of the coke breeze.

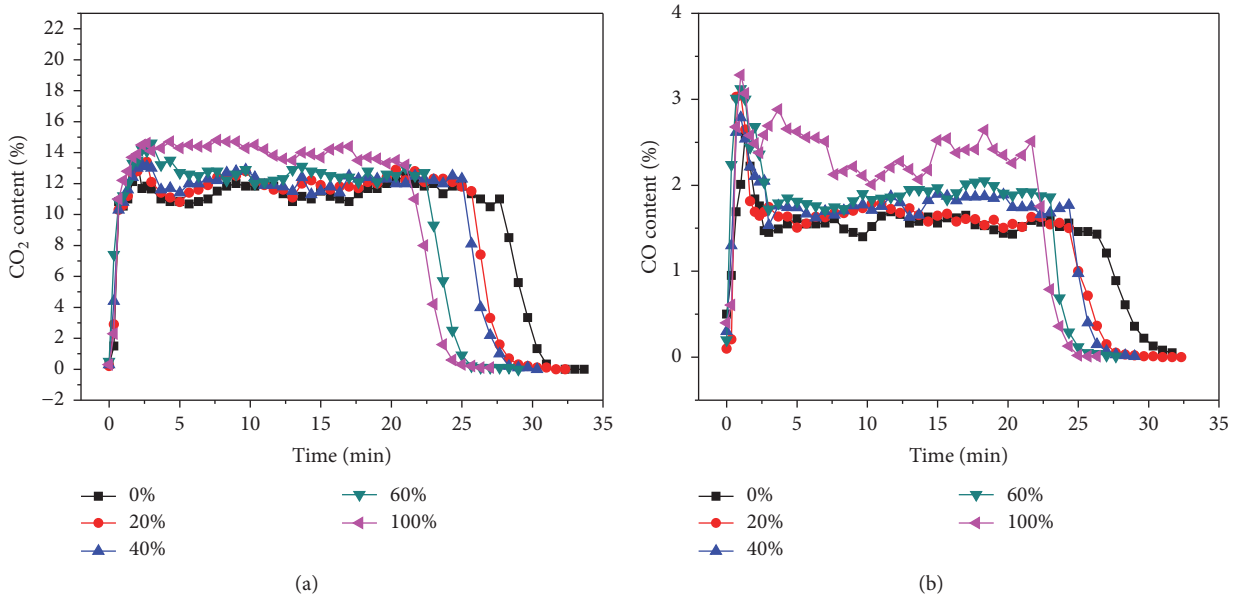

Figure 6: Effect of proportion of biochar replacing coke on COx concentrate of flue gas.

3.2. The Effect of Biochar on Sintering. The effect of proportion of biochar replacing coke at equal heat substitution on sintering process was studied. The effect of biochar replacing coke breeze on the emission of CO_2 and CO during sintering was shown in Figure 6. With the increase of substitute proportion, the content of CO_2 and CO in flue gas increased. More fuel was burned per unit time due to the increasing of burning speed when using biochar in sintering. When the substitute proportion increased from 0% to 100%, the average concentration of CO_2 and CO in flue gas increased from 10.32% and 1.43% to 12.27% and 2.14%, respectively.

Combustion efficiency refers to the ratio of complete combustion to the whole combustion. The ratio of $CO_2/(CO + CO_2)$ can reflect the combustion efficiency. When C is combust at high temperature, the reaction on the surface of C is the gasification reaction between C and CO_2, and the produced CO diffuses outward and reacts with O_2 diffusing inward to generate CO_2. Therefore, combustion efficiency was affected by the rate of $CO_2 + C = 2CO$ reaction on the surface of carbon particle. The influences of biochar replacing coke breeze on combustion efficiency were illustrated in Figure 7. Evidently, combustion efficiency was decreased with the increase of biochar ratios, and when they were 20%, 40%, 60%, and 100%, the average combustion efficiency was decreased from 87.83% to 87.82%, 86.92%, 86.04%, and 85.15%, respectively, which indicated that incomplete combustion developed with the increase of biochar ratios in sintering process. The heat released by the combustion of carbon was just 29.25% of its total calorific value when it combusted incompletely, which meant a high heat loss portion of 70.75%. Therefore, biochar replacing coke breeze would lower the efficiency of heat utilization.

From the above, it is known that biochar was characterized by higher reactivity than coke breeze and could react with CO_2 rapidly. Therefore, more CO was generated

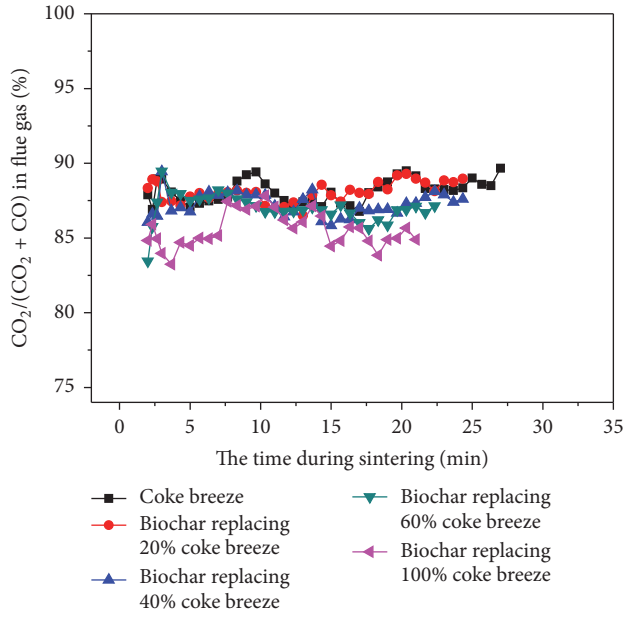

Figure 7: Influence of biochar replacing coke breeze on combustion efficiency.

on the surface of biochar. Furthermore, as biochar burned quickly, more O_2 was consumed per unit time and the concentration of O_2 in flue gas was relatively low, which limited the secondary combustion reaction of CO and finally made combustion efficiency drop, which finally decreased the production and quality index of sintering.

The effect of biochar replacing coke breeze at equal heat substitution on the yield and quality of sinter was shown in Table 4. With the increase of substitute proportion, the sintering speed accelerated, while the sinter yield, tumble

Table 4: Effect of biochar replacing coke breeze on sintering indexes.

Biochar replacing coke ratio/%	Suitable moisture/%	Sintering speed/mm·min^{-1}	Yield/%	Tumble strength/%	Productivity/t·m^{-2}·h^{-1}
0	7.25	21.94	72.66	65.00	1.48
20	7.25	24.58	68.69	64.40	1.52
40	7.50	24.73	65.30	63.27	1.43
60	7.50	27.20	55.35	54.67	1.32
100	7.75	27.17	41.11	23.87	0.93

Table 5: Effect of heat replacement ratio on sintering indexes.

Heat replacement ratio	Sintering speed/mm·min^{-1}	Yield/%	Tumble strength/%	Productivity/t·m^{-2}·h^{-1}
1.00	24.73	65.30	63.27	1.43
0.85	24.29	67.27	64.47	1.41
0.75	23.88	69.63	64.18	1.46

strength, and productivity decreased. When the substitute proportion of biochar was relatively low, the decreasing extent was not significant. However, when the substitute proportion exceeded a certain value, the sinter yield and quality index deteriorated greatly. Therefore, the proportion of biochar replacing coke breeze had an appropriate value. When the substitute proportion was more than 40%, the sinter yield and quality index dropped rapidly, indicating that the appropriate substitute proportion was 40%.

The main reason why sinter yield and tumble strength decreased was that the biochar burnt too fast, causing the deterioration of combustion efficiency and the drop of bed layer temperature. Consequently, reducing the heat replacement ratio of biochar for raising the temperature of bed layer could improve the yield and tumble strength of sinter. The effect of heat replacement ratio on sintering indexes was shown in Table 5. When the ratio of the heat released by biochar replacing that for the coke reduced from 1.00 to 0.75, the yield of sinter increased from 65.30% to 69.63%, and the tumble strength increased from 63.27% to 64.18%. Therefore, reducing the heat replacement ratio of biochar could improve the yield and quality of sinter.

4. Conclusion

(1) The initial temperature and the final temperature of the gasification reaction between biochar and CO_2 were low, the speed was fast, and the maximum weight loss rate and heat absorption were both higher than those of the coke breeze. Dynamic parameters showed that the gasification activation energy of biochar was 56.26 kJ/mol, lower than coke breeze, which indicated that the biochar had better reactive activity.

(2) Due to biochar's high reactivity, the degree of incomplete combustion in the sintering process increased and the thermal efficiency reduced, which was not conducive to the high-temperature mineralization process. As a result, the sinter yield, tumble strength, and productivity decreased with the increase of biochar's substitute proportion. Therefore, the proportion of biochar replacement of coke breeze at equal heat substitution should be controlled no more than 40%. Reducing the heat replacement ratio of biochar could improve the temperature of sinter bed, improving the yield and tumble strength of sinter.

Conflicts of Interest

The authors declare that they have no conflicts of interest.

Acknowledgments

The research was financially supported by the State Key Program of National Natural Science Foundation of China (no. U1660206), Natural Science Foundation of Hunan Province in China (no. 2015JJ3164), Hunan Provincial Co-Innovation Center for Clean and Efficient Utilization of Strategic Metal Mineral Resources and Innovation Driven Plan of Central South University (no. 2015CX005), Hunan Provincial Innovation Foundation for Postgraduate (CX2016B054), and Open-End Fund for the Valuable and Precision Instruments of Central South University (CSUZC201703).

References

[1] Z. Z. Hao, S. L. Wu, and X. G. Duan, "Practice of reducing sintering process energy consumption in Baosteel," *Sintering Pelletizing*, vol. 35, article 46, 2010.

[2] S. Q. Li, Z. J. Ji, L. Wu et al., "An analysis on the energy consumption of steel plants and energy-saving measures," *Industrial Heating*, vol. 39, no. 5, pp. 1–3, 2010.

[3] X. M. Liang, D. Q. Zhu, T. Jiang et al., "Present State of Sintering Energy Saving Techniques and Prospect," *Sintering and Pelleting*, vol. 25, no. 4, pp. 1–4, 2000.

[4] Y. G. Chen, Z. C. Guo, Z. Wang, and G. S. Feng, "NOx reduction in the sintering process," *International Journal of Minerals, Metallurgy and Materials*, vol. 16, no. 2, pp. 143–148, 2009.

[5] Y. Chen, Z. Guo, and Z. Wang, "Influence of CeO2 on NOx emission during iron ore sintering," *Fuel Processing Technology*, vol. 90, no. 7-8, pp. 933–938, 2009.

[6] P.-A. Glaude, R. Fournet, R. Bounaceur, and M. Molière, "Adiabatic flame temperature from biofuels and fossil fuels and derived effect on NOx emissions," *Fuel Processing Technology*, vol. 91, no. 2, pp. 229–235, 2010.

[7] J. Liu, G. Zhai, and R. Chen, "Analysis on the characteristics of biomass fuel direct combustion process," *Journal of Northeast Agricultural University*, vol. 3, pp. 290–294, 2001.

[8] C. Bartolomé and A. Gil, "Emissions during co-firing of two energy crops in a PF pilot plant: Cynara and poplar," *Fuel Processing Technology*, vol. 113, pp. 75–83, 2013.

[9] H. Spliethoff and K. R. G. Hein, "Effect of co-combustion of biomass on emissions in pulverized fuel furnaces," *Fuel Processing Technology*, vol. 54, no. 1-3, pp. 189–205, 1998.

[10] R. C. Guo, J. R. Tang, H. Xu, and H. C. Ma, "The status and vision for utilization of lignified biomass energy," *Forest Inventory & Planning*, vol. 32, no. 1, pp. 90–94, 2007.

[11] R. Lovel, K. Vining, and M. Dell'Amico, "Iron ore sintering with charcoal," *Transactions of the Institutions of Mining and Metallurgy, Section C: Mineral Processing and Extractive Metallurgy*, vol. 116, no. 2, pp. 85–92, 2007.

[12] M. Zandi, M. Martinez-Pacheco, and T. A. T. Fray, "Biomass for iron ore sintering," *Minerals Engineering*, vol. 23, no. 14, pp. 1139–1145, 2010.

[13] T. C. Ooi, E. Aries, B. C. R. Ewan et al., "The study of sunflower seed husks as a fuel in the iron ore sintering process," *Minerals Engineering*, vol. 21, no. 2, pp. 167–177, 2008.

[14] S. N. Silva, F. Vernilli, D. G. Pinatti et al., "Behaviour of biofuel addition on metallurgical properties of sinter," *Ironmaking and Steelmaking*, vol. 36, no. 5, pp. 333–340, 2009.

[15] H. Helle, M. Helle, H. Saxén, and P. Frank, "Mathematical optimization of ironmaking with biomass as auxiliary reductant in the blast furnace," *ISIJ International*, vol. 49, no. 9, pp. 1316–1324, 2009.

[16] L. Lu, M. Adam, M. Kilburn et al., "Substitution of charcoal for coke breeze in iron ore sintering," *ISIJ International*, vol. 53, no. 9, pp. 1607–1616, 2013.

[17] L. Lu, M. Adam, M. Somerville, S. Hapugoda, S. Jahanshahi, and J. G. Mathieson, "Iron ore sintering with charcoal," in *Proceedings of the 6th Int. Cong. of the Science and Technology of Ironmaking – ICSTI 2012*, Brazilian Association for Metallurgy, Materials and Mining, Rio de Janeiro, Brazil, 2012.

[18] M. Gan, X. Fan, X. Chen et al., "Reduction of pollutant emission in iron ore sintering process by applying biomass fuels," *ISIJ International*, vol. 52, no. 9, pp. 1574–1578, 2012.

[19] X. Fan, Z. Ji, M. Gan, X. Chen, Q. Li, and T. Jiang, "Influence of charcoal replacing coke on microstructure and reduction properties of iron ore sinter," *Ironmaking and Steelmaking*, vol. 43, no. 1, pp. 5–10, 2016.

[20] X. Fan, Z. Ji, M. Gan, X. Chen, L. Yin, and T. Jiang, "Preparation technologies of straw char and its effect on pollutants emission reduction in iron ore sintering," *ISIJ International*, vol. 54, no. 12, pp. 2697–2703, 2014.

[21] M. Gan, X. Fan, Z. Ji, X. Chen, T. Jiang, and Z. Yu, "Effect of distribution of biomass fuel in granules on iron ore sintering and NOx emission," *Ironmaking and Steelmaking*, vol. 41, no. 6, pp. 430–434, 2014.

[22] H. P. Tseng and T. F. Edgar, "Identification of the combustion behaviour of lignite char between 350 and 900 ∘C," *Fuel*, vol. 63, no. 3, pp. 385–393, 1984.

Hindawi
Advances in Materials Science and Engineering
Volume 2017, Article ID 9407259, 7 pages
https://doi.org/10.1155/2017/9407259

Research Article

Preparation and Properties of Agricultural Residuals-Iron Concentrate Pellets

Zhulin Liu,[1] Xuegong Bi,[2] Zeping Gao,[1] and Yayu Wang[2]

[1]*School of Metallurgical and Materials Engineering, Hunan University of Technology, Zhuzhou, Hunan 412007, China*
[2]*State Key Laboratory for Refractory Materials and Metallurgy, Wuhan University of Science and Technology, Wuhan, Hubei 430081, China*

Correspondence should be addressed to Xuegong Bi; 1575595611@qq.com

Received 22 May 2017; Accepted 18 September 2017; Published 22 October 2017

Academic Editor: Merrick Mahoney

In this paper, carbon-containing pellets were prepared by using crop-derived charcoal made from agricultural residuals and iron ore concentrates, and their pelletizing performance and properties were studied. Experimental results showed that the strengths of pellets were related to the particle size of concentrates and the content of moisture, bentonite, and crop-derived charcoal fines in the pelletizing mixture and the temperature of roasting and reduction. That the granularity of raw materials was fine and the bentonite content increased was beneficial to the improvement of pellet strengths. The suitable molar ratio of carbon to oxygen was 1.0 and the proper proportioning ratios of moisture and binder were 8.0% and 6.5%, respectively. The pellet strengths increased accordingly with increasing the reduction temperature, and when the temperature reached 1200°C, accompanied by the fast reduction of iron and the formation of crystal stock, the dropping strength of product pellets was 15 times and the compressive strength was 1650 N; this may be improved by grinding of the concentrate, leading to acceptable strength for the blast furnace.

1. Introduction

The sustainable development of the steel industry is severely restricted by natural resources, energy supply capacity, and the earth environmental bearing capacity [1]. Crops are artificial plants and grow and develop by absorbing CO_2 in the atmosphere and utilizing solar energy. Therefore, crops waste not only is a renewable energy, but also could not additionally increase CO_2 in the atmosphere during combustion; it is completely carbon neutral, that is, has a feature of zero CO_2 emission [2].

Further, because the ash generated by biomass combustion appears to be alkaline, it is possible to restrain the formation of contaminants such as SO_2, NO_x, and so on [3]. Moreover, burning in the open air of a large number of surplus crop straw will produce a great deal of gases and aerosol components. This will not only lead to a great waste of resources and destroy soil fertility, but also bring about serious air pollution [4]. Therefore, the application of crop wastes will improve the ecological environment. China owns extremely abundant biomass resources; the output of residues from forests and agricultural industry is 2 billion 29 million tons per annum. There mainly are crops straw, forestry residues, livestock manures, and energy crops [5]. The carbon content in wheat and corn straws is about 40% while that in rice husk accounts for 43% [6].

The product of crop wastes carbonization is essentially the same with charcoal in respect to chemical composition, being based on carbon and also having hydrogen, oxygen, nitrogen, and a few other elements, but very low ash and sulphur. Therefore, it is feasible to reduce iron ores with crop wastes [7, 8]. More importantly, to substitute agricultural and forestry biomass charcoal for coal for producing carbon-bearing pellets can not only realize the reuse of wastes and protect the environment, but also save coal and mitigate CO_2 emission [9].

Babich et al. [10] studied charcoal behavior by its injection into the modern blast furnace. Specific surface area was measured with BET technique and the results showed that specific surface area of charcoals (150~350 m^2/g) is 60~350 times greater than that for PC (1.0~2.6 m^2/g). This result is coincident with the higher reactivity that was determined

Table 1: Chemical composition of concentrate.

Component	T.Fe	S	P	SiO_2	FeO	Al_2O_3	CaO	MgO	MnO	H_2O	I.L.
Mass%	60.67	0.11	0.05	12.00	9.23	1.07	0.50	1.00	0.33	10.96	−1.30

Note. I.L. is ignition loss.

by the Simultaneous Thermal Analysis (Netzsch, STA 409) method, the pilot injection plant test, and the coke bed simulator experiment. Pore characteristics were quantified by optical microscope with Soft Imaging Analysis. The overall porosity varies between 1/3 and 1/2 among the charcoal samples, but for PC no pores were identified. Although there are so far few measured data of porosity, surface area and reactivity for crop-derived charcoal were reported; it can be reasonably presumed that crop-derived charcoal is also superior to PC in terms of these three qualities.

Mathieson et al. [11] analyzed the potential for biomass-derived charcoal to reduce net greenhouse gas emissions from the Australian steel industry and proposed many applications such as sintering solid fuel, cokemaking blend component, BF tuyere fuel injectant, BF nut coke replacement, BF carbon/ore composites of BOF prereduced feed, and steelmaking recarburiser. Actually, as early as in the 1980s, aiming at the application of abundant tropical forest resources in Brazil, Martins et al. [12] made a preliminary study on sponge iron production by using green pellets made of iron ores and charcoal mix. The binders used in their research consisted of water glass, lime, and cement. Hayashi and Iguchi [13] studied the possibility of partly substituting cedar flour for coal to produce carbon composite iron ore hot briquettes. Nakano et al. [14] have proposed that unreduced carbon-ore composite pellets or briquettes be added as blast furnace feed and manufactured nonspherical carbon composite in lab-scale. In their study on charcoal composite iron oxide pellets, Konishi et al. [15] derived charcoal from Japanese cypress and mixed it into Fe_2O_3 agent of 98% purity pellets at a ratio of 1/4 with an addition of 3 mass% bentonite. And then pellets of about 10 mm in diameter were manually made and reduced at 1273, 1373, and 1473 K in N_2 gas atmosphere. More recently, Li et al. [16] added straw fiber (without carbonization) to substitute for coal into South African iron ore for the preparation of metallized pellets. Pellets sized 22 ∗ 10 mm were produced under 20 MPa pressure without heating and binder addition. It was demonstrated that the strength of green pellets met the requirement of Rotary Hearth Furnace process. It is noted that there are few reports in the literature so far on the preparation and properties of crop-derived charcoal containing iron ore pellets.

In this work, feasibility of preparation of carbon composite iron ore pellets by using crop-derived charcoal was assessed and appropriate technological conditions were experimentally determined.

2. Test Materials and Methods

2.1. Chemical and Size Compositions of Concentrate. The raw materials for pellets preparation were concentrates provided by Hualing Xiangtan Iron and Steel Corporation (Group); the chemical composition is shown in Table 1. The reducing agent was self-made crop-derived charcoal; the composition is shown in Table 2. The binder used was bentonite; the composition is shown in Table 3.

Table 2: Approximate analysis of crop-derived charcoal.

Component	A_d	V_d	FC_d	$S_{t,d}$	M_{ad}
Mass%	3.48	32.10	61.82	0.05	2.60

Note. A_d is ash content; V_d is volatile content; FC_d is fixed carbon content; $S_{t,d}$ is total sulfur content; M_{ad} is moisture content.

Table 3: Chemical composition of bentonite.

Component	Al_2O_3	CaO	MgO	SiO_2	K_2O	Na_2O	I.L.
Mass%	12.65	1.02	4.19	53.25	0.43	0.30	14.39

The crop-derive charcoal was prepared from rice husk and peanut shell through crushing, molding, and low temperature carbonization (300~350°C) for the purpose of including more residual volatile matter.

The cumulative size distribution curve of concentrate is shown in Figure 1.

As can be seen from Figure 1, the size of this concentrate was a little too coarse for pelletizing ores; the cumulative percentage of minus 0.04 mm approximately accounted for 30% and that of minus 0.074 mm approximately accounted for only 80%. As can be seen from Table 2, the fixed carbon content in the self-made crop-derived charcoal was relatively low at only 61.82% while the volatile content was as high as 32.10%. The reason is that the blocks made of crop wastes were relatively large, the carbonization temperature was lower, and the time was shorter, resulting in an insufficient carbonization. However, the ash content of biochar was only 3.48%, which is favorable to the reduction of flux consumption and to the smelting of low Si content pig iron [17]. As can been seen in Table 3 that the MgO content in bentonite was relatively high, it belongs to Ca-based bentonite with a poorer bonding capacity.

2.2. Test Method. In the experiment, a vacuum heating furnace was used for carbonizing the collected crop wastes such as peanut hull and rice husk. After carbonization, they were crushed and ground. The concentrate and self-made crop-derived charcoal fines were, respectively, screened with 150, 180, and 200 mesh sieves; the obtained materials of corresponding sizes were used for pelletizing. The diameter of green balls was 8~12 mm. In the tests, the water content of green balls was designated as 7.5%, 8.0%, and 8.5%. By taking into account the fact that the addition of crop-derived charcoal fines will decrease the strength of green balls, bentonite proportioning ratio was set as 6%, 6.5%, and 7%. According to investigation results of other researchers [18, 19], the molar ratio of carbon to oxygen (C/O ratio) usually is

Table 4: Material ratios of carbon-bearing pellets, mass%.

Test number	Size of concentrate and char/mesh	C/O —	Concentrate	Crop-derived charcoal	Binder	H_2O
1	200	0.9	67.9	18.6	6.0	7.5
2	200	1.0	65.6	19.9	6.5	8.0
3	200	1.1	63.4	21.1	7.0	8.5
4	180	0.9	66.8	18.2	6.5	8.5
5	180	1.0	65.6	19.9	7.0	7.5
6	180	1.1	64.5	21.5	6.0	8.0
7	150	0.9	66.8	18.2	7.0	8.0
8	150	1.0	65.6	19.9	6.0	8.5
9	150	1.1	64.5	21.5	6.5	7.5

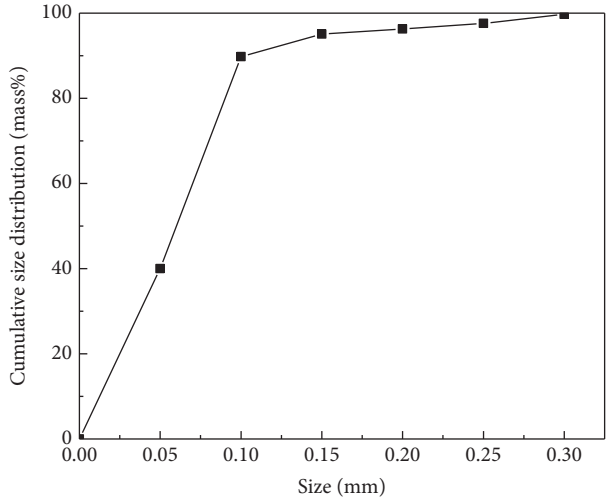

Figure 1: Cumulative size distribution of concentrate.

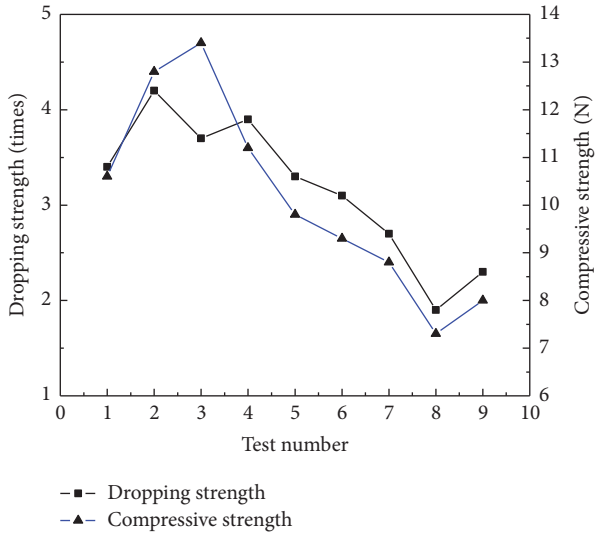

Figure 2: The dropping strength and compressive strength of green balls.

around one. In this experiment, C/O ratio was assigned as 0.9, 1.0, and 1.1; the corresponding material ratios calculated are seen in Table 4. The measurements of pelletizing performance mainly included the compressive strength, dropping strength, and shock temperature of green balls.

Measurement of the dropping strength of green balls: in each test, ten green balls of 10~12 mm in diameter are selected at pleasure and dropped onto a steel sheet of 10 mm in thickness, the height of dropping is 500 mm, and the mean value of the number of dropping where there appeared flaws in any green ball or it broke into pieces is taken as the dropping strength of green balls in this test.

Measurement of the compressive strength of green balls: in each test, ten green balls of 10~12 mm in diameter are picked at random, they are pressed vertically at a compression speed not exceeding 10 mm/min, and the mean value of the exerted loads where flaws appeared in any green ball is taken as the compressive strength of green balls in this test.

Measurement of the shock temperature of green balls: in each test, ten green balls of 10~12 mm in diameter were selected at random, and, in the tubular furnace with a 320 to 520°C temperature range, the temperature where the percentage of green balls that generated flaws inside achieves 10% is measured and taken as the shock temperature of green balls.

3. Test Results and Analysis

3.1. Properties and Their Analysis of Carbon-Containing Green Balls. After the disc pelletizer started running, the pelletizing mixture accounting for about one-third of the total weight of green balls was firstly added and water was dropped with a bottle onto the materials to form seed balls. The size of seed balls was controlled at around 2 mm, and it was also required that the grain size was uniform. After seed balls formed, mist water was sprayed while materials were added according to the situation of balls growing. When most green balls grew up to 8~12 mm in diameter, it was stopped to add materials into the disc pelletizer and the pelletizer continued running for 3~5 min. The green balls properties of nine tests are shown in Figures 2 and 3.

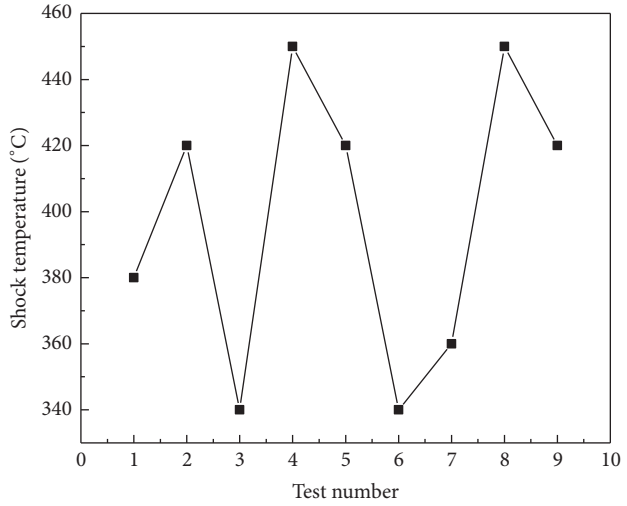

Figure 3: The shock temperature of green balls.

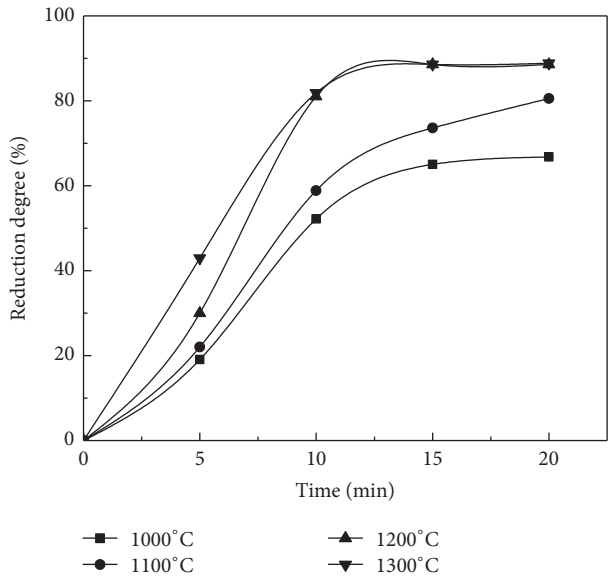

Figure 4: Reduction degree of carbon-bearing pellets versus time.

As can be seen from Figures 2 and 3, the quality of green balls dropping strength of test number 2 and the quality of green balls compressive strength of test number 3 were the best, respectively, achieving 4.3 times the dropping strength and 13.4 N compressive strength. However, the green balls shock temperature of test number 3 was only 340°C, unfavorable to the high temperature reduction and calcination of pellets.

Making a comprehensive comparison, the overall property of test number 2 was the best: the dropping and compressive strengths were 4.2 times and 12.8 N, respectively, and the shock temperature could reach 420°C. The size of raw materials of test number 2 was 200 mesh, C/O ratio was 1.0, binder blending ratio was 6.5%, and H_2O content was 8%.

The size of raw materials of the first three tests was smaller and accordingly the dropping strength and compressive strength were higher. The finer the raw materials size, the higher the surface free energy and, after water addition for lubrication, the smaller the diameter of the capillaries generated. The greater the capillary force, the stronger the binding force, and thus the dropping strength as well as the compressive strengths would increase.

Generally speaking, the dropping and compressive strengths of green balls increase with increasing the content of bentonite binder. The supper fine particles in bentonite and concentrate form gelatinous substance, and this kind of colloids fills up among iron ore particles, playing a good role of adhesive bridges. In addition, after absorbing moister, bentonite forms a colloid, which has a gelatinous structure of a "card room" type 3D network form. This gelatinous structure could improve the viscous resistance and shear strength of binding bridges, and thus increase the dropping strength, compressive strength, and shock temperature.

Why the shock temperature of test number 3 appeared abnormal is probably because C/O ratio was higher and crop-derived charcoal contained more volatile matters; thus the volatilization of volatile matters would be the primary cause that leads to green balls bursting and decreases the shock temperature. Similarly, due to the higher C/O ratios, the shock temperature of tests number 6 and number 9 were decreased in different extents, but number 9 is actually still quite strong.

3.2. Metallized Pellets Properties and Analysis. For studying the effect of temperature on the reduction property of pellets, after drying at 110°C, the green balls with 1.0 C/O ratio of test number 2 were isothermally autoreduced for 5, 10, 15, and 20 min, respectively, at various temperatures and under the condition of nitrogen protection.

In the weight loss of carbon-containing pellets, apart from oxygen loss, the carbon loss, the amount of volatile matters separated, and remaining water vaporized are also included. In this paper, the modified weight loss approach was utilized, that is, by taking carbon-containing alumina balls as a reference, to indirectly measure the separation ratio of volatile matters and water and to evaluate the degree of reduction with (1), which originated from a reference and was modified in this work.

$$R = \frac{4}{7M_O}\left(f_\Sigma - f_{A\text{-}P}\right)W \times 100, \%, \quad (1)$$

where M_O is oxygen amount in iron oxides, g; f_Σ is the percentage of total weight loss, %; $f_{A\text{-}P}$ is the percentage of weight loss of volatile matters and moisture in carbon-containing alumina balls, %; W is the weight of carbon-containing pellets, g.

The maximum weight loss rate and the reduction degree at 20 min were obtained as shown in Table 5. The plots of reduction degree against time are described in Figure 4.

It can be seen from Table 5 and Figure 4 that, for carbon-bearing pellets, the maximum reduction degree and the maximum weight loss rate at 1200°C and 1300°C are all essentially identical. This is presumably because the porosity of crop-derived charcoal fines is relatively large, having bigger

Table 5: Results of carbon-bearing pellets reduction at different temperatures.

Temperature, ˚C	Weight loss rate at 20 min, %	Reduction degree at 20 min, %
1000	27.36	66.76
1100	32.21	80.56
1200	34.79	88.66
1300	34.86	88.85

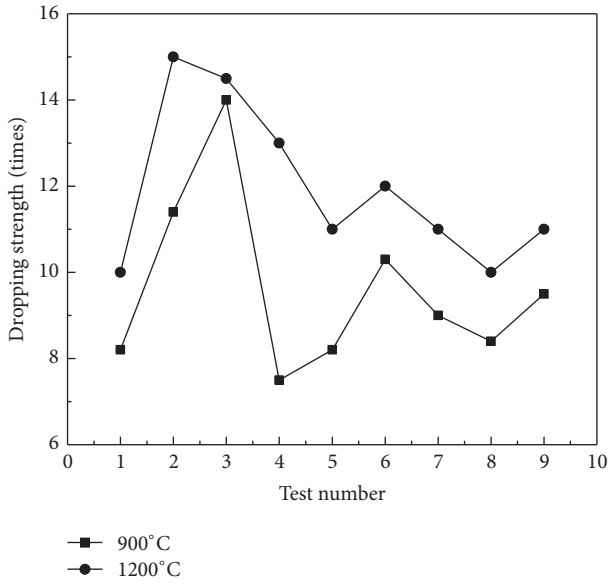

Figure 5: The dropping strength of pellets after reduction.

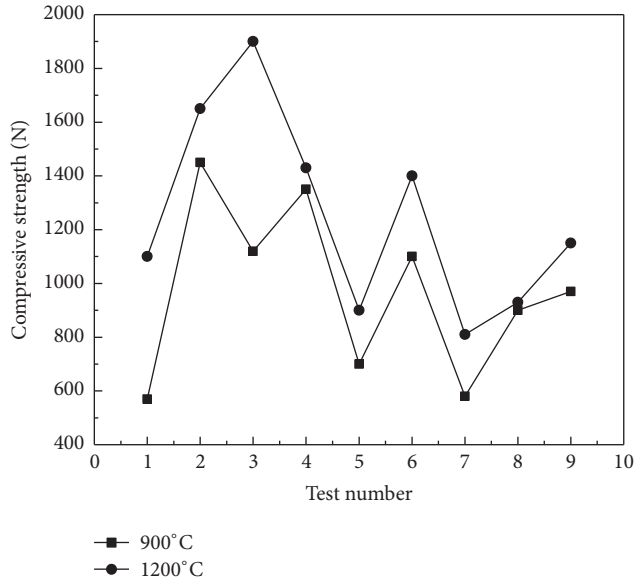

Figure 6: The compressive strength of pellets after reduction.

areas of reaction and also possessing higher degree of CO_2 reaction compared to PC; see Section 1, and with the addition of reduction by the CO and H_2 in abundant volatile matters, the reduction process could rapidly proceed at only 1200˚C. Over 1200˚C, however, further increasing temperature had no great raising effect on the reduction extent of pellets. It is true that the reduction degree of pellets increased with temperature increasing, but, from the economic point of view, the appropriate reduction temperature of these carbon-containing pellets would be 1200˚C, with a reduction time of 15 min.

Green balls of the above-mentioned nine tests were treated isothermally at 900˚C for 20 min; at this moment, direct reduction had not taken place in quantity in the pellets, and dropping and compressive strengths were measured. Again, the green balls were isothermally treated at 1200˚C for 20 min, metallized pellets were obtained by reduction, and dropping strength and compressive strength were measured and shown in Figures 5 and 6, respectively.

It can be seen from Figures 5 and 6 that, under the condition of 1200˚C, the dropping and compressive strengths of metallized pellets of each test are all higher than the pellets of their corresponding tests which were obtained under the condition of 900˚C reduction temperature and had lower extents of direct reduction. The highest dropping strength and compressive strength of pellets reduced at 1200˚C were 15 times and 1900 N. The best was the pellets of test number 2 in respect to comprehensive properties; their dropping strength and compressive strength were 15 times and 1650 N, respectively.

Reduction temperature has a positive impact on increasing the postreduction strength of pellets, and thus a lower temperature will bring about various physicochemical reactions proceeded slowly; above all, for carbon-containing pellets that give priority to the direct reduction, it is hard to achieve the consolidation effect. As temperature increases and the direct reduction reaction proceeds, more metallic iron forms and the metallic iron sinters increasing pellet strength.

3.3. Consideration of How to Decrease the Blending Ratio of Bentonite. As shown in Table 4, the blending ratio of bentonite in this work was rather high, ranging from 6.0 to 7.5 mass%, which will bring about a higher production cost of pellets and a lower iron grade of pellets, meaning a higher slag volume and a greater fuel consumption of the blast furnace. The main reason why so much bentonite has to be proportioned into the pelletizing mixture is, in comparison with pulverized coal, crop-derived charcoal is poor in hydrophilia and ballability. The secondary cause is the blending ratio of charcoal being necessarily higher for a given C/O ratio, due to its lower carbon content and its lower density. As a consequence, the bulk density of pelletizing

mixture is smaller and the voidage between material particles is larger; thus more binder has to be blended.

There are some potential countermeasures [20] to solve this problem, including reducing the concentrate size to 325 mesh with use of the technique of wet-grinding or high-pressure roller grinding, applying alkali-based bentonite of higher efficiency, and partly blending organic binders. This is the subject of future work.

4. Conclusions

(1) Under the condition that pelletizing time and pelletizer parameters are constant, the properties of carbon-containing pellets are related to the particle size of pelletizing materials, the content of moisture, the amount of bentonite blended, the amount of crop-derived charcoal fines addition, and the temperature of reduction. The finer the raw materials particle size and the higher the binder content, the better the comprehensive performance of pelletizing. The water content needs to be appropriate. Too high a C/O ratio could cause a decrease of the shock temperature of green balls.

(2) Under the condition that the particle size of concentrate and crop-derived charcoal fines were both 200 mesh, C/O ratio was 1.0, the bentonite content was 6.5%, and water content was 8%, the quality of green balls was better: the dropping strength reached 4.2 times, the compressive strength was 12.8 N, and the shock temperature was 420°C.

(3) The reduction process of crop-derived charcoal composite iron ore pellet could quickly be conducted at only 1200°C; a 15 min holding time of high temperature was suitable.

(4) The dropping strength and the compressive strength of metallized pellets obtained by high temperature reduction at 1200°C were all higher than the pellets with lower direct reduction extents that were obtained under the reduction condition of 900°C. The main reason was that the rapid reduction of metallic irons and the formation of a crystal stock between them significantly improved the mechanical strength of pellets. The dropping strength and compressive strength of pellets of test number 2 with a good comprehensive performance were, respectively, 15 times and 1650 N, basically meeting the requirements of blast furnace feed materials in terms of strength.

Blast furnace pellets should have an average compression strength of 2500 N. Future work should try to increase this strength.

Conflicts of Interest

The authors declare that there are no conflicts of interest regarding the publication of this paper.

Acknowledgments

Thanks are due to Hunan Province (A research project supported by the Hunan Province Science and Technology Program Foundation Grant no. 2012FJ3037).

References

[1] Z.-L. Liu, X.-G. Bi, and S.-Z. Shi, "Development of ecological blast furnace in 21st century," *Kang T'ieh/Iron and Steel (Peking)*, vol. 43, no. 7, pp. 1–6, 2008.

[2] Y.-K. Liu, Q.-F. Sun, D.-M. Li, and Zh.-Q. Chen, "Current status and prospect of the utillization of biomass wastes," *Chemical Engineer*, no. 3, pp. 28–30, 2011.

[3] S. V. Loo and J. Koppejan, *Handbook of Biomass Combustion and Co-firing*, Twente University Press, Netherlands, 2002.

[4] M.-L. Li, J. Gu, H. Gao, Q.-J. Qin, and M.-J. Liu, "Preparing and application of bio-organic fertilizer and organic-inorganic fertilizer," *Soils and Fertilizers Sciences in China*, no. 1, pp. 56–59, 2008.

[5] M. Mandalakis, Ö. Gustafsson, T. Alsberg et al., "Contribution of biomass burning to atmospheric polycyclic aromatic hydrocarbons at three european background sites," *Environmental Science & Technology*, vol. 39, no. 9, pp. 2976–2982, 2005.

[6] Zh.-Q. Song, "High-value utilization of agricultural and forestry residues resources," *Jiangsu Science and Technology Information*, no. 12, pp. 1–3, 2008.

[7] M. Kawakami, T. Karato, T. Takenaka, and S. Yokoyama, "Structure analysis of coke, wood charcoal and bamboo charcoal by Raman spectroscopy and their reaction rate with CO2," *ISIJ International*, vol. 45, no. 7, pp. 1027–1034, 2005.

[8] H. Konishi, K. Ichikawa, and T. Usui, "Effect of residual volatile matter on reduction of iron oxide in semi-charcoal composite pellets," *ISIJ International*, vol. 50, no. 3, pp. 386–389, 2010.

[9] N. Li, W.-F. Jiang, S.-J. Hao, and Y.-Q. Wang, "Effect of addition agent on the strength of high carbon bearing pellets," *Journal of Hebei Polytechnic University*, vol. 31, no. 3, pp. 20–24, 2009.

[10] A. Babich, D. Senk, and M. Fernandez, "Charcoal behaviour by its injection into the modern blast furnace," *ISIJ International*, vol. 50, no. 1, pp. 81–88, 2010.

[11] J. G. Mathieson, T. Norgate, S. Jahanshahi et al., "The potential for charcoal to reduce net greenhouse gas emissions from the Australian steel industry," in *Proceedings of the 6th International Congress on the Science and Technology of Ironmaking 2012, ICSTI 2012*, pp. 1602–1613, bra, October 2012.

[12] J. Martins et al., "Primary tests of sponge iron production by using green pellets made of iron ores and charcoal mix," *Sintering and Pelletizing*, vol. 1, pp. 54–56, 1989.

[13] S. Hayashi and Y. Iguchi, "Reaction behavior of wood flour added coal composite iron ore hot briquettes at high temperatures," in *Proceedings of the Asia Steel International Conference*, pp. 372–377, Fukuoka, Japan, 2006, May 9-11.

[14] M. Nakano, M. Naito, K. Higuchi, and K. Morimoto, "Non-spherical carbon composite agglomerates: Lab-scale manufacture and quality assessment," *ISIJ International*, vol. 44, no. 12, pp. 2079–2085, 2004.

[15] H. Konishi, T. Usui, and T. Harada, "The Preparation and Reduction Behavior of Charcoal Composite Iron Oxide Pellets," *Journal of High Temperature Society*, vol. 34, no. 1, pp. 14–19, 2008.

[16] D.-W. Li, Ch.-Sh. Yue, H.-L. Han, and D.-P. Duan, "Application of straw fiber as the reducing agent in production of metallic pellets," *Environmental Engineering*, vol. 34, no. 1, pp. 119-112, 2016.

[17] Zh.-L. Liu, J.-L. Wang, Zh.-J. Su, X. Yang, and K. Liu, "Analysis of the measurement on reducing the fuel rate of blast furnace in pingxiang iron and steel co," *Journal of Hunan University of Technology*, vol. 26, no. 1, pp. 96–100, 2012.

[18] Zh.-G. Ren, Y.-Sh. Zhou, L.-J. Wang, and W.-Zh. Li, "Study on the metallurgical properties of cold-boned carbon-bearing pellets," *Sintering and Pelletizing*, vol. 21, no. 6, pp. 12–22, 1996.

[19] T. Du and K. Du, "Application-basis study of key technologies in carbon-bearing pellets-iron bath smelting reduction process," *Jinshu Xuebao/Acta Metallurgica Sinica*, vol. 33, no. 7, pp. 727-728, 1997.

[20] J. Pan, D.-Q. Zhu, K.-Ch. Zhang, F.-Ch. Tian, A.-P. He, and X.-F. Xu, "Experimental Study of Improving Green Balls Properties by Modifying Bentonite," in *Proceedings of 2005 National Technical Communication Congress of Sintering and Pelletizing*, pp. 32–36.